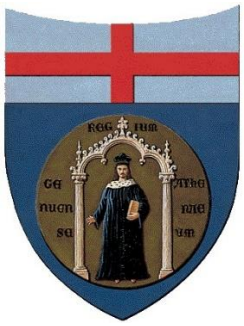

Università degli Studi di Genova

Dottorato di Ricerca in Fisica – XXXII Ciclo

Tesi per il conseguimento del titolo di Dottore di Ricerca

Nanofluidic platforms for sensing applications in biomedical and environmental fields

Supervisors:

Dr. Luca Repetto

Dr. Elena Angeli

Candidate:

Denise Pezzuoli

Abstract

Nowadays, nanofluidic platforms are powerful tools for carrying out fundamental studies on molecular-scale phenomena. Typically, the use of these systems results in being crucial both in biomedical and environmental fields. In fact, they are widely exploited for many applications such as detection, concentration, sorting, counting and sizing of several nano-objects such as nanoplastics, viruses, antibodies and DNA. This is the context in which my Ph.D. research project is inserted.

I have worked on the development of elastomeric nanofluidic platforms, equipped with different nanostructures, that are the functional areas of the entire fluidic system, useful for different applications among which single nanoparticles detection, high-sensitivity immunoassay analysis and DNA sensing.

Typically, nanofluidic platforms are composed of two U-shaped microchannels connected by nanostructures with suitable geometries. All devices were fabricated starting from a pre-patterned silicon mold on which nanostructures were etched using the Focus Ion Beam (FIB) milling technique. Then, the molds were replicated through a, Poly(DiMethylSiloxane)(PDMS) based, double REplica Molding (REM) technique. Although FIB is a high-resolution but expensive technology with REM technique, that is a low-cost and simple approach, I was able to fabricate many polymeric replicas with high precision re-using the mold for several times. This combination allowed obtaining

high-resolution nanofluidic platforms reducing fabrication costs, a method that is potentially applicable to processes with high production rate.

However, when the dimension shrinks from micro to nanoscale, PDMS presents significant limits. In particular, polymeric nanostructures suffer from the “roof collapse” phenomenon that occurs when the replica is sealed with a glass substrate, a necessary procedure to obtain watertight devices. It is possible to overcome this problem both by exploiting the Junction Gap Breakdown (JGB) technique and by using hard-PDMS (h-PDMS) during the fabrication process.

During my Ph.D. research activity, I have initially worked on an asymmetric structure that was a funnel-shaped nanochannel in which the tip, after experiencing “roof-collapse”, was re-opened, thanks to the Junction Gap Breakdown procedure. From an electrical investigation of the devices fabricated with this strategy, we observed an ion current rectification characteristic and analyzing the electro-kinetic transport properties we observed that, in few minutes, intra-funnel accumulation occurs, and this phenomenon results in being stronger for low ionic strength solutions.

Combining intra-funnel accumulation of biomolecules, governed by electro-hydrokinetic phenomena, that occurs applying high voltage across the device, and an appropriate functionalization of nanochannel polymeric surface with antibodies, it was possible to decrease sensing limit for the detection of one or several targeted antigens for clinical diagnostics. It was possible to identify through fluorescence optical microscopy and electrical measurements, the uptake of a specific antigen, diluted in solution (down to 1 pg/ml), to the nanochannel surface when functionalized with antibodies. So, in this condition, we successfully detected antigen-antibody binding on the nanostructure surface, a promising step for realizing a high-sensitivity nanofluidic immuno-assay sensor.

Successively, I have developed other nanofluidic devices equipped with symmetric nanostructures for single-particle sensing. These devices were made using h-PDMS (hard- PDMS) in order to confer higher rigidity to the nanostructures, i.e. the functional part of the device, avoiding collapse problems. H-PDMS was used in exploiting a “focused drop-casting” approach in order to make only the nanostructure region stiffer,

while leaving the other regions of the device flexible enough to avoid the formation of cracks along the device. Combining the nanoscale dimension of the sensing gate with the Resistive Pulse Sensing (RPS) technique, it was possible to analyze single nanoparticles (NPs) and the motion of single λ-DNA molecules through the nanochannel as transient variations in ionic current during the translocation events, allowing a real-time, label-free and high-sensitivity detection. In particular, it was possible to demonstrate the possibility of counting nano-objects depending on selected characteristics (i.e. charge and size ranging from 40 nm to 100 nm) that is a crucial step, useful in many fields such as medicine (drug delivery, imaging, cell-secreted carriers), environment (groundwater remediation, nanoplastics detection) and food production (nano-agrochemicals, nano-encapsulated additives, anti-microbials).

SUMMARY

1. Nanotechnology

1.1 Introduction

Nowadays the term nanotechnology, introduced for the first time by Richard P. Feynman in 1959 during his lecture “There’s a plenty of room at the bottom” at the American Physical Society meeting [1] and definitively coined by Professor Norio Taniguchi in 1974 [2], it is usually used for describing a branch of technology, science and engineering carried on at the nanoscale. Nanoscale concerns structures having dimensions ranging from 1 to hundreds of nanometers at which fluctuations in the averaged properties (due to the motion and behavior of individual particles) begin to have significant effects on the system behavior and cannot be neglected. Nanotechnology is a very wide and interdisciplinary field, relevant in several research areas as chemistry, physics, biology, food, electronics, medicine and materials science. Scientists' tendency to focus on the nanoscale is because, on this nanoscopic scale, matter shows novel features and potentialities. For example, the ability to study and manipulate nano-sized materials has allowed a lot of possibilities in many industrial and scientific activities.

Currently, a large part of nanotechnology is widely exploited in the electronics, optics and fluidics fields to obtain ever smaller and more performing devices / systems useful for sensor applications.

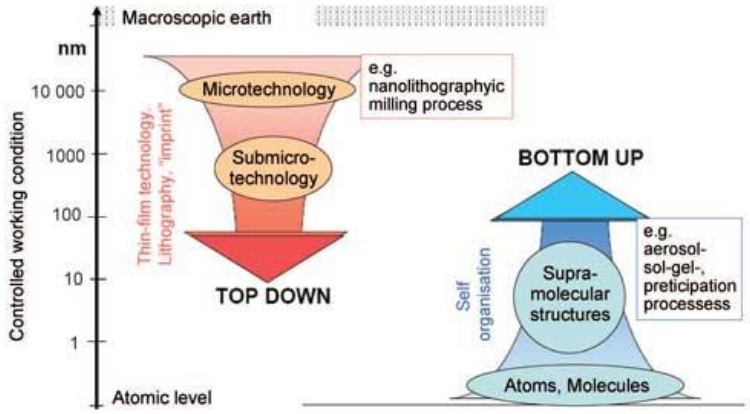

Fig.1.1 Methods of nanodevices production: top-down and bottom-up. (Image: Laboratory for Micro and Nanotechnology, Paul Scherrer Institut).

This kind of approach, schematically presented in Fig 1.1, is called “top-down” because starts from bulk material and subsequently uses finer and finer tools for creating smaller structures or devices that can have several functions such as:

- Extracting information from the system in which they are applied for investigation or control activities;

- Reducing to sub-micrometric and nanometric scale macroscopic functionalities with evident advantages;

- Getting new functionalities that do not exist at the macroscale.

However, it is possible to create nanostructure through “bottom-up” nanotechnology. This approach is based on the self-assembly properties of the matter. Self-assembly is

defined as the capability of small components of atomic or molecular dimensions to self-assemble together, according to a natural physical principle or an externally applied driving force, to give rise to larger and more organized systems, until the macroscale[3].

As disclosed before, nanotechnology is a very wide sector and here, in my PhD thesis, I focused on a nanotechnology section that regards the study and the development of nanofluidic devices for nano-biosensing applications that result useful in biomedical and environmental fields.

1.2 Nanofluidics and its properties

Nanotechnology and nanomaterials offer the opportunity to work with nanofluidics that is defined as the study of the behavior, manipulation and control of fluids that are confined into structures of almost one dimension ranging from 1 to 100 nm.

The general advantages of working at this scale are the use of less reagents, the possibility of parallel analysis, faster operation, and the possibility to develop new analytical tools allowing single molecule studies of objects such as biomolecules[4,5], DNA [6,7], and viruses[8–10] at a size-scale comparable to their intrinsic dimensions.

However, when a fluid is confined in a nanostructure the dominating forces and physics process involved tend to change because of the high surface-to-volume ratio. The influence of surface interactions into a nanofluidic device leads to transport phenomena that are impossible at larger length scales [11–13]. The transport of fluids and electrolytic solutions within micro and nanochannels can be controlled by applying a pressure difference or by applying an electrical potential across the nanofluidic system. The presence of an electric potential generates several electro-kinetic effects that can be exploited when using these structures as nano-biosensors. Among the most important effects that govern the transport of objects of interest at nanoscale there are: electric double layer, electrophoresis and electroosmosis.

1.2.1 Electric Double Layer

When a charged solid surface comes into contact with an electrolyte solution, a counterion layer builds in its proximal region.

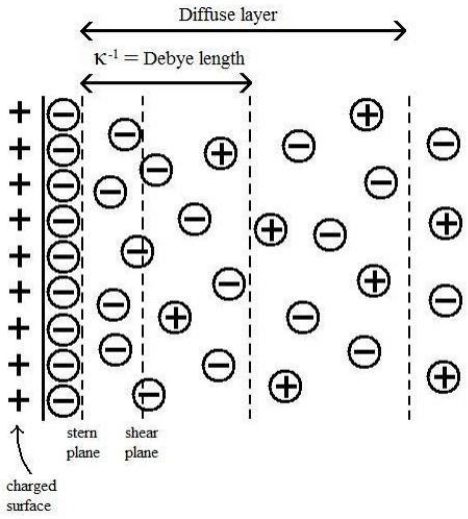

Fig.1.2 Scheme of Electric Double Layer formation and parameters that describe this phenomenon.

In particular, as it is possible to observe in Fig. 1.2 the counterions in the solution are attracted towards the charged surface while the co-ions are repelled. The resulting charge distribution, at the solid-liquid interface, is called Electric Double Layer (EDL) [14]. This condensed charge layer provides an electric shield against the surface charge, and when dealing with electric measurements, it is analogous to a capacitor.

The most common model, used to describe EDL, is the Gouy-Chapman-Stern (GCS) model [15]. It describes the EDL as composed by two layers: (i) a layer called “stern layer” that consists in ions bound at the solid surface due to the Coulomb interaction and (ii) a “diffuse layer” that is formed by mobile ions, next to the Stern layer, where ions follow the Boltzmann distribution until they are free to move as in the bulk solution. The virtual plane that separates the fixed ions from the mobile ones in solution, is named shear plane or slip surface. At this plane, no-slip fluid flow conditions can be considered, and the electric potential is named zeta potential. The electric potential decays exponentially in the diffuse layer, and the characteristic distance, called Debye length κ^{-1}, corresponds

to the EDL thickness that can vary with the surface charge and with the ionic strength of the solution. It is defined as:

$$\kappa^{-1} = \left(\frac{\varepsilon_r \varepsilon_0 k_B T}{2\, C_\infty e\, N_A}\right)^{1/2} \qquad (1.1)$$

where ε_0 is the permittivity of vacuum, ε_r is the relative permittivity of water, k_B is the Boltzmann constant, C_∞ is the bulk concentration of the electrolyte, T the temperature of the fluid, e the electron charge and N_A the Avogadro's number [16].

Typically, the Debye length ranges from one-tenth of nanometer at high ionic strengths to hundreds of nanometers. Many of the characteristic properties of nanofluidic structures arise because when the EDL could has a size comparable to the nanochannels that are the functional part of the nanofluidic devices.

1.2.2 Electroosmosis

The electro-osmotic flow consists in the movement of a fluid through a membrane, a micro / nanochannel, a porous material or other similar structures [17].

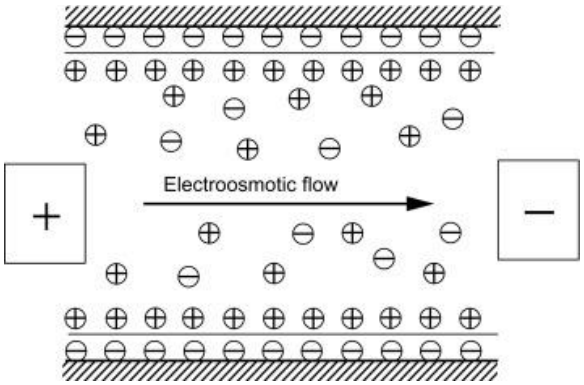

Fig.1.3 Scheme of electroosmotic flux within nanochannels.

The electroosmotic flow is due to the Coulombian forces acting on the mobile charged particles in solution. As shown in Fig. 1.3 when a charged solid surface is immersed in a

fluid EDL formation occurs and when an electric field is applied, the mobile part of EDL (diffuse layer) is set in motion because of the Coulombian forces. The resulting liquid movement is called "electrosmotic flow" (EOF) [18]. For example, if the surface of the nanostructure has a negative charge the positive mobile charges present in the diffuse layer will move towards the cathode. The mathematical representation of EOF velocity is:

$$v_{EOF} = \frac{-\zeta \varepsilon_r E}{\eta} \qquad (1.2)$$

and the EOF mobility is defined as:

$$\mu_{EOF} = \frac{v_{EOF}}{E} = \frac{-\zeta \varepsilon_r}{\eta} \qquad (1.3)$$

This means that the EOF mobility depends on the charge of the solid surface, viscosity, ionic strength and pH of the electrolytic solution.

1.2.3 Electrophoresis

Electrophoresis is another important electro-kinetic effect that occurs when an electric field is applied across a nanofluidic device. Electrophoresis differs from electroosmosis because, in the latter, it is the liquid that moves respect to a solid body when an electric field is applied, while in electrophoresis it is the particle, present in solution, that moves in relation to the liquid under the electric field influence [16].
Electrophoresis is the basis of numerous analytical techniques, used to separate molecules based on their shape, or their charge [19].

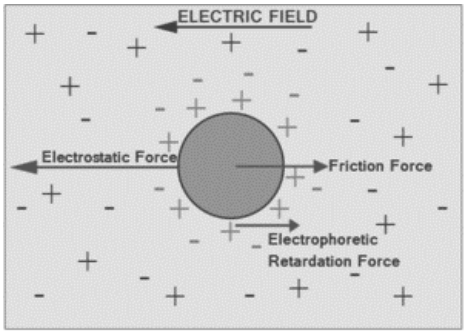

Fig. 1.4 Scheme of electrophoretic phenomenon.

The electrophoresis movement is schematically shown in Fig. 1.4 and is mathematically described by the Smoluchowski theory [20] that relates the electrophoretic mobility μ_e with particles characteristics and fluid parameters as follow:

$$\mu_e = \frac{\varepsilon_r \varepsilon_0 \zeta}{\eta} \qquad (1.4)$$

where ε_r is the relative dielectric constant, ε_0 the vacuum permittivity, η the dynamic viscosity of the fluid and ζ is the particle zeta potential.

This relation does not take into account the Debye length effect even if it plays a fundamental role. In fact, in the standard theory for electrophoresis, a particle's electrophoretic mobility is due to (i) the electrostatic force acting on the bare charge of the particle, (ii) the hydrodynamic friction force at the particle-liquid interface and (iii) a retardation force that is caused by the presence of a EDL around the particle.

When the EDL increases, the retardation force also tends to increase and when EDL becomes bigger than particle radius the electrophoretic mobility is not well described by Smoluchowski theory but it is possible to describe this parameter through the Huckel model [21] that relates the electrophoretic mobility as follow:

$$\mu_e = \frac{2\varepsilon_r \varepsilon_0 \zeta}{3\eta} \qquad (1.5)$$

1.3 Lab-on-chip devices

The understanding of fluid motion at nanoscale is at the base of the development of more complex nanofluidic platforms called Lab on Chip devices. Lab on chip (LOC) is a term that indicates a device that integrates multiple functions conventionally conducted in standard laboratories and facilities. In other words, it is possible to define LOC devices as miniaturized laboratories built on small and portable chips able to make sequences of laboratory processes to do specific analysis.

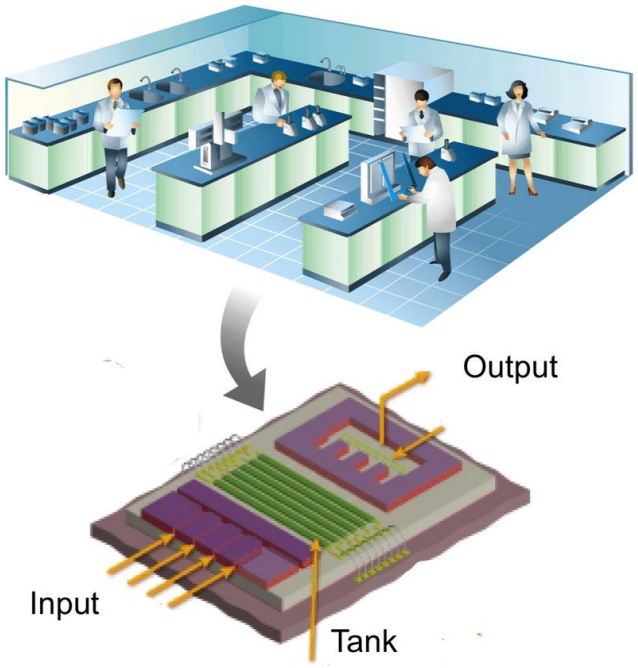

Fig. 1.5 Schematic representation of integration of laboratory process in a LOC device (Image: Hugo Salmon. Medical Physics, Université Paris)

As shown in Fig 1.5 a LOC device is composed by a network of micro- and nanochannels, electrodes, sensors, and electrical circuits and applying electric fields, or other driving forces, along the device, it is possible to control the liquid flow and make other operations that allow to analyze the liquid sample inside the chip. This means that the

understanding of electrokinetic-driven liquid flow in micro- and nanochannels is fundamental for designing and controlling lab-on-a-chip (LOC) devices. In fact, as disclosed before, all solid-liquid (aqueous solutions) interfaces “carry” electrostatic charge that means the increase of EDL at the interface on the liquid side which in turn is responsible of electroosmosis and electrophoresis [22].

The use of LOCs provide several advantages compared to common laboratories such as:

- Low sample volume required;
- Low fabrication costs;
- Faster analysis time thanks to the short diffusion distances and high surface to volume ratio;
- Good process control because of the faster response of the system;
- Compactness and parallelization allowing high-throughput analysis.

These enormous advantages help make LOC technology a good candidate for improving global health, for example through the installation of Point of Care (POC) in remote areas of the world. So, the main goal is to create nanofluidic platforms that allow to perform in poorly equipped clinics specific diagnostic tests without laboratory support [23].

2. Fabrication of nanofluidic devices

The majority of nanofluidic devices are made of solid-state materials, such as silicon, silicon oxide or quartz suitably machined. Among the most popular machining techniques are Focused Ion Beam (FIB) and Electron Beam Lithography (EBL).
These techniques result in being convenient because they allow obtaining stable nanostructures, which are the functional part of nanofluidic devices, with high precision and resolution. But, on the other hand, they present several drawbacks including high production costs and time-consuming character.

Therefore, for limiting these negative aspects, a promising manufacturing option is offered by soft-lithography methods that consist in the replication of a mold by using, as principal compounds, elastomers and allowing a great reduction of production costs. The most famous soft-lithography technique is called Replica Molding (REM).

2.1 Electron Beam Lithography

Electron Beam Lithography (EBL) is a technique derived from the development of electron microscopy that consists in the emission and scanning of a focused electron beam on the surface of the sample covered with a sensitive resist.

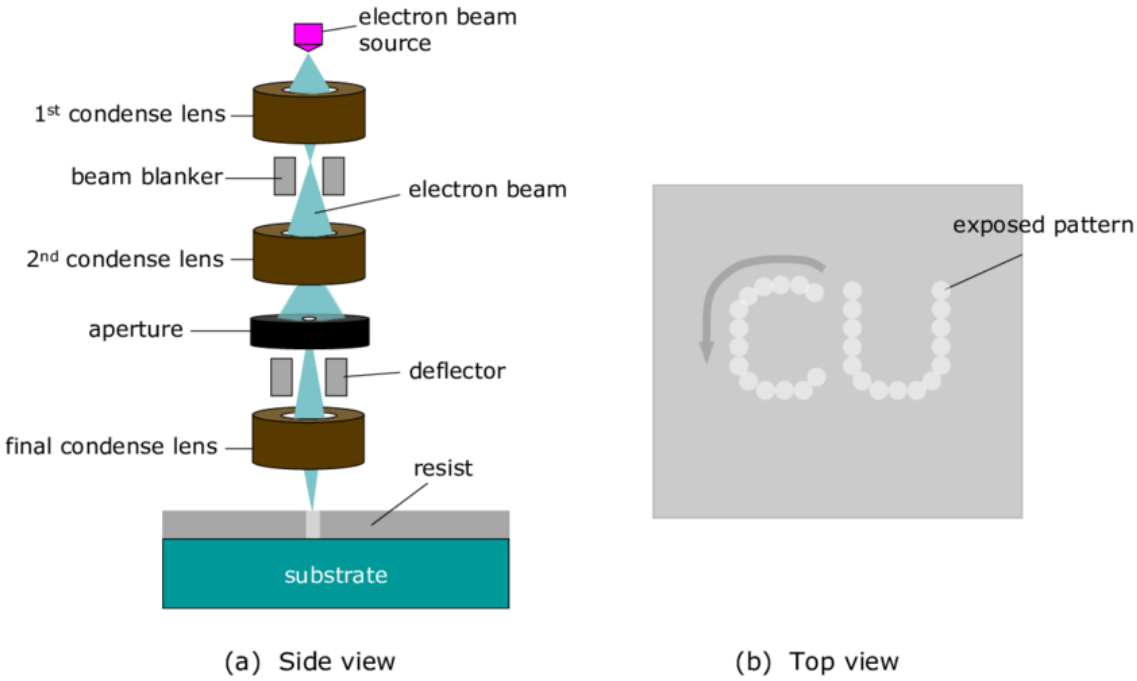

Fig. 2.1. (a) Working principle of EBL and (b) an example of machining.

When electrons, with high energy, interact with the positive resist, an increase of its solubility occurs allowing the selective removal of the exposed regions. As a typical 30 KeV electron beam have a much smaller wavelength than UV light, which is used in convectional photolithography, structures around 10 nm, or even smaller, can be created with EBL. So, with EBL it is possible to fabricate complicated micro/nanofluidic patterns, even if EBL is not a suitable tool for mass production of nanofluidic devices because of its relatively high cost and low scanning speed [24,25].

2.2 Focused Ion Beam Technique

Focused Ion beam (FIB) technique is used in several fields such as material science, biology and semiconductor industry for its capabilities of analysis, implementation and ablation of samples. Its structure is similar to an electron microscope; in fact, it is composed by a column in which ions can be accelerated and focused onto the sample.

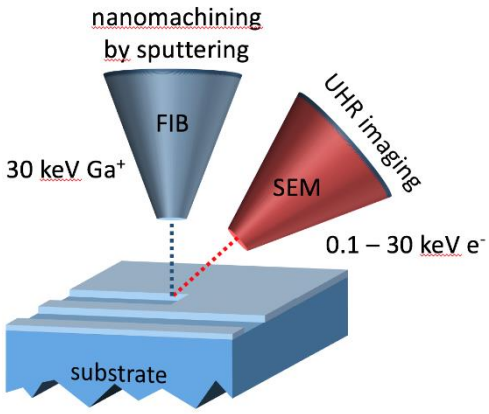

Fig. 2.2 Scheme of FIB milling procedure.

Generally, as shown in Fig 2.2 FIB is incorporated in a system with both electron and ion beam columns, allowing the same feature to be investigated using both beams.

In the field of nanofabrication, FIB milling has attracted the attention of many researches because it is able to manufacture nanopatterns directly without the use of photo resist or electrons. Comparing it to EBL it has significant advantages in terms of sensitivity, backscattering and proximity effects [26].

FIB milling principle consists in the setting up of a gallium ions beam with a size, current and energy able to cause a collision cascade providing target atoms with enough energy to overcome the surface binding allowing to pattern the sample surface. In this way, it is possible to fabricate nanostructure with high precision and resolution. In fact, it is possible to successfully fabricate nanochannel with at least one dimension close to tens nanometers [27,28].

Definitively, the FIB technique results a crucial technique for the fabrication of nanofluidic devices even if it remains a high-cost technique [24].

2.3 Soft-lithography: the use of PDMS

Soft lithography includes a set of patterning methods that utilize elastomeric compounds for fabricating nanofluidic devices. As stated before, the principal advantage of this method is not only a relatively low cost, easy setup, and high throughput, but also a pattern resolution that can range from nanometer to micrometer precision.
Soft lithography needs to utilize FIB or EBL technique to fabricate the initial stamp. This step needs only to be done once because with soft lithography it is possible to replicate the stamp hundreds of time decreasing fabrication costs [29]. In soft lithography, the most used elastomeric material is polydimethylsiloxane (PDMS), a polymeric compound characterized by viscoelastic properties and weak intermolecular force that gives it a rubbery behavior.

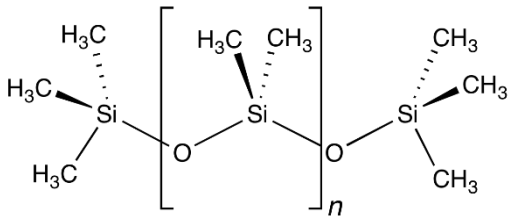

Fig. 2.3 PDMS Monomer chemical structures.

Fig. 2.3 shows the chemical structure of PDMS which consists of a repetition of $[SiO(CH_3)_2]$ units. In the field of nanofluidic this polymer results to be widely exploited for the fabrication of devices thanks to several useful properties, that make it suitable for biomedical applications, such as:

- Young's modulus of approximatively 2-3 MPa
- Optical transparency and low autofluorescence;
- Thermal stability up to 200°C;
- Chemical modification of its surface with different molecules;

- Low cost;
- Low toxicity;
- Good biocompatibility and biodurability.

Thus, thanks to these advantages, regarding costs, simplicity of fabrication techniques, versatility and biocompatibility, the use of PDMS results crucial for the production of different miniaturized nanofluidic devices [30].

2.3.1 Replica Molding (REM) technique

Replica Molding is a technique that allows obtaining surface patterns with dimensional characteristics lower than 100 nanometers without requiring, as in other protocols, the use of specific equipment.

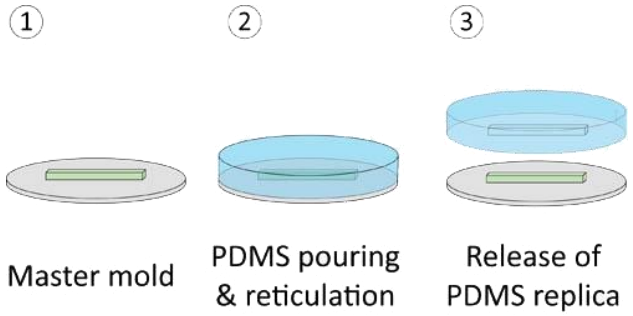

Fig. 2.4 PDMS replica molding procedure.

Fig 2.4 shows the REM procedure schematically. A liquid PDMS prepolymer is poured on the original master whose surface is pre-patterned with nanometeric structures, made by using advanced lithographic techniques such as FIB or EBL. The initial master can be made of SiO_2, Si_3N_4, metals, or photoresists. After curing, PDMS is carefully peeled-off from the mold producing polymeric nanostructures that are the same of those on the surface of the original master [31]. The replica molding process could be repeated once

or twice depending on the nanostructures patterned on the original master if they are in relief or etched.

3. Applications of nanofluidic devices

Nanofluidic devices offer powerful versatility in terms of shape and size, and the unique phenomena that occur in nano-confined conditions offer interesting opportunities for applications not easily achievable at the microscale. In particular, nanochannel is a powerful tool to investigate nanoscale physical and chemical phenomena such as ion concentration polarization, nonlinear electrokinetic flow and transport in confined regions in order to create bio- or nanosensors (able to separate, manipulate and detect single molecules) that result useful not only in biomedical but also environmental field.

3.1 Biomedical Field

In the biomedical field, biosensors are used for collecting information deriving from the interaction between biomolecules and the surrounding environment. The term “biosensor” appeared after shortening the term “bioselective sensor” proposed by Rechnitz in 1977 [32] for an arginine-selective electrode that used living organisms as sensing elements that now is widely used for self-monitoring of glucose or for pregnancy tests. However, there is still need for the development of cheap and ultrasensitive

biosensing platforms with the aim of detecting multiple analytes and of overcoming the problems that afflict traditional biosensors. In this context, the use of nanofluidic platforms as biosensors offer a lot of advantages such as (i) the reduction of the sample volume, (ii) the possibility of integrating of several laboratory functions into a unique miniaturized chip and (iii) high sensitivity, up to single molecule level, thanks to the characteristic dimension of their functional part closer to intrinsic dimensions of biomolecules to be analyzed. The possibility of manipulating biological objects such as viruses, nucleic acids or proteins in a liquid medium allowed the development of nanodevices for electrophoretic analysis for detection/separation of biomolecules, biomolecules concentration, immunoassay analysis, and single molecule sensing.

3.1.1 Biomolecules separation and transport

Nanofluidic platforms are often used for biomolecular separation. The most common molecules that are separated taking advantage of nanostructures are DNA and proteins. The separation mechanism are based on several different phenomena including steric, hydrodynamic, electrical and entropic [33].

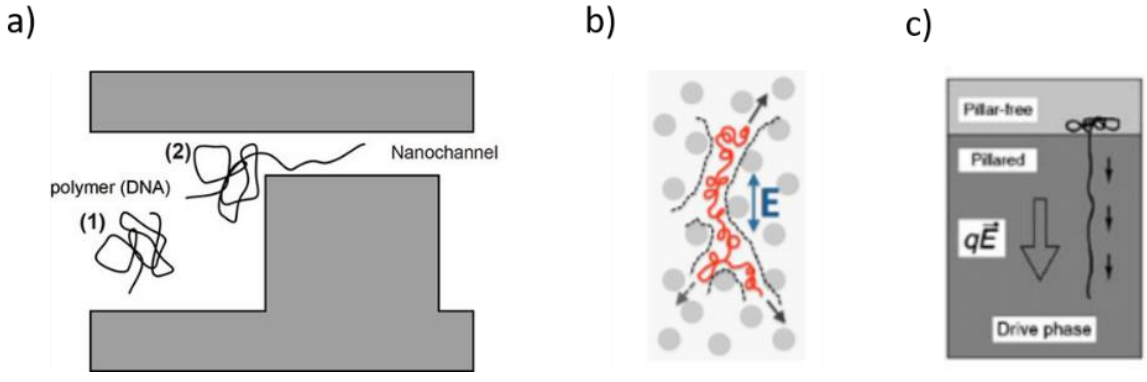

Fig. 3.1 Scheme of biomolecules analysis through nanofluidic devices. a) DNA conformational change analysis by entropic trapping methods b) DNA reptation along nanostructures and c) DNA separation exploiting electrophoretic effect.

Typically, DNA separation, that exploits conformational changes in biomolecules induced by steric interactions (Fig. 3.1) with the channel walls, results crucial for genome sequencing, biometric fingerprinting and identification of pathogens and genetic diseases. Applying an electric field it is possible to induce DNA motion or reptation, between obstacles, along nanochannels in a controllable manner achieving a DNA length-based separation that results extremely short in time in comparison with traditional gel electrophoresis [34,35].

Moreover, it is possible to obtain DNA separation exploiting entropic effects (Fig 3.1) thanks to the possibility of shaping a nanochannel to be an alternating sequence of shallow-deep wells that must have a depth smaller than DNA gyration radius. When the DNA molecules are electrokinetically driven inside that structure they are trapped at the wells' entrance and, in particular, longer molecules have a higher escape rate from the traps due to the larger surface area in contact with the boundary that corresponds to a higher probability of escaping from the wells. This means that is possible to differentiate DNA molecules depending on length [36,37].

Also the electrokinetic transport and separation of ionic species in nanofluidic channels result in a fast, selective and effective technique. The principle of electric separation exploits the EDL thickness inside the nanochannels that, in particular conditions, is of the same order of the characteristic channel dimensions that leads to non-uniform velocity profiles and strong electric fields transverse to the flow. These effects are shown as a good method to achieve the separation of small biomolecules and short strands of DNA in a gel-free environment (Fig 3.1)[38,39].

All these separation mechanisms are not only limited to DNA but recent studies have shown that it is possible to work more generally with proteins [40–42] but unfortunately proteins have the drawback of being prone be absorbed by the nanochannel walls [43,44].

Besides that protein transport and separation experiments there are the realization of a nanofluidic biosensor able to (i) monitor the binding affinity of two proteins, (ii) to

study the diffusion kinetics of biomolecules under nanoconfinement, and showed that such confinement leads to a deviation from Fick's law and (iii) allow label-free electrical detection of biomolecule binding reactions [33].

Typically, nanofluidic devices require small amounts of sample that is typically highly diluted, so the need of a pre-concentration mechanism of analytes results crucial.

3.1.2 Biomolecules concentration

One of the main challenges of nanofluidic-based biosensors is detecting extremely dilute analytes in solution. A simple strategy consists in being able to concentrate the analytes in a particular area of the device.

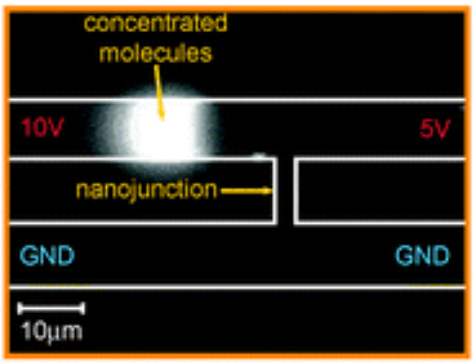

Fig. 3.2 Biomolecules concentration effect under electric field application.

For example, it is possible to insert a polyester membrane composed of nanometric structures and since, for this kind of device , concentration is a mechanism of charge entrapment, among the molecules that are electrokinetically guided through the channel, those that have opposite charge from the inner walls of the nanostructures cannot pass the membrane starting to accumulate and concentrate in a certain area as shown in Fig. 3.2 [45,46].

Another exciting feature of nanofluidic devices is the fact that various analytes can be concentrated together, as long as they have the same charge, since it is found that

electrophoretic mobility has a negligible effect on the concentration factor. In this way, the device can potentially be used also as a microreactor [38].

Another mechanism of preconcentration is based on electrokinetic trapping. Here, the device is generally composed of two microchannels connected to each other by a nanochannel and applying appropriate external voltages, the coupling between the electric fields is able to create a region of space charge at the micro/nano interface where the biomolecules are collected and trapped [48].

In all these cases, this phenomenon involves very high concentration factors, ranging from 10^6 to 10^8 [33].

3.1.3 Immunoassay analysis

Immunoassays are biochemical test that detects particular analyte exploiting the antigen-antibody reaction. This analysis usually involves (i) measurement that must be performed at very low concentrations (ii) low molecular weight drugs and (iii) biomolecules of pharmaceutical interest or biomarkers, in order to indicate disease diagnosis. The importance of immunoassay analysis in biomedical fields is attributed to their intrinsic specificity, high-throughput, and high sensitivity for the analysis of a wide range of analytes and when these immunoanalytical reagents are mixed and incubated, the analyte binds to the antibody forming an immune complex. Analysis is achieved by measuring the label activity (e.g. radiation, fluorescence, or enzyme) of the bound part [49].

The use of nanofluidic devices allows increasing the efficiency of immunological assays. In particular, by adequately functionalizing the nanostructured part of the device and exploiting the concentration phenomenon that can occur within the nanochannel, it is possible to increase the efficiency of the antigen-antibody reaction by managing to detect extremely diluted amounts of analytes in solution with the aim of being able to get an early diagnosis [46].

3.1.4 Single-molecule sensing

Nanofluidic devices are also fundamental for the detection of single molecules thanks to the fact that they have dimensions comparable to the molecules of interest. It is possible to detect single molecules both with optical and with electrical methods. For example, for a label-free detection, electrical methods are used, i.e. in a nanochannel that connects two fluidic cells on each side, it is set by applying an electrical polarization and the current is monitored.

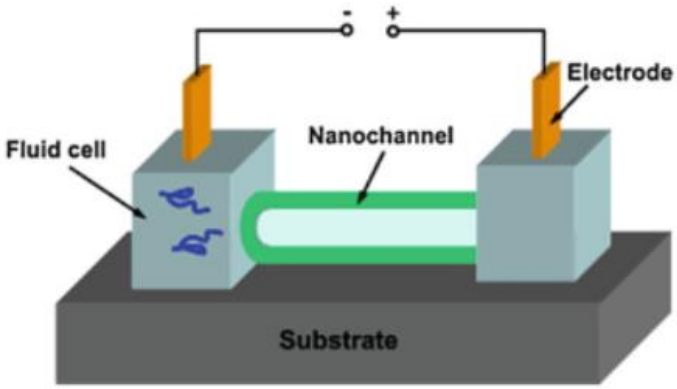

Fig. 3.3 Scheme of nanofluidic platform for electric single-molecule sensing [50].

Fig.3.3 shows a schematic diagram of nanofluidic systems that electrically detect single molecules and this mechanism was first implemented in pioneering work on single DNA detection using a natural nanopore, an α-hemolysin, that has 10 nm of length and inner diameter of about 1.4 nm[51]. The working principle of label-free detection of single molecules is based on the variation of ionic current that is generated when a molecule crosses a nanostructure. Specifically, when the molecule crosses a nanochannel it generates an obstruction and therefore a consequent increase in the measured resistance which is reflected in a sudden reduction of the monitored current. From this reduction, it is then possible to obtain different information regarding the molecule as charge and size[6,50].

Even single-molecule detection on nanofluidic devices coupled with scanning microscopy or optical microscopy, is an excellent method to obtain information, with a high resolution, regarding structure, composition and other properties that are not easily accessible in bulk solutions. Exploiting the fluorescence of the molecules, which are usually introduced into nanochannels through the phenomenon of electrophoresis, is possible to perform specific analysis.

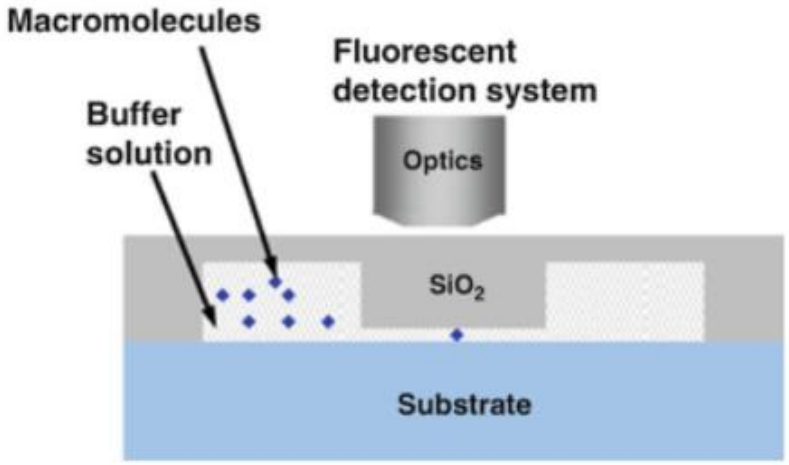

Fig. 3.4 Scheme of nanofluidic platform for optical single-molecule sensing [50].

Fig. 3.4 shows a schematic diagram of nanofluidic systems that allow detecting single molecules through optical methods.

Among the main advantages of using nanofluidic devices coupled with optical methods for single-molecule detection there are: (i) the increased probability of finding the molecule in the focal volume since the sample is confined to a nanometric space, (ii) the increase of the residence time of the molecule in the focal volume since the diffusion coefficient in the nanochannels greatly decreases (iii) the aid to reduce the background noise of other molecules and impurities in the solution to obtain a higher signal-to-noise ratio indeed the noise is proportional to the size of the detection volume and (iv) the possibility of forcing long molecules, such as DNA, to unroll inside the nanochannels

allowing to distinguish the various molecules by length or to favor the counting of the number of proteins anchored to the strand of DNA [50,52,53].

3.2 Environmental Field

Monitoring the compounds that represent a risk for the environment and consequently also for human and animal health is an essential part of the efforts made by the scientific community and nanofluidic devices are an excellent tool. In fact, nanofluidic devices can be exploited in this field for several applications like detection of pollutants, heavy metals, contaminants and nanoplastics. The main advantages of using nanofluidic devices are (i) ease of handling, (ii) economic manufacturing, (iii) ease of disposal after use, but above all (iv) the possibility of performing in-situ and real-time analysis using quantities of extremely small samples and allowing, for example, a much better control on contaminants such as nanoplastics and heavy metals present in aqueous samples [54].

3.2.1 Nanoplastics detection

The huge production, use and subsequent disposal of plastics have caused over the years a big environmental problem. In fact, nowadays, plastic represents more than 80% of marine litter causing extensive damage to marine ecosystems.

The main problem is that plastic is a long-lasting pollutant because it is resistant to natural biodegradation processes, in other words the microbes that breakdown other substances do not recognize plastic as food and generally the plastic fate is to be fragmented by light in smaller and smaller debris over time reducing to nanoscale [55,56].

These small debris can enter the food chain, through the contamination of aquatic organisms, causing important consequences. For example, many studies [57–60] show that they can permeate through the lipid membrane and affect the cellular function. In

particular, carboxylated nano-polystyrene particles ranging from 40 nm to 50 nm can enter cells irreversibly. They can also accumulate in the liver, the lungs, the gastrointestinal tract and in the lymphatic system inducing alteration of the oxidative stress, of energy and lipid metabolism causing inflammation response and neurotoxic effects [61].

Hence the importance of detecting, characterizing and quantifying the presence of nanoplastics in aqueous solutions.

4. Materials and Methods

In this section, I will illustrate the main materials and methods used for the study and characterization of nanofluidic devices.

In particular, we will see how the devices were manufactured and characterized by means of atomic force microscopy, optical microscopy and electrical measurements. The technique of the “junction gap breakdown” will be described in detail. Finally, the strategies used for accumulation, functionalization and sensing, exploited for testing the performance of these devices as biosensors, will be reported.

4.1 Fabrication of Nanofluidic devices

The devices were made entirely of polydimethylsiloxane by replicating the micro and nanofeatures patterned on a silicon substrate through micromachining and FIB milling techniques.

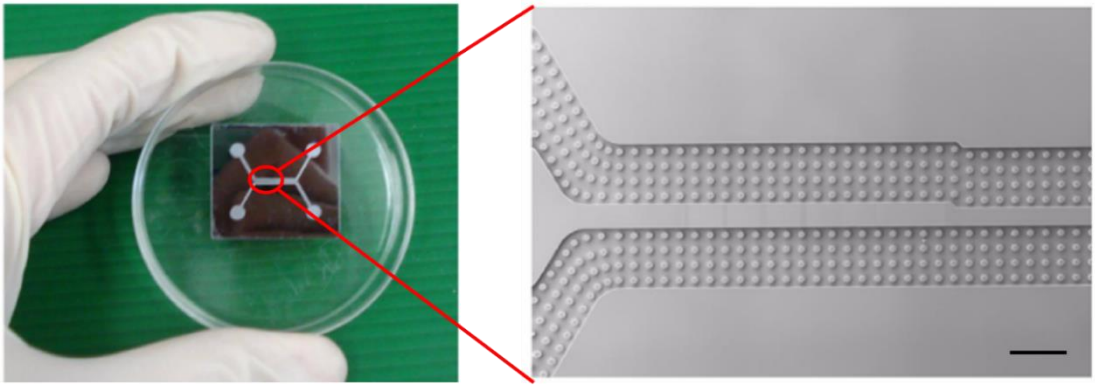

Fig. 4.1 Micropatterned silicon substrate and its SEM microscope image. Scale bar 500 µm.

As shown in Fig. 4.1, the silicon substrate is firstly micromachined by standard lithographic techniques in order to pattern four reservoirs and two U-shaped microchannels, 50 µm high and 500 µm wide. These latter are separated by a minimum gap of 100 µm where functional nanostructures are patterned.

Microstructures are equipped with cylindrical pillars, arranged along all the microchannels in order to sustain the channels avoiding the polymeric replica collapse. Pillars are 50 µm high and have a diameter of 50 µm.

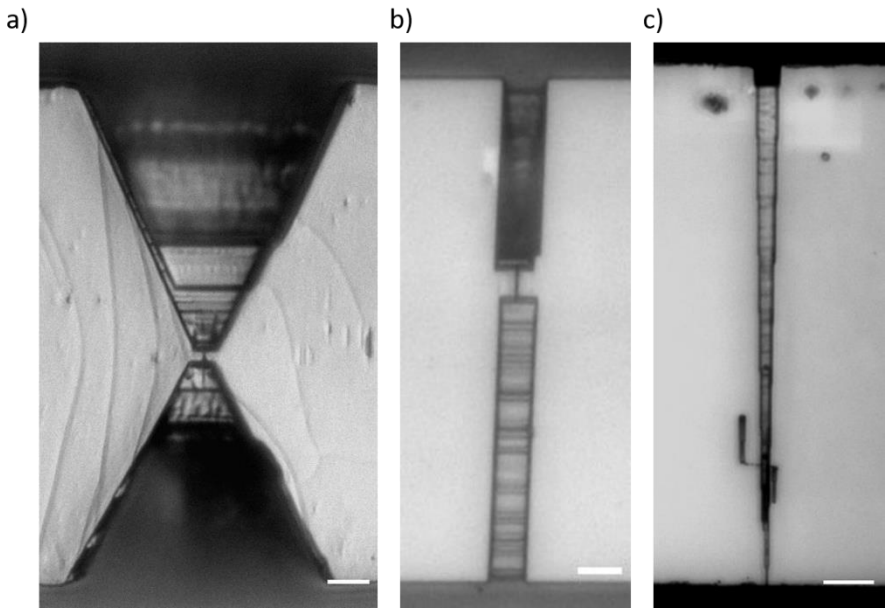

Fig. 4.2 a) Symmetric nanochannel with an hourglass shape b) Symmetric structure with rectangular access regions and c) Nanochannel with a funnel-shape access region. Scale bar 10 µm.

As shown in Fig. 4.2 three different types of structures are patterned, along the gap between microchannels, using a CrossBeam @workstation 1540XB model (Zeiss) that combines an ultra-high-resolution scanning electron microscope (UHR-SEM) with a Focused Ion Beam (FIB).

For the first nanostructure (Fig 4.2 a) FIB was used to fabricate two trapezoidal excavations having 114 µm of larger base, 6.5 µm of smaller base and 45 µm height while the depth flagged gradually from 20 µm to 2 µm. These excavations allowed to reduce the gap between the two microchannels and to create a short nanochannel of 2 µm of length, 500 nm of width and 90 nm of depth. The nanostructures in Fig. 4.2 b was fabricated with the same strategy, but with rectangular access regions and a nanochannel bigger in dimensions than the other one (i.e. length 6 µm, width 300 nm and depth 800 nm).

The third nanostructure (Fig. 4.2 c) has an asymmetrical funnel-shaped geometry and is equipped with a nanometric tip that has a length of 8 µm, a width of 500 nm and a depth

of 90 nm. These structures constitute the only fluidic connection between the two U-shaped microchannels.

The silicon masters, suitably designed and fabricated, are then used as a mold allowing to obtain a series of high-fidelity replicas using the double replica molding process.

4.1.1 Soft Lithography: Double Replica Molding

Double REplica Molding (REM) is a soft lithography procedure that exploits elastomeric compound to replicate an initial silicon mold [62,63].

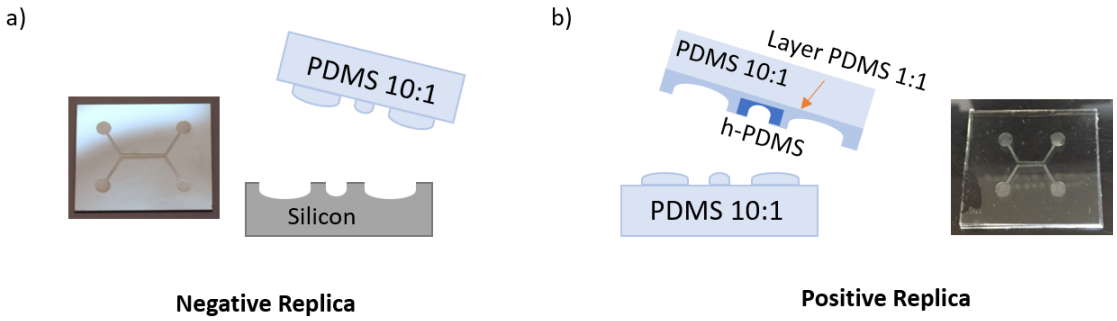

Fig. 4.3 Scheme of Double Replica Molding procedure. a) Negative replica step b) Positive replica step

As shown in Fig 4.3 double REM process is divided into two principal steps. The first step, called Negative Replica, consists in a degassed mixture (prepolymer and curing agent w/w ratio) of standard PDMS (DOWSIL™ 184 Silicone Elastomer Kit) that was poured on the silicon master and, after 4 hours of curing at 65 °C in oven, the cross-linked polymer is peeled-off from the mold. The resulting replica has the patterned structures in relief and must be used in turn as a "negative mold". In the second step, called Positive Replica, different formulations of the same polymer: standard (DOWSIL™ 184) PDMS 1:1 and PDMS 10:1 and in some cases also hard-PDMS (h-PDMS) were used. In this last

case, a drop of h-PDMS was deposited with a syringe on the region of the negative replica with the nanostructures. The volume of h-PDMS was opportunely sized to confine it only in that region. In the following sections, I refer to this method as “focused drop casting” procedure. After deposition, the drop was left curing for 30 minutes at 70 °C. After that, a layer of PDMS 1:1 was poured all over the negative replica, spun at 1000 rpm for 60 s (resulting in a layer around 50 µm thick) and cured for an hour at the same temperature. Then, a thick layer of standard PDMS 10:1 (about 5 mm) was deposited and left curing for 4 h at 70 °C. Finally, the positive replica was peeled off the mold and further incubated at 150 °C overnight to ensure complete cross-linking and for further hardening of the replica.

The obtained positive replica was drilled, in the reservoirs area, using a needle in order to have fluidic access for solutions.

4.1.2 h-PDMS

The conventional soft lithography allows to easily produce nanostructures of small dimensions down to about 500 nm. This means when using this methodology for replicating structures having at least a size below 100 nm, various problems, related to the reduced Young's modulus of the PDMS, may arise.

In fact, nanostructures tend to collapse on themselves [64], and this process result to be irreversible if the elastic energy due to the deformation of the structures is less than the energy gained by the system thanks to the decrease in surface area. This often makes the samples unusable.

This means that the mechanical properties of the elastomers used in soft lithography represent a critical aspect.

For this reason, h-PDMS represents a good compromise for its use in soft lithography. In fact, it is an elastomeric compound similar to the standard PDMS but with a Young's modulus between 8 and 12 MPa a value significantly higher than standard PDMS (2-3 MPa) [65].

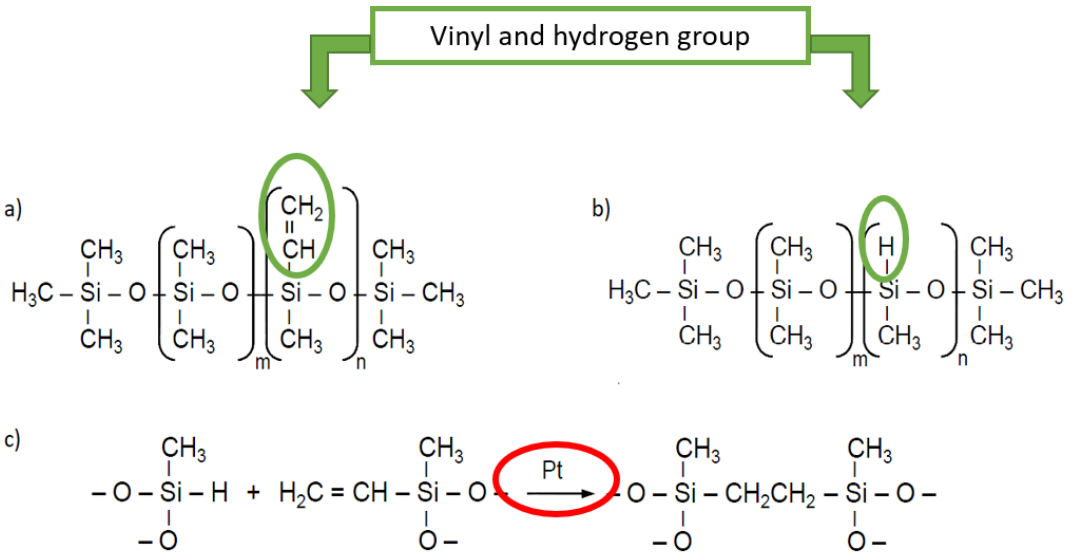

Fig. 4.4 a) Dimethylsiloxane with part of the methyl groups replaced with vinyl groups. (b) Dimethylsiloxane with part of the methyl groups replaced with a hydrogen. (c) Reaction with a platinum catalyst between the hydrogen and the vinyl group of the two reagents, which leads to the formation of a silicon - ethyl - silicon bond between the two siloxane molecules.

In particular, h-PDMS is a two-component system of linear dimethylsiloxane molecules, which is cross-linked through the use of a platinum catalyst. The two components differ for the different functionalization of the molecules: part of the methyl groups is in fact replaced with a vinyl group or with hydrogen, and it is between these two groups that cross-linking takes place (Fig. 4.4).

Experimentally, h-PDMS was prepared by mixing four compounds: (i) 1.7 g of a vinyl PDMS prepolymer (VDT-731, Gelest Corp. USA), (ii) 4.5 µl of Pt-based catalyst (platinum divinyltetramethyldisiloxane, Gelest Corp.), (iii) 0.05 g of modulator (1, 3, 5, 7 tetravinyl-1, 3, 5, 7 tetramethyl cyclotetrasiloxane, Gelest Corp.) and (iv) 0.3 g of hydrosilane prepolymer (HMS-301 Gelest Corp.).

4.1.3 Silane treatment

Between each replica step, described before, it was necessary to perform a surface silanization treatment of both the silicon master and the negative mold. Silanizing the master is important to avoid the PDMS sticking to the master, to ease the peeling and to preserve the PDMS replica from damaging.

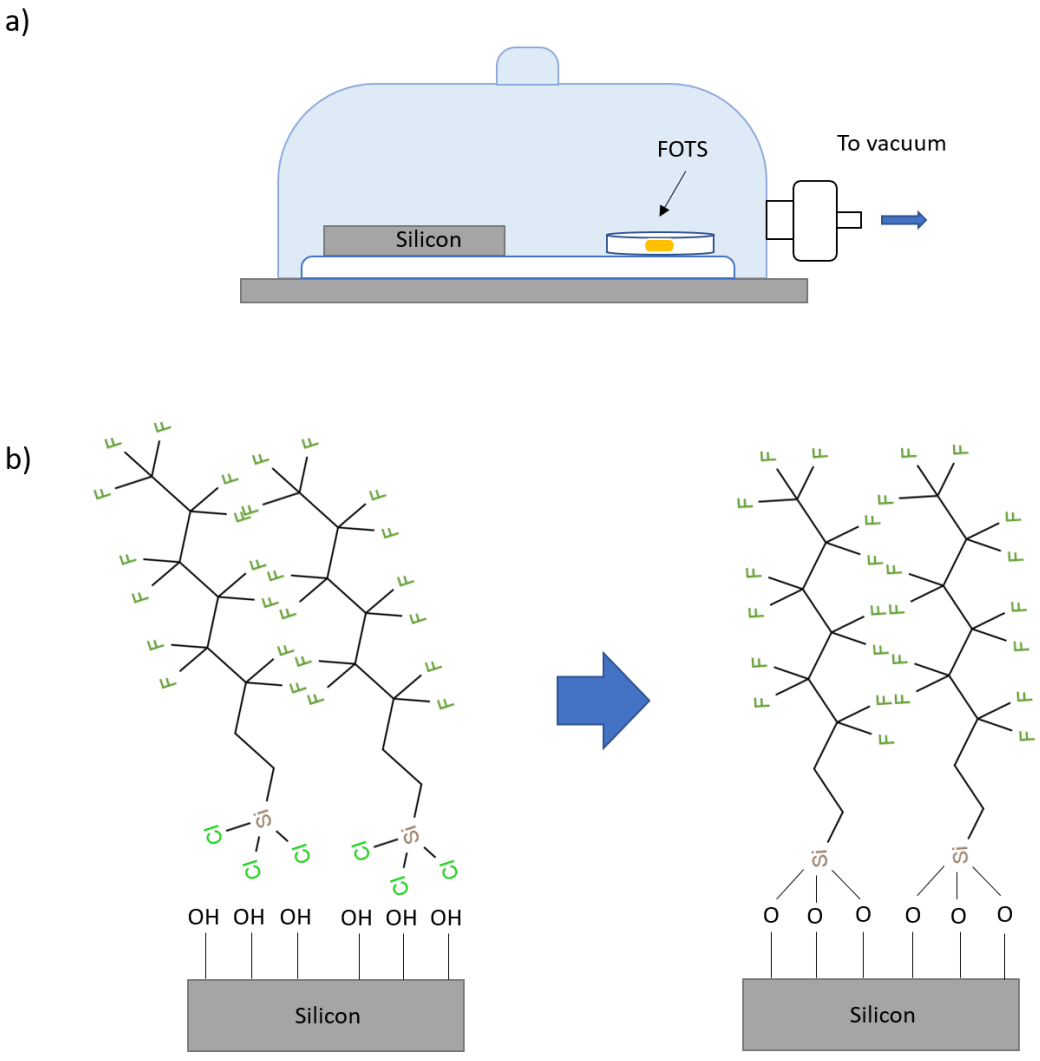

Fig. 4.5 a) Schematization of the FOTS silane treatment, b) chemical reaction that leads to the formation of a silane monolayer on silicon and/or PDMS surfaces.

As schematized in Fig 4.5, a drop (nearly 5 µl) of 1H,1H,2H,2H-perFluoroOctylTrichloroSilane (FOTS – Sigma Aldrich) is placed in a vial and inserted in a desiccator with the masters. The desiccator is placed under a vacuum for 5 minutes causing the silanizing agent to evaporate and form a monolayer on the surface of the master that prevents the PDMS sticking and bonding to the master's surface allowing a better replica release. To promote the formation of the silane monolayer it was necessary to expose the surface to an oxygen plasma for 30 s at 70 W.

4.1.4 Bonding Procedure

For obtaining a functional nanofluidic device, it was necessary to seal the PDMS replica with a glass coverslip. PDMS is quite hydrophobic with an overall non-reactive surface, making it difficult for it to bond with other surfaces. By exposing PDMS to an oxygen plasma, the PDMS surface becomes hydrophilic and reactive, promoting an irreversible bonding when it encounters glass, silicon, or another PDMS piece exposed to the same plasma process. This contact must be made immediately after the treatment because the PDMS surface tends to recover its hydrophobic state after a short time, preventing the sealing between the glass and the replica.

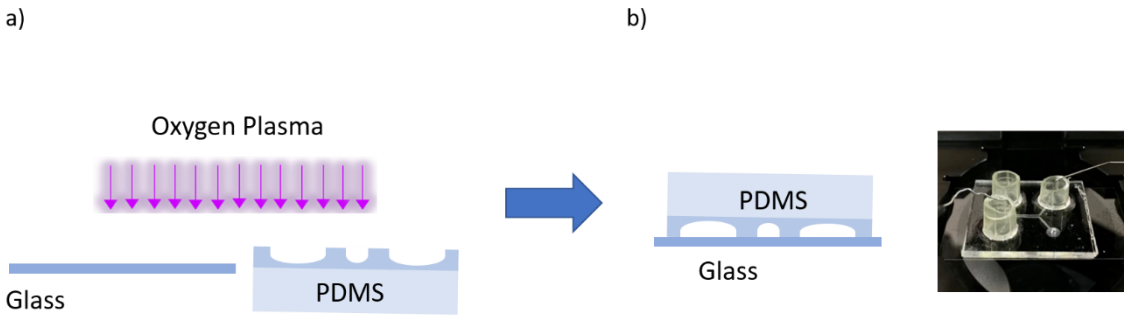

Fig. 4.6 a) Glass and PDMS replica under oxygen plasma exposition b) Bonding procedure contacting PDMS and glass and a picture of the final nanofluidic device.

As shown in Fig. 4.6, the polymeric replica and a glass coverslip were treated in oxygen plasma (Gambetti Tucano TUC-1B-MF) for 60 s at 50 W and then brought into conformal contact obtaining a sealed and water-tight nanofluidic device ready to be filled with sample solutions.

In particular, during the exposure to oxygen plasma the (-Si-CH_3) groups of the PDMS are converted into hydrophilic silanol (-Si-OH) groups.

This functional group can condense with the adjacent silanol to form a SiO_2 layer that increases the PDMS surface hydrophilicity and allow an irreversible bonding with the glass [66].

Before oxygen plasma treatment, PDMS replica was sonicated into a solution of milli-Q water and acetone (ratio w/w 4:1) for 10 minutes and the glass coverslip in a solution of ethanol for the same time in order to clean them and avoid residual of dust.

4.2 Atomic Force Microscopy (AFM) characterization

In order to estimate the size of the nanochannel after the sealing/bonding procedure, AFM measurements were performed on a cast obtained inserting a resin into a nanofluidic device closed with a silicon substrate with a conformational contact approach (i.e. without plasma oxygen treatment).

After curing, I peeled off the positive replica thus obtaining a cast that was successively imaged by AFM. This analysis provided information on the geometry and size of the nanochannels after the device closure.

The AFM measurements were performed in tapping mode by a Dimension 3100 microscope (Veeco Instruments, Plainview, USA) and an Olympus silicon nitride tip. The software WSxM [67] was used to process and analyze the images.

4.2.1 Cast fabrication

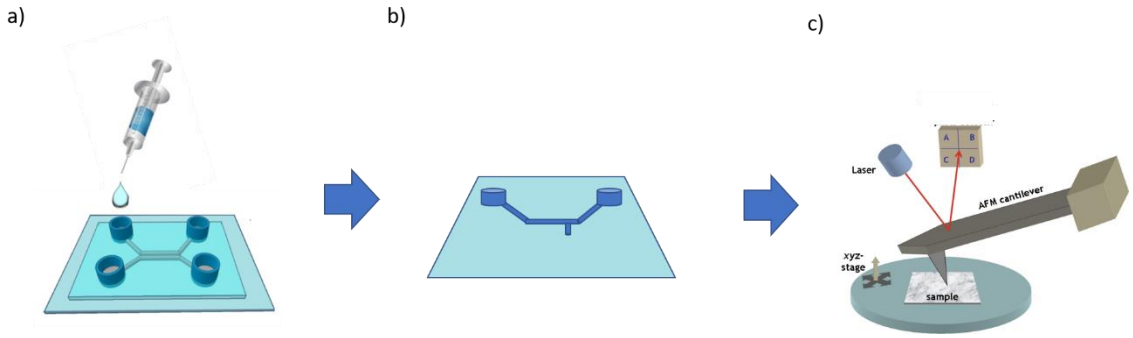

Fig. 4.7 a) Scheme of NOA resin insertion b) NOA cast after curing and positive replica peel-off and c) Schematic representation of AFM imaging.

The process for the realization of the cast is schematized in Fig 4.7. The resin 81 Norland Optical Adhesive (NOA) was used together with a silicon wafer and the positive replica.

The positive replica was placed in conformal contact with the silicon substrate and then the NOA resin diluted in acetone (1:1 v/v), was inserted in one of the two microchannels, let fill the nanochannel, and cured under UV irradiation for 2 hours with a Biolink lamp (UV lamp 365 nm -Vilber Lourmat). At this point, the replica was peeled-off and the cast was ready to be characterized by AFM.

4.3 Optical and Electrical characterization of the devices

Optical microscopy images of the devices were acquired during and after the fabrication with an Olympus BX51 microscope equipped with an F-View II camera controlled by CellB Software.

Then, the devices were electrically characterized in order to obtain an evaluation of the nanochannel resistance and of its electrical behavior. In particular, after filling the device with a solution of KCl 1 M solution, current–voltage (I–V) curves were acquired by using

an electronic amplifier (EPC 10 Usb, Heka Electronik, Multi-Channel Systems MCS GmbH, Reutlingen, Germany) connected to Ag/AgCl electrodes. All the electrical measurements were performed in a Faraday cage for minimizing the electrical noise from electromagnetic interference. The sampling rate was 10 kHz, and traces were filtered by a low-pass Bessel filter with cut-off at 2.9 kHz.

4.4 Junction gap breakdown

This kind of process was necessary to re-open the nanostructures of collapsed nanofluidic devices.

For the junction gap breakdown procedure, I used a Keithley 6487 sourcemeter connected to the device with two platinum (Pt) electrodes. An increasing voltage bias (up to a maximum value of 150 V) was applied, across the device filled with KCl 1 M while monitoring the ionic current.

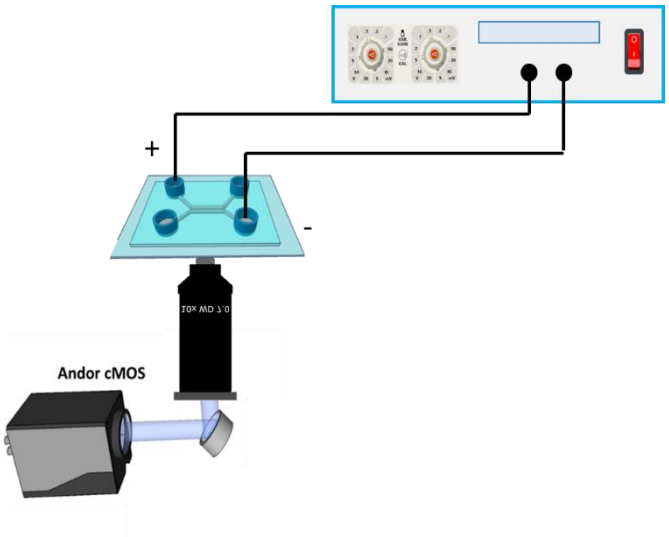

Fig. 4.8 Scheme of experimental set-up used for junction gap breakdown procedure

A schematic representation of the set-up used for the junction breakdown procedure is reported in Fig. 4.8. During the process the sourcemeter was controlled, through a GPIB

interface, by a computer and the current traces were acquired by using a custom-designed LabVIEW software.

During the junction gap breakdown procedure, dielectric breakdown occurs in correspondence to a sudden and steep increase in current, caused by an increment of the voltage applied to the structure.

There are different ways in which the breakdown can be detected during a Direct Current (DC) measurement:

1. A spike in the current draw;
2. A consequent decrease of the nanochannel resistance;
3. A visual change of the polymer material

Typically, the procedure led to the formation of a nanoporous network as a connection between microchannels.

4.5 Accumulation measurements

After the formation of the nanoporous network, by junction gap breakdown, the accumulation process of fluorescein diluted in 1 M, 100 mM, and 10 mM KCl solutions at pH 8 were monitored in order to characterize concentration capabilities into the nanochannel of nanofluidic device.

The solution, with the diluted fluorescent probe, was inserted inside one microchannel, while the other one was filled with a KCl solution of the same molarity.

For concentrating molecules inside the funnel, it was necessary to apply a constant voltage bias across the device. To do this, the same electrical apparatus used for the junction gap breakdown procedure was used. Simultaneously, the nanochannel was optically monitored by a Nikon Eclipse Ti inverted microscope, equipped with an Andor Zyla 5.5 camera (Imaging parameters: gain 1, exposure time 0.8 s, no binning). 60x λ-oil lens and a B-1E filter 540/20 nm were used for epifluorescence measurements.

4.6 Nanofluidic device's functionalization process

Chemically functionalizing a surface of a material means properly modify it through specific treatments. Functionalization can be performed on inorganic or organic materials or on a region of interest of a device, in order to create a biosensor able to recognize a specific bio-analyte or exploiting a transduction mechanism related to it.

Surface modification allows the material surface to recognize several biological molecules (i.e. proteins, antibodies or individual DNA chains) and, in particular, allows to bind biological species in a permanent way.

Generally, the functionalization processes are based on chemical reactions performed in liquid and/or vapor phases assisted by cold low-pressure plasma.

In our case, the PDMS surface has been functionalized using the antibody Antihuman anti-interleukin 10.

Concerning the immobilization of proteins, PDMS is hydrophobic in native form, therefore, proteins tend to bind quickly and in a non-specific way to the surface. So, a proper functionalization of the surface is necessary for immobilizing the proteins on the surface of the device and imparting it recognition capabilities.

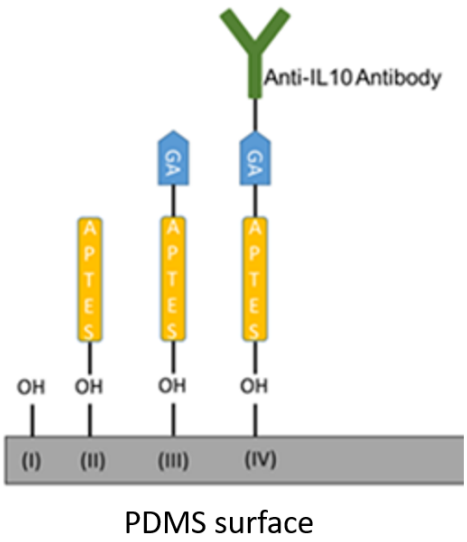

Fig. 4.9 Representation of PDMS surface functionalization with IL-10 antibodies.

Fig. 4.9 shows a scheme of the functionalization process that was performed as follows. The device was treated in an oxygen plasma for 10 minutes at 70 W, in order to obtain the exposition of hydroxyl (-OH) groups on the PDMS surface making it hydrophilic.
Then, the device was placed in vacuum chamber together with 5 µl of (3-aminopropyl) triethoxysilane (APTES – Sigma Aldrich) for 5 minutes. APTES treatment was necessary because APTES is a compound that can bind to the hydroxyl functional groups of PDMS at one end and possess an amine functional group on the other end to facilitate covalent linkage with proteins.
After the treatment with APTES, the microchannels were filled with a glutaraldehyde (GA – Sigma Aldrich) solution and placed on an agitator for 1 hour at 25°C in order to promote the diffusion of the solution. GA was used because it is a bi-functional linker that allow to covalently immobilize protein to the support.
Successively, microchannels were washed with PBS 1X solution for 5 times and subsequently with DI water for others 3 times for removing the excess part of the previous solutions used.

breakdown

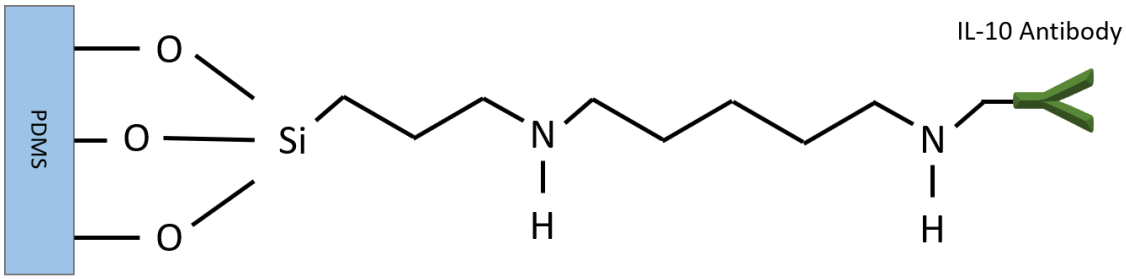

Fig. 4.10 Bonding of APTES with GA and antibodies on the PDMS surface.

Then, a solution of IL-10 antibodies (Mouse monoclonal Anti-Human Interleukin-10 - Invitrogen) in PBS, with a concentration of 6.25 ng/ml, was inserted in the microchannel linked with the nanochannel entrance, while a PBS 1X solution was inserted into the

other microchannel. The device, filled with these solutions, is placed on an agitator for 2 hours at 25 °C [68].

Fig. 4.10 shows the chemical bonding formation with this functionalization process. Microchannels were rewashed with PBS solution and then a Bovine Serum Albumin (BSA) solution (5% in weight in PBS) is injected in both the microchannels to “block” non-specific binding sites of PDMS surface.

The device was left, with BSA solution inserted, for 1 h on the agitator and then was washed with PBS and deionized water [69]. After this procedure, the device results to be conveniently functionalized and ready to be used.

4.6.1 FTIR-ATR measurements

Fourier Transform Infrared Spectroscopy (FTIR) was used to analyze the surface of the PDMS after the functionalization process and to be able to understand if the latter correctly occurs.

The working principle of this technique is based on the interaction between infrared radiation (IR) and matter. When IR passes through the sample, a photon absorption, through a transition between the vibrational energy levels of the molecule, can occur.

This means that, with this technique, it is possible to study the vibrational modes of the molecules (stretching and deformation vibrations).

Moreover, in this work, the FT-IR spectroscopy technique is used in conjunction with Attenuated Total Reflectance (ATR) that can measure the changes occurred in a totally internally reflected infrared beam when the beam encounters a sample.

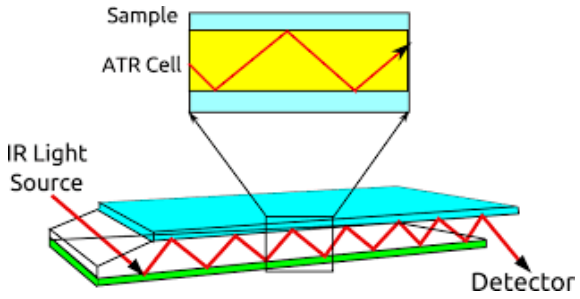

Fig. 4.11 Scheme FTIR-ATR working principle: IR beam encounters the sample passing through a diamond crystal. The IR ray crosses the crystal with a specific angle and is captured by a detector.

As shown in Fig. 4.11, FTIR - ATR requires the contact between the sample and a crystal able to transmit IR radiation and with a high refractive index. When IR radiation crosses the crystal, with a specific angle, it is subjected to total internal reflection at the interface with the sample. However, the evanescent field of IR radiation can partially penetrate the sample. The penetration depth depends on crystal refractive indexes, the incident angle and from IR radiation wavelength.

Following the absorption of the evanescent radiation by the sample, attenuated radiation is collected at the exit from the crystal and subsequently analyzed. The analysis was made both by comparison with the reference spectra collected in commercial databases and by attributing each peak to the vibration of a specific functional group.

From the analysis, I was able to recognize the characteristic groups present within the molecules, both organic (i.e. groups CH_2, C = O, etc.) and inorganic (carbonates, sulphates, etc.) [70,71].

PDMS samples with a diameter of 3 mm and a thickness of 1 mm were examined, different spectra were acquired for each phase of the functionalization of PDMS. After the crystal area is cleaned and the background collected, the polymeric material is placed onto the prism area. Typical spectra were collected with 10 scans in the range of 500-4000 cm-1 at atmospheric pressure and room temperature, with the PDMS samples hold against the prism with a standardized pressure.

4.7 Antigen – Antibody Recognition

In order to prove the biosensing capabilities of the functionalized nanofluidic device, I filled it with a solution of matching biotinylated recombinant human (rh) IL-10 antigen (Fluorokine® Biotinylated Human IL-10 - R&D system NF100 kit) diluted in PBS 1X in a concentration range of 12.5 to 1.25 pg/ml.

The accumulation phenomenon described above (Section 4.5), was used to promote the reaction between the antigens in solution with the antibodies anchored to the PDMS surface. In particular, to accumulate antigens and thus to increase the local concentration, a voltage bias was applied cyclically to the device. Cycles consisted in 10 minutes at 10 V and in a resting interval at 0 V for 10 minutes. Cycles were repeated 3 times.

After the accumulation procedure, the antigen solution was removed and a solution of fluorescent avidin (R&D system NF100 KIT) was inserted and left to interact with the biotinylated antigens for 30 minutes at 25°C under agitation and in a dark environment. Then, the device was opportunely washed with PBS 1X solution and deionized water in order to remove the excess of avidin-fluorescein solution.

The device was observed through optical fluorescence microscopy using a Nikon Eclipse Ti inverted microscope, equipped with an Andor Zyla 5.5 camera, 60x λ-oil lens and a B-1E filter 540/20 nm.

In addition, negative tests were performed following the same protocol described above but using a non-matching antigen (negative control reagent - R&D system NF100 KIT).

4.8 Resistive Pulse Sensing Technique

Resistive pulse sensing (RPS) is a technique widely exploited to study, detect and measure the size of individual particles in fluids [8,72–74].

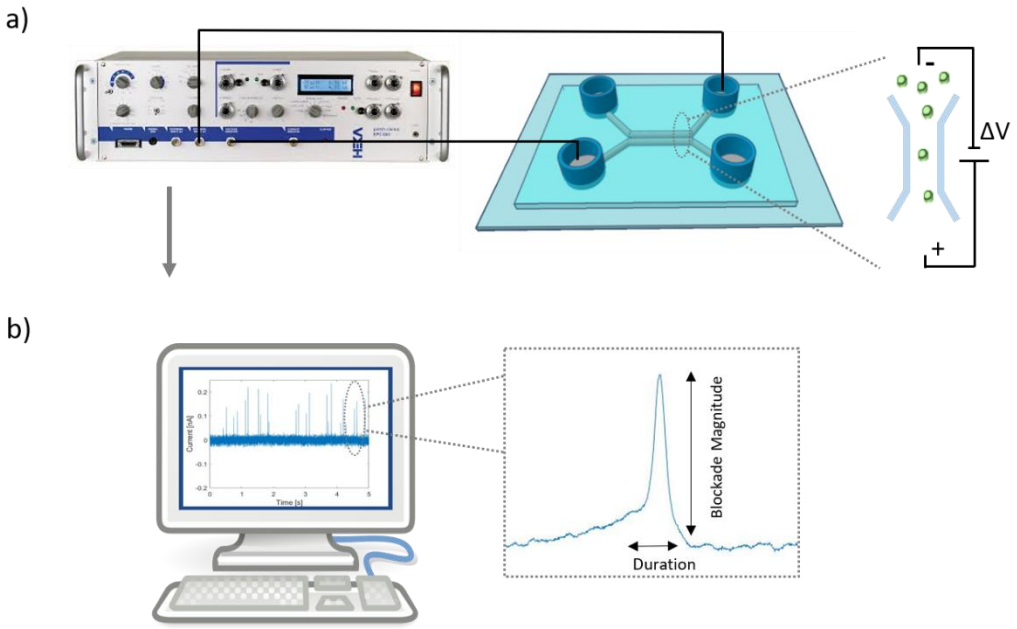

Fig. 4.12 Scheme of RPS measurements. (a) Experimental set-up for detecting translocations of "nano-objects" through the nanochannel. (b) Typical current trace recorded. The inset shows how a single translocation event reflects into the current trace.

.

Fig 4.12. represents the experimental set-up for RPS measurements. Constant voltages across the device are applied through a patch clamp amplifier (HEKA epc 10 USB, HEKA Elektronik, Germany), using two Ag/AgCl electrodes, while ionic current traces are recorded with a sampling rate of 200 kHz, using PATCHMASTER software. Acquired data are filtered by using a low pass Bessel filter-1 at 10 kHz and Bessel filter-2 at 2.9 kHz.

Across the device, filled with electrolytic solutions an electric field is generated. This field drives charged nano-objects through the nanochannel by means of electrokinetic effects (Fig 4.12 a). Each nanobead passage generated a change in the ionic current trace (Fig 4.12 b).

The device and the headstage of the amplifier, during measurements, were put in a shielded box, connected to the ground in order to minimize environmental electromagnetic noise.

Processing and analysis of acquired data were carried out through LabVIEW and Matlab home-made programs.

4.8.1 Nanoparticles solutions preparation

48 nm carboxylated fluorescent nanoparticles (Molecular Probes® USA, F8795) with a stock concentration of 10^{15} beads/mL and 100 nm polystyrene beads (Sigma-Aldrich, USA LB1-2mL) with a stock concentration of 1.8 10^{14} beads/mL were used for experiments.

Nanoparticles were diluted 1:1000 and 1:100 respectively in a KCl 1M buffered solution at pH 8. KCl solution was obtained by dissolving KCl (Carlo Erba Reagents, Italy) into milliQ water. Tween 20 (Sigma-Aldrich USA, P1379) 0.1% was added to avoid nanoparticle aggregation caused by the high ionic strength of the solution. Before insertion, solutions were sonicated for at least 20 minutes in order to break clusters due to nanoparticle aggregation.

4.8.2 λ-DNA solution preparation

λ-DNA (48.5 kbp) was purchased from WAKO-Japan and freshly marked with YOYO-1 intercalant (Molecular Probes® USA Y3601) in a dye-to-base pair ratio of 10:1. Labeled molecules were diluted in a TE 5X solution at a concentration of 0.5 µg/ml. TE 5X was made of 5 mM of EDTA (Sigma Aldrich, USA) and 50 mM of Tris-HCl (Sigma Aldrich, USA) diluted in MilliQ water.

5. Results and Discussion

In order to test the performances of the nanofluidic devices I developed in the framework of my Ph.D. research activity, both for biomedical and environmental applications, different kind of experiments, studies and characterizations have been performed, they include:

1. The application of the “junction gap breakdown” technique to obtain PDMS ionic rectifiers by the formation of an in-situ nanoporous network close to the tip of asymmetric structures.
2. The electrical characterization of the devices, before and after the “junction gap breakdown” procedure, by using working solutions of different ionic strength and pH, in order to understand the electrical behavior of the devices.
3. Analysis of the electro-kinetic transport properties of nanofluidic devices filled with fluorescein solution in order (i) to observe if any accumulation phenomenon, inside the nanostructure, occurs and (ii) to understand how it can be exploited to create high-sensitivity biosensors.

4. Functionalization of the nanofluidic devices, equipped with asymmetric nanostructure suitably re-opened through JGB procedure, with antibodies (Anti IL10) able to recognize specific antigens (IL 10). Successful functionalization was proved by FTIR-ATR measurements and the recognizing antigen-antibody performances were evaluated by optical fluorescence microscopy.
5. Optimization of the fabrication process of nanofluidic devices using h-PDMS, a polymeric compound with higher Young modulus than standard PDMS. Optimization occurs in a "focused drop casting" approach, this strategy consists of the confinement of h-PDMS only on the nanostructured region of the nanofluidic device. This contributes making the nanostructured region of the devices stiffer avoiding the roof collapse phenomenon. The simplicity of this method makes it suitable for increasing the device fabrication yield and allows reducing the fabrication costs.
6. Development of a new class of nanosensors useful for real-time single nanoparticle sensing, with a label-free approach, exploiting the resistive pulse sensing technique.

All these experiments and studies are illustrated and commented in the following sections.

5.1 Roof collapse phenomenon

Polymeric nanofluidic structures are good candidates for tackling the bottleneck preventing the passage of Micro and Nanofluidics' from research labs to the market. The advantages offered by polymeric materials, such as polydimethylsiloxane (PDMS) or polymethylmethacrylate (PMMA), to the production of fluidic devices, are mainly related to their low cost and ease of handling, compared to semiconductor industry-derived materials. Nevertheless, when the size of fluidic structures is shrunk from micro to nanoscale the limits of these polymeric materials become evident. In particular, PDMS nanostructures (nanochannels or nanoslits) are usually affected by "roof-collapse"

problems during the bonding process. "Roof collapse" is defined as partial or complete closure of the nanostructures that occurs when the PDMS positive replica is put in contact with glass coverslip during the bonding procedure. This means that shallow nanochannels characterized by a low aspect ratio < 0.4 (height to width) tend to buckle on the closing substrate under the action of adhesion forces [75–77].

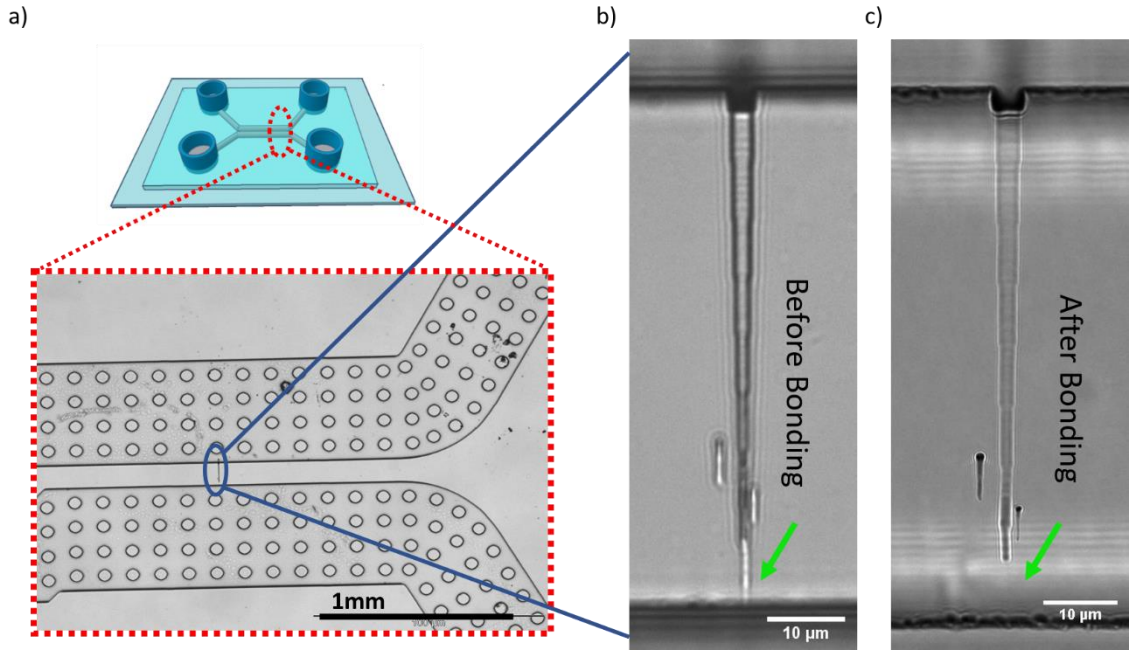

Fig. 5.1 (a) Scheme of nanofluidic device and optical microscope image of the device. (b) Optical microscope images of polymeric positive replica before the bonding procedure and (c) the nanochannel image after bonding procedure.

Fig. 5.1 shows the first nanofluidic device studied. It consists in an asymmetric funnel shape microstructure (98.3±0.2) µm long and a half-cone of 2° connected with a nanometric tip 8 µm long, 500 nm wide and 90 nm deep (these nominal dimensions are referred to the silicon master). In turn, the entire funnel connects two bigger parallel microchannels.

Before the bonding procedure, the tip results is visible in the bright field microscope image while, when the replica is put in contact with a glass coverslip, after the oxygen plasma treatment, the funnel tip disappears from the optical microscope image.

This means that roof-collapse occurs, causing a reduction of the nanochannel dimensions, that, in the worst cases, results in complete closure of the structure, making the device unusable as hindering the passage of fluids and molecules or “nano-objects” from one microchannel to the other. This is also confirmed by the high resistance values (typically a few GΩ) measured across the microchannels, filling the device with 1 M KCl solution.

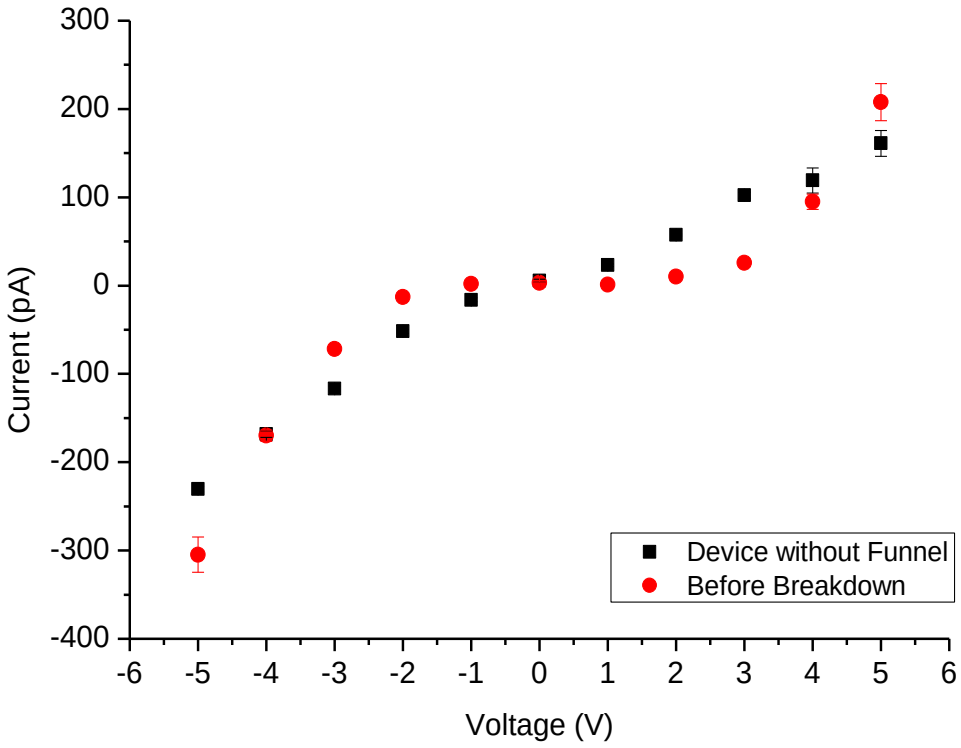

Fig. 5.2 I-V ramp from -5 V to +5 V of nanofluidic device acquired after bonding procedure (i.e. after tip collapse)(black line), in comparison with I-V ramp of a device made only with microchannel (i.e. without nanochannel as point of connection between them) (red line).

In fact, as shown in Fig. 5.2, current versus voltage (I-V) curves acquired on devices with no funnel connecting the microchannels and on devices with a collapsed tip show similar currents values meaning that the tip is effectively collapsed.

To investigate the effects of the roof collapse phenomenon on the nanochannel size and geometry, a cast of the closed device was fabricated by using a photocurable resin, whose commercial name is NOA.

The cast was fabricated by simply putting a PDMS replica into conformal contact with a silicon substrate and filling the closed device with a solution of NOA diluted in acetone (see section 4.2.1 for details). The cast profile was acquired by using an AFM microscope.

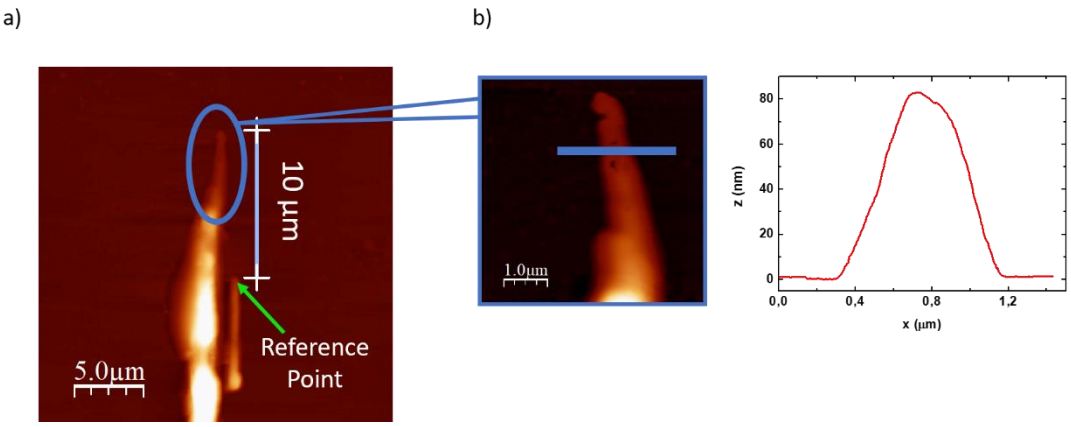

Fig. 5.3 (a) AFM image of the cast of a positive replica brought into conformal contact with a silicon substrate. The final part of tip (~ 5 µm) was not reproduced by the casting procedure. (b) Zoom of cast tip and height profile close to the collapsed region.

AFM image of the NOA cast is shown in Fig. 5.3. Nominally, the distance from the reference point to the tip of the PDMS positive replica has a value of about 15 µm. From the cast, it is possible to observe that the tip has not been filled by the resin for a length of nearly 5 µm, in fact, the distance from the reference point-to the tip is around10 µm. This confirms the effective tip collapse, after the bonding procedure, which hindered the resin from entering in the tip.

The profile of the final part of the cast (blue line in Fig. 5.3 b) is reported in the graph. It confirms that the nanochannel has a cross-section shape which can be approximated as a triangle.

From the analysis of the profile, it was possible to estimate the height and the width of the funnel tip close to the collapsed region that resulted to be: (85 ± 5) nm and (850 ± 70) nm respectively.

5.2 PDMS ionic rectifiers – Junction Gap Breakdown technique

In this section, it is showed how, exploiting the Junction Gap Breakdown (JGB) technique, it is possible to overcome the mechanical limits of PDMS when employed fot the fabrication of polymeric sealed fluidic nanostructures, allowing to use them as concentrators and ionic rectifiers.

JGB consists in the application of constant voltages across collapsed nanofluidic devices until sudden and significant current increases, associated to variations in the nature of the material, are registered.

I observed that the value of the voltage necessary to re-open the nanostructure during the JGB procedure never exceeded, in absolute value, 150 V, due to the small length of the gap (around 5 µm) and to the funnel shape of the structure that allows to focus the electric field at the tip. The applied voltages produce an electric field intensity around 25-30 V/µm that is higher than the dielectric strength of PDMS (21 V/µm - Sylgard 184 datasheet).

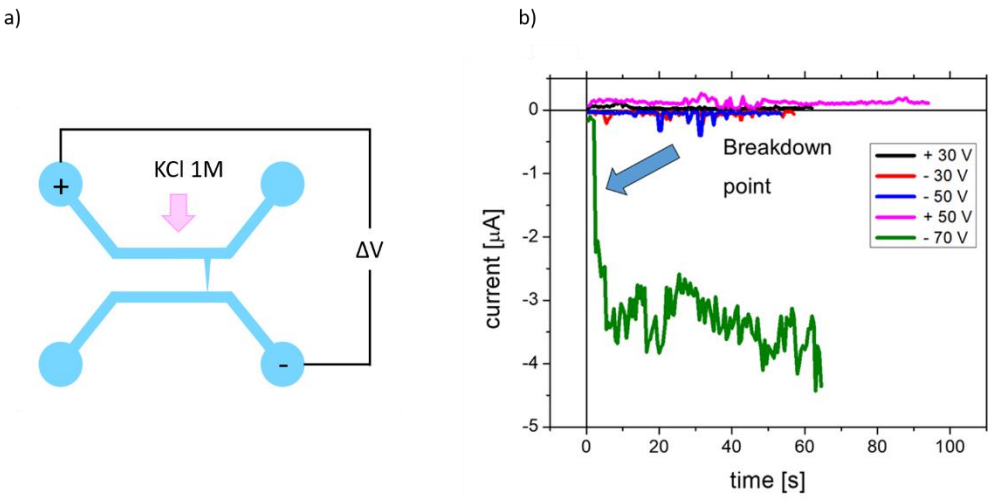

Fig. 5.4 (a) Scheme of electrodes configuration during JGB procedure. (b) Current versus time curves recorded during a typical JGB process. Voltages of increasing intensity and alternate polarity (-30, +30, -50, +50, -70 V) are applied to the device filled with a 1 M KCl solution. For a tension of -70 V the current intensity abruptly increased to values around 3 μA.

As shown in Fig. 5.4, constant voltages across the device, filled with 1 M KCl, were applied while monitoring the ionic current (see section 4.4 for details). A picture and a schematic representation of the set-up used for the dielectric breakdown procedure are reported in Fig. 4.8.

The values of the voltage bias that were applied for "opening" a passage in correspondence of the tip were progressively increased with steps (in absolute value) of 20 V and was kept constant for 1 minute. If, during this time interval, no significant resistance decrease was observed, the intensity of the voltage was increased.

Both positive and negative voltage biases were applied but the "re-opening" of the funnel tip occurred only when the anodic side was in the microchannel connected to the funnel entrance.

The typical behavior of a device, during JGB experiments, is described by the ionic current traces reported in Fig. 5.4. The recorded ionic current did not significantly vary in the voltage range from -50 to 50 V. Instead, when a voltage of -70 V was applied to the device (green curve), the absolute value of the ionic current increased abruptly to 3 μA. This means that the breakdown of the material occurred in the collapsed region of

the nanofluidic device, , in fact the sudden increase of the current proves that the nanostructure has re-opened and correctly connects the two main microchannels of the nanofluidic device. This hypothesis was supported by optical and electronic microscopy images reported in the following section.

5.2.1 Optical and electronic images of the nanostructures after JGB

After the JGB procedure, optical microscope images of the nanofunnel were acquired in order to analyze the differences and compare the images with those made before the breakdown.

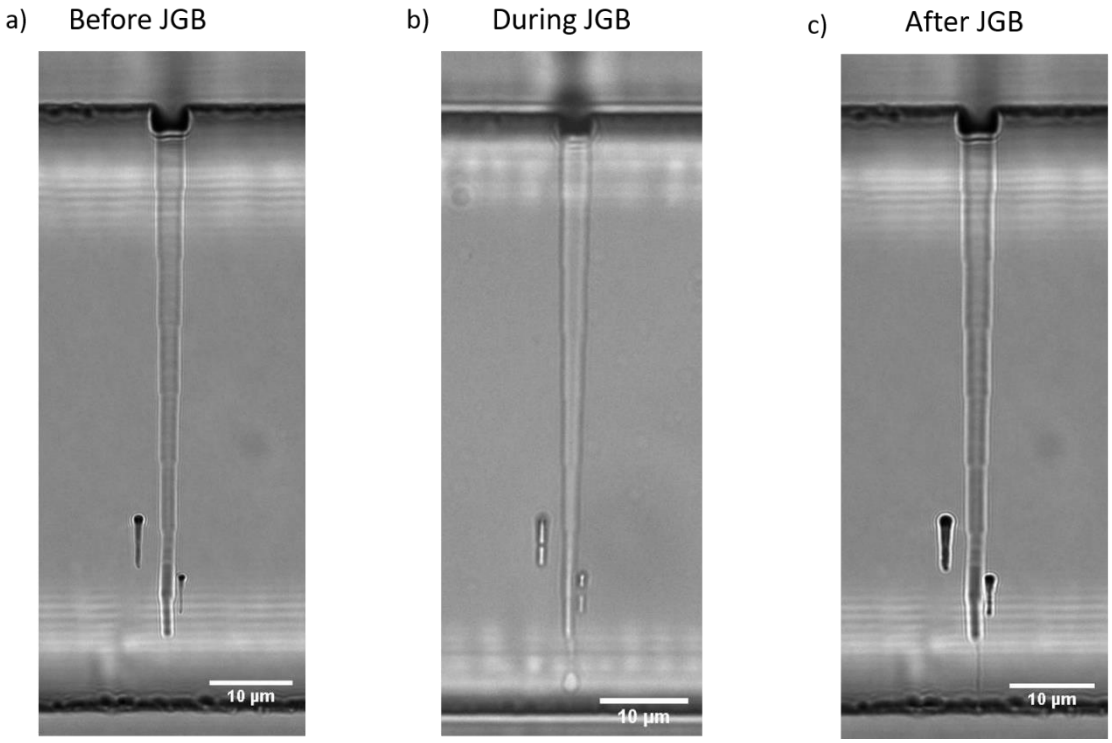

Fig. 5.5 Bright-field images of the funnel tip before (a), during (b) and after (c) breakdown process. Funnel tip, which is not visible before the breakdown, because of elastomeric collapse, is visible at the end of this process, demonstrating a change in the material near the tip.

From Fig. 5.5, it is possible to observe that after JGB, the tip becomes visible again while during the procedure bubble formation, in proximity of the funnel tip, usually occurs due to high voltages applied. Bubbles tend to spontaneously disappear when the device is left to stabilize after the JGB procedure.

Moreover, to understand and analyze the effects of high voltage on PDMS, different regions of the device were observed by Scanning Electron Microscopy (SEM).

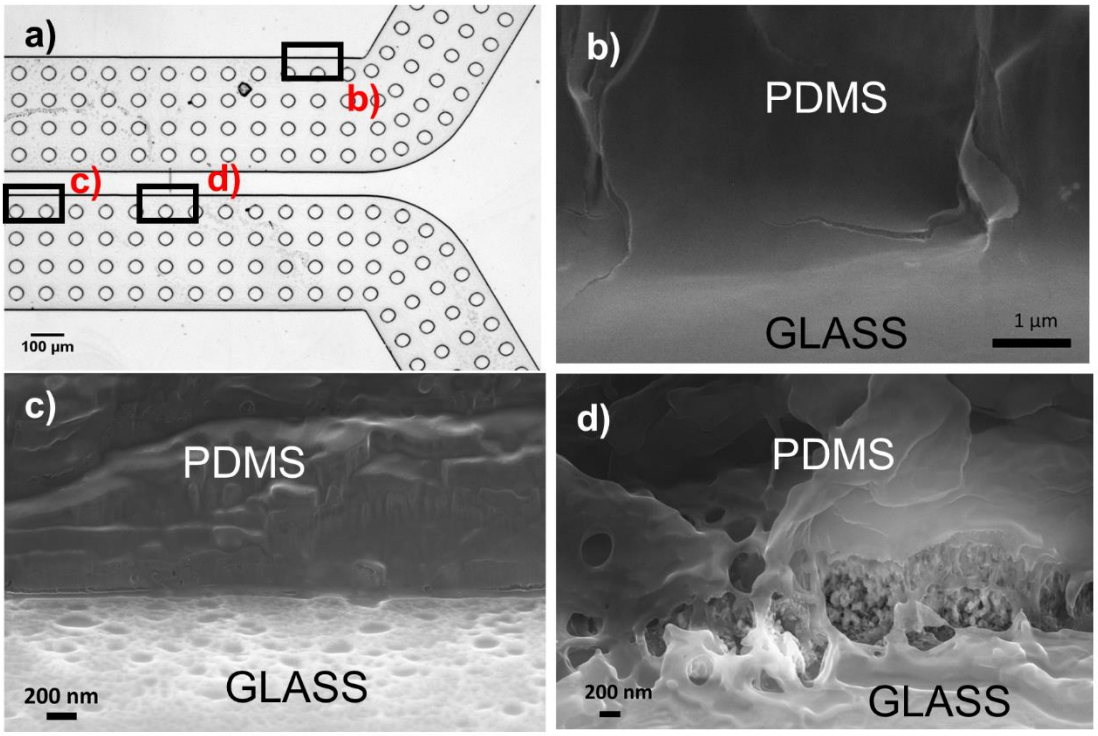

Fig. 5.6 (a) Optical image of the device in which are highlighted three different regions observed with SEM and whose images are reported in b), c) and d).

Fig. 5.6 shows a map of the device in which is marked the three regions observed through the SEM microscopy. The first two regions (see Fig. 5.6 b and c) refers to the wall at the PDMS/silica interface (see label "b" and "c" in Fig. 5.6 a) of both microchannels nearly 500 microns far away from the funnel tip. In both images PDMS appears compact and uniform.

In the region corresponding to the funnel tip, panel d of Fig. 5.6, the polymer shows a different structure. The PDMS at the interface with the glass substrate is nanoporous, with a porosity of a few tens of nanometers.

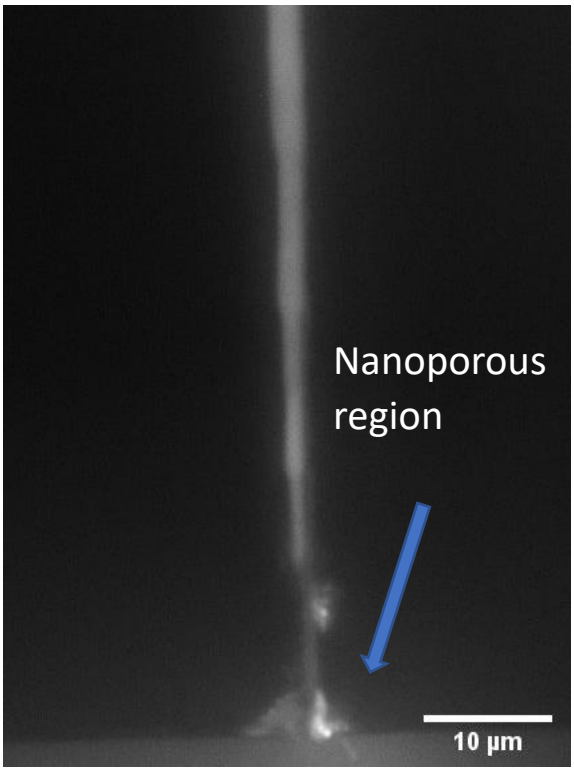

Fig. 5.7 Epifluorescence image of the funnel tip "re-opened" through the JGB procedure. The nanoporous region broadens close to the edge in correspondence of the microchannel

The nanoporosity was also confirmed by epifluorescence image of the funnel (Fig. 5.7) acquired inserting fluorescein diluted in an electrolytic solution and applying a voltage bias of -10 V. From this image, the tip structure, consisting in a nanoporous network, is clearly visible and it covers several microns connecting the funnel tip with the microchannel.

5.2.2 Electrical behavior of the device

Before and after the JGB procedure, I-V curves were recorded. The data are shown in Fig.5.8.

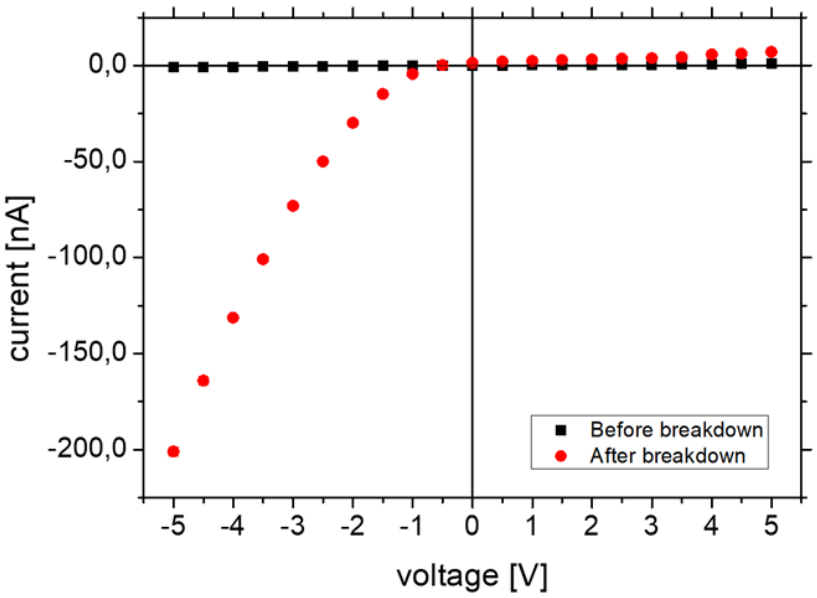

Fig. 5.8 I-V curves of the nanofluidic device with funnel nanostructure acquired before and after the breakdown procedure. Working solution: KCl 1 M.

The curves show different trends, and, after the breakdown procedure, the device clearly shows a rectifying behavior.

In order to evaluate the effects of ionic strength and pH on the electrical behavior, I-V curves were recorded on the same device filled with solutions of KCl of different molarities (1 mM, 10 mM, 100 mM to 1 M) and pH values (4, 6, 8 and 11).

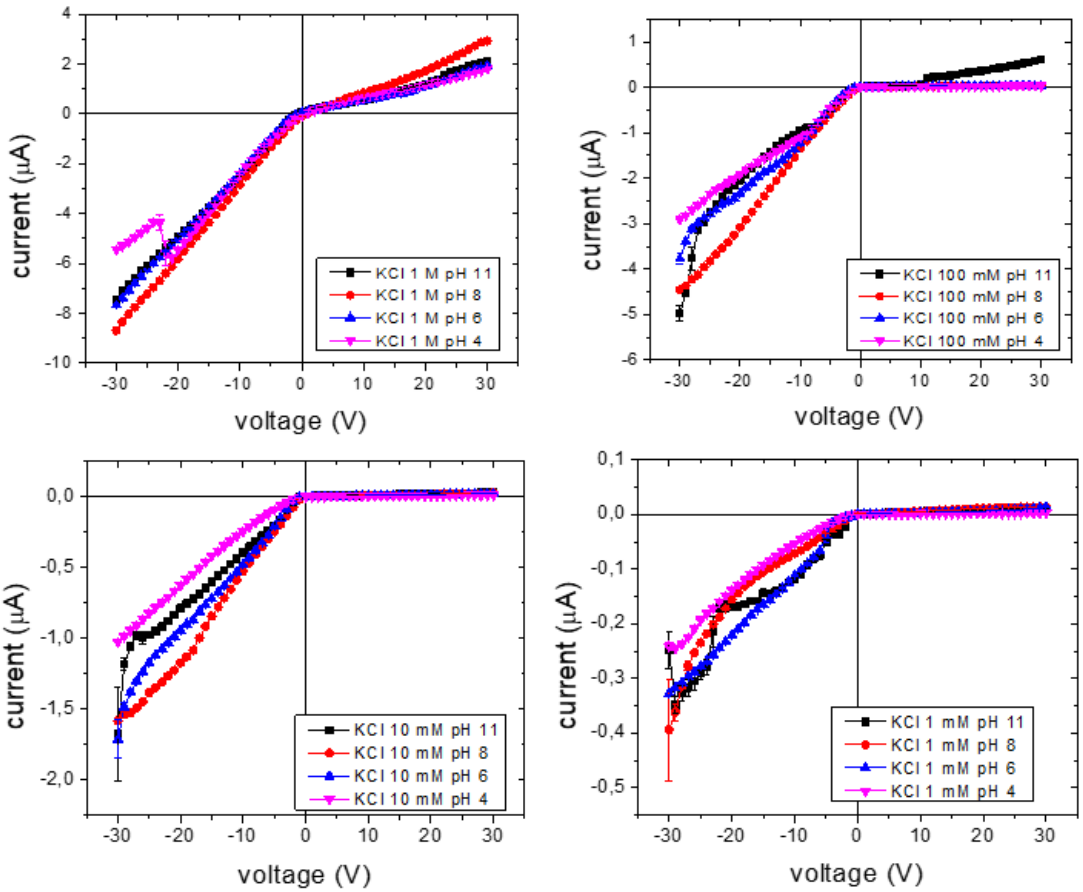

Fig. 5.9 I-V curves recorded after filling the device with (a) KCl 1M (b) KCl 100 mM (c) 10 mM and (d) 1mM at different pH: 4 (pink line), 6 (blue line), 8 (red line) and 11 (black line). Scan rate: 0.14 V/s.

From Fig. 5.9, it is possible to observe larger current values for negative voltages (i.e. anode on the tip side of the nanostructure). This is compatible with the presence of a negative surface charge on PDMS.

This rectifying behavior was observed for all ionic strengths, even for the highest (KCl 1 M). These measurements were conducted on tens of devices, confirming the same results.

Moreover, based on the work of Momotenko and Girault [78], who observed the dependence of rectification properties on the scan rate direction, I-V scans with both

polarities (from -30 V to +30 V and vice-versa) were performed, obtaining a good overlap.

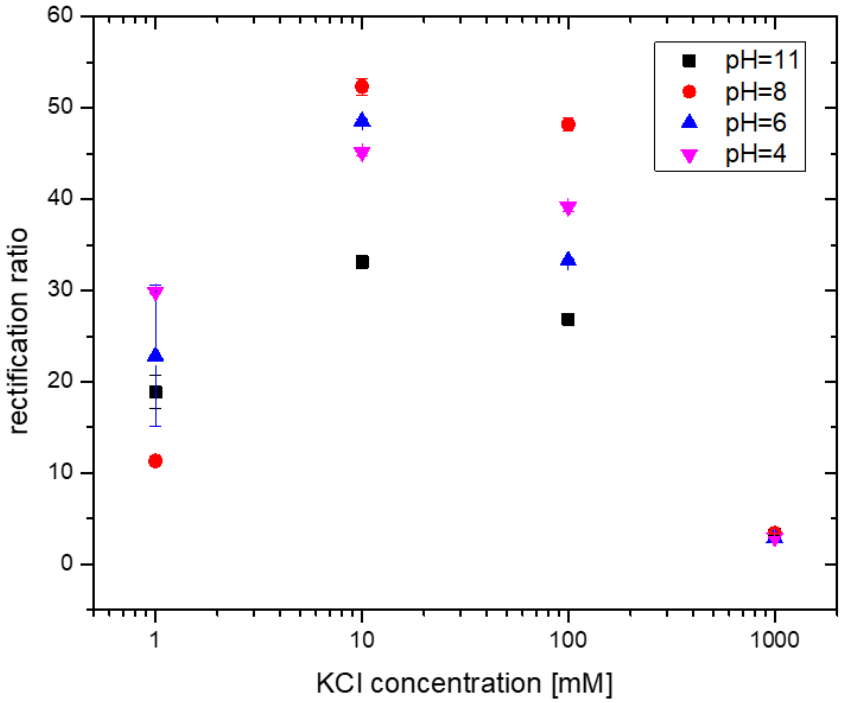

Fig. 5.10 Dependence of the rectification ratio (RR) calculated for -5V and +5V as a function of KCl molarity at different pH.

Fig. 5.10 shows the rectification ratio (RR), i.e. the ratio of the absolute value of the ionic current measured for negative and positive voltages of opposite polarity as a function of KCl concentration. Considering Fig. 5.10, it is possible to observe that RR increases when decreasing the ionic strength of the electrolyte, but this increase is not monotonic as the data collected for devices filled with 1 mM KCl show lower values compared to higher ionic strength electrolytes. A similar behavior was observed by several previous studies performed on silica conical nanopores [79] and nanocapillaries [80]. Moreover, it is worth noting that, in our system, consisting in the combination of a nanoporous network (created in-situ) with an asymmetric microstructure, high values of RR were observed.

5.3 Accumulation experiments depending on ionic strength

After the “re-opening” of the nanochannel tip through the JGB procedure, I studied and characterized the accumulation of fluorescein, inside the funnel structure, in order to evaluate the concentration capabilities of the nanofluidic device.

The device was filled with a solution of KCl 10 mM in which fluorescein molecules were previously diluted and both negative (-10 V) and positive (+10 V) voltages were applied across the device for several minutes while it was optically monitored through fluorescence microscopy.

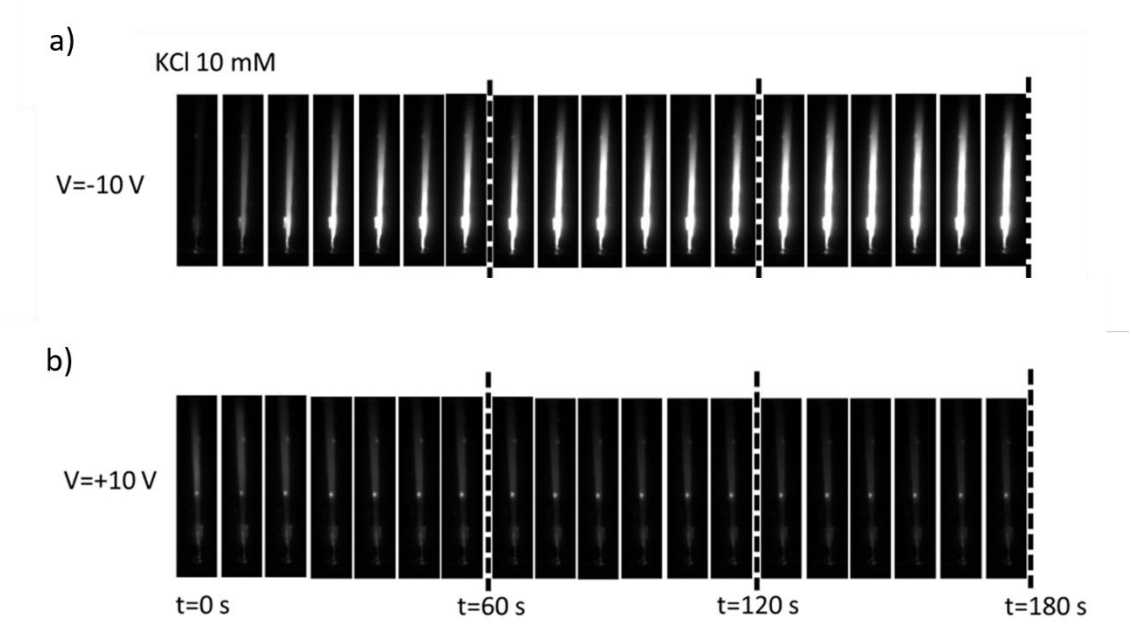

Fig. 5.11 Sequence of fluorescence images, acquired with an interval of 10 s during the application of a constant bias of (a) -10 V and (b) +10 V, with the device filled with 10 mM KCl.

Fig. 5.11 shows a sequence of fluorescence microscopy images of the nanofunnel, acquired every 10 s, from these images it is possible to note a gradual increase of the

fluorescence intensity during the application of a negative bias, while for positive bias no accumulation was observed.

IIn addition, I-V ramps from -30 V to +30 V were applied in order to correlate the previously studied rectification behavior of the device with its accumulation capabilities.

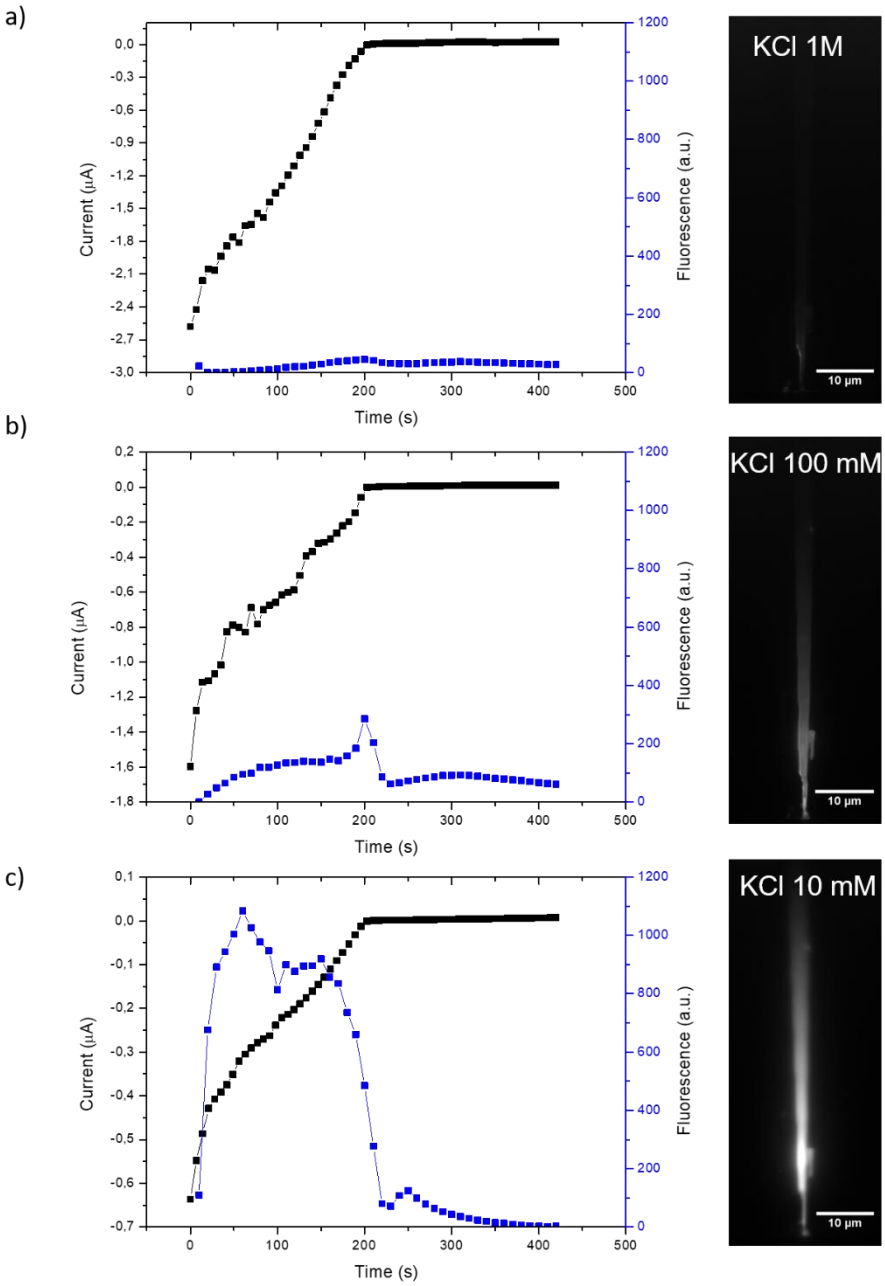

Fig. 5.12 I-V curves (black line), fluorescence signal along the nanofunnel axis (blue line) and fluorescence microscopy images of the nanofluidic devices filled with (a) 1 M, (b) 100 mM and (c) 10 mM KCl.

Three I-V ramps (black line), with fluorescein diluted in KCl solutions at different ionic strengths (1 M, 100 mM and 10 mM), were acquired. They are reported in Fig. 5.12. During the ramps, images of the nanofunnel were recorded through fluorescence microscopy, and the fluorescence intensity signals (blue line), were also acquired on a region of the image covering the whole funnel area.

For fluorescein diluted in KCl 10 mM, the I-V curve and the fluorescence intensity signal have a similar trend indicating that the accumulation occurs when the funnel is in its high conductance state, and that it gradually empties when the positive bias increases. For high ionic strength solutions (100 mM and 1 M), the accumulation phenomenon is less evident while the rectifying behavior of the I-V curves is still marked.

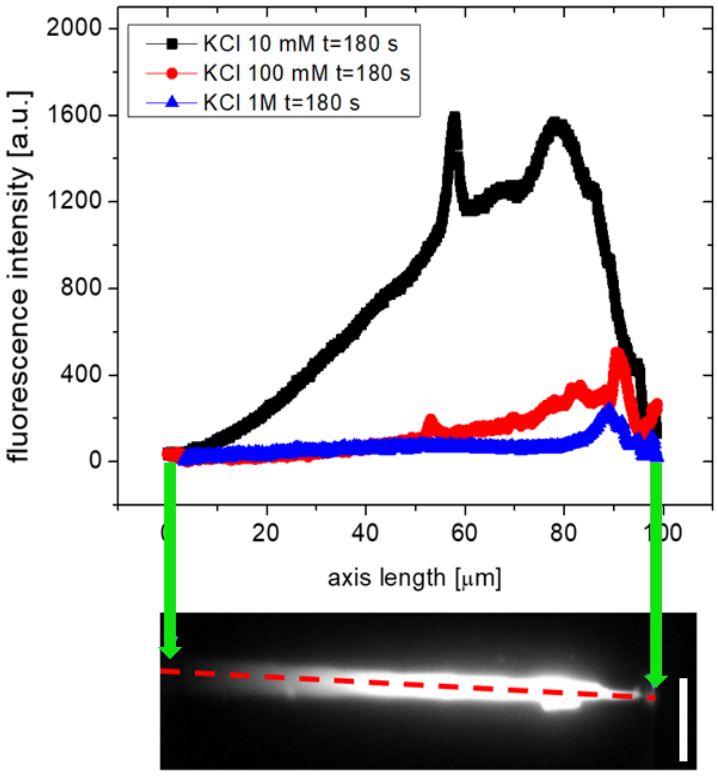

Fig. 5.13 Fluorescence intensity profile acquired along the funnel axis (red dashed line) for fluorescein diluted in KCl 1 M, 100 mM, 10 mM. Scale bar 10 µm. During the acquisition a constant voltage of -10 V was applied across the device. Profiles were acquired after 180 s.

The same result also emerges from the analysis of the intensity profiles acquired along the funnel axis (Fig. 5.13). In fact, considering the same acquisition conditions and image analysis for all the measurements, the accumulation effect results significantly stronger for low ionic strength solutions.
Moreover, it is evident that the highest accumulation point is close to the funnel tip or rather at the microfunnel/nanoporous network interface, confirming the crucial role of this part of the device in order that the accumulation process may occurs.

Definitely, inside these nanostructures, the physical constraints due to the particular geometry, charge and chemistry of the surface can affect the behavior of the fluid. In particular, in these conditions, the thickness of the Debye layer is non-negligible compared to the nanochannel and to the nanoporous network dimensions. This means that when the size of the fluidic structures are shrink until to the nanoscale, EDL overlap occurs. Considering this overlap and applying an electric field across the nanochannel, a concentration phenomenon called ICP "Ion Concentration Polarization" [81,82] take place and, as demonstrated in this section, it results useful for accumulating specific analytes inside the nanostructures.

5.4 Functionalization of a PDMS nanofunnel with antibodies

After the JGB procedure for "re-opening" the nanochannel tip and the characterization of the accumulation capabilities, the nanofluidic device was chemically functionalized by protein (i.e. anti-IL10 antibodies) immobilization on the nanochannel wall. The purpose of this functionalization is to make the device a nano-biosensor able to perform high sensitivity immunoassay analysis by exploiting the concentration phenomenon, for a rapid detection of one or several targeted diluted antigens. These capability is crucial for the improvement in clinical diagnostics field.
Concerning protein immobilization, it is well-known that PDMS is hydrophobic in its native form, so proteins tend to readily and non-specifically bind on its surface **[83]**. Therefore, an activation of the adsorptive surface, in a specific and organized manner,

is necessary to immobilize proteins on the device surface and impart it recognition capabilities.

In this case, the protein immobilized on the PDMS surface was an antibody called IL-10 (i.e. Mouse monoclonal Anti-Human Interleukin-10). The functionalization process was performed as reported in the materials and methods chapter - section 4.6. The final concentration of antibodies on the PDMS surface was 62.5 ng/ml.

5.4.1 Characterization of the PDMS surface after the functionalization procedure

In order to prove and confirm that the device had been successfully functionalized with IL-10 antibodies, FTIR-ATR measurements on native PDMS and on two layers of PDMS with partial and complete functionalization were performed.

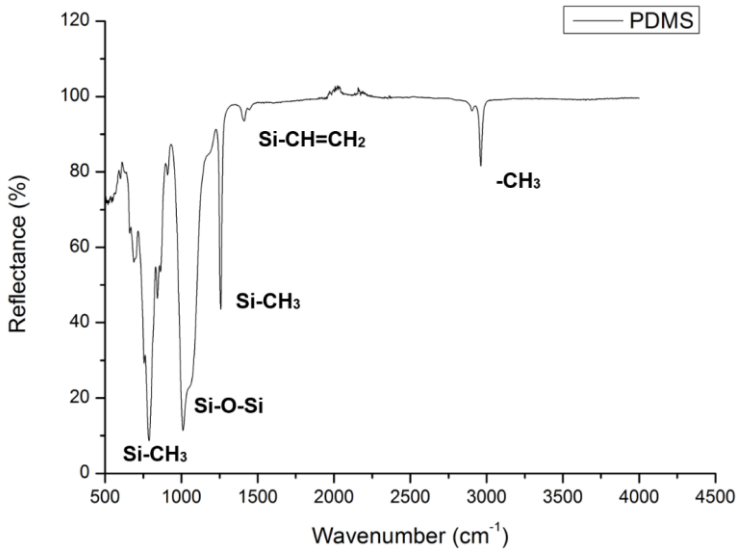

Fig. 5.14 FTIR-ATR spectrum of native/not functionalized PDMS.

Fig. 5.14 shows an FTIR-ATR spectrum of native PDMS that is characterized by the presence of several sharp negative peaks corresponding to specific functional groups of the polymeric material.

In particular, peaks at 2950 and 810 cm^{-1} correspond to the stretching and rocking –CH3 groups, the peak at 700 cm^{-1} is characteristic of the Si-CH3 group and the peaks at 1110 cm-1 and 1410 cm^{-1} are related to Si-O-Si and and Si – CH = CH2 functional groups respectively. Finally, the broad peaks between 1240–1020 and 980–880 cm−1 are attributed to Si–O stretches of the PDMS layer.

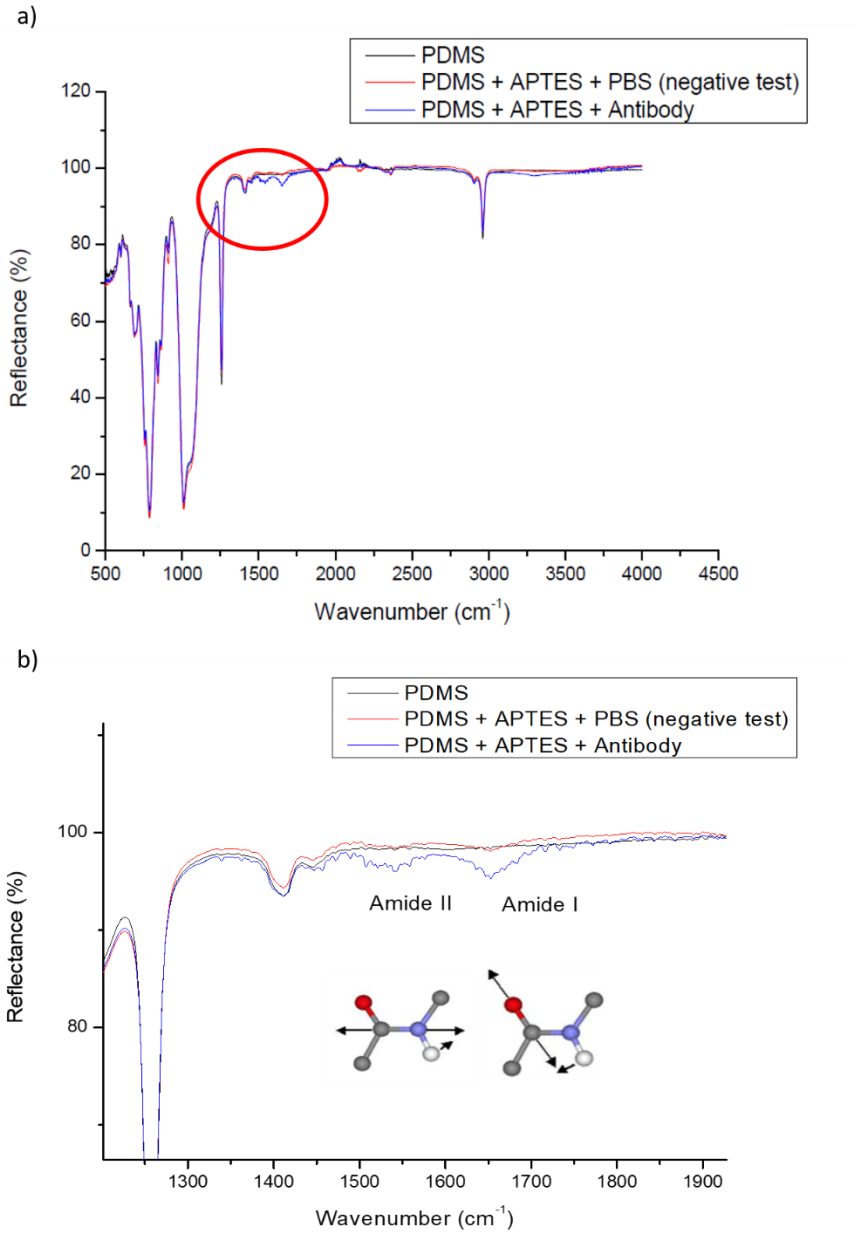

Fig. 5.15 (a) Spectra overlap of native PDMS, PDMS with APTES treatment + PBS and PDMS functionalized with antibodies. (b) Zoom of spectra from 1200 to 1950 cm^{-1}(red circle in (a)).

Spectra were acquired for three PDMS samples: (i) on native PDMS, (ii) on PDMS treated with APTES and PBS and (iii) on PDMS functionalized with IL 10 antibodies. These spectra are compared in Fig. 5.15.

The main difference between them is in the range of 1200-1900 cm^{-1}, in fact the bands relative to Amide I and Amide II at 1650 and 1550 cm^{-1} respectively, which are typically associated to the presence of proteins on the sample, were only detected on the PDMS functionalized with antibodies (blue curve in Fig. 5.15).

Infrared spectroscopy resulted in being very useful for identifying the presence of a protein.

However, thanks to these measurements, it was possible to confirm the presence of the antibody's typical chemical groups on the sample surface. The presence of the peaks proved that the functionalization process was successful and that this protocol was an effictive strategy for immobilizing the IL10 antibody on the PDMS surface.

5.4.2 Immunoassay analysis – IL 10 antigen sensing

After the functionalization of surface of the PDMS device with antibodies, a solution of PBS containing biotinylated IL10 antigens was inserted in both the microchannels of the nanofluidic device and left under agitation for 30 min at room temperature.

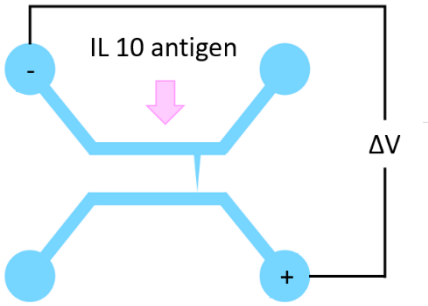

Fig. 5.16 Electrodes configuration used for accumulation/concentration measurements.

For accumulating antigens inside the funnel, and, thus, increasing the local concentration, taking advantage of the ion concentration polarization phenomenon, previously described in section 5.3, a voltage bias was applied cyclically to the device using two Pt electrodes placed in the configuration shown in Fig. 5.16. Cycles consisted in 10 minutes at -10 V and in a resting interval at 0 V for 10 minutes.

The micro/nanoconfinement of these molecules inside the funnel, through the accumulation procedure, allowed to increase the antigen-antibody recognition probability even if the solution with antigens was extremely diluted.

After this procedure, microchannels were washed with a PBS solution in order to clean and remove the unreacted antigens from the device and the avidin-fluorescein solution was inserted in microchannels. The device was placed under agitation protected by an aluminum foil, to avoid photobleaching of fluorescent molecules, for 20 minutes.

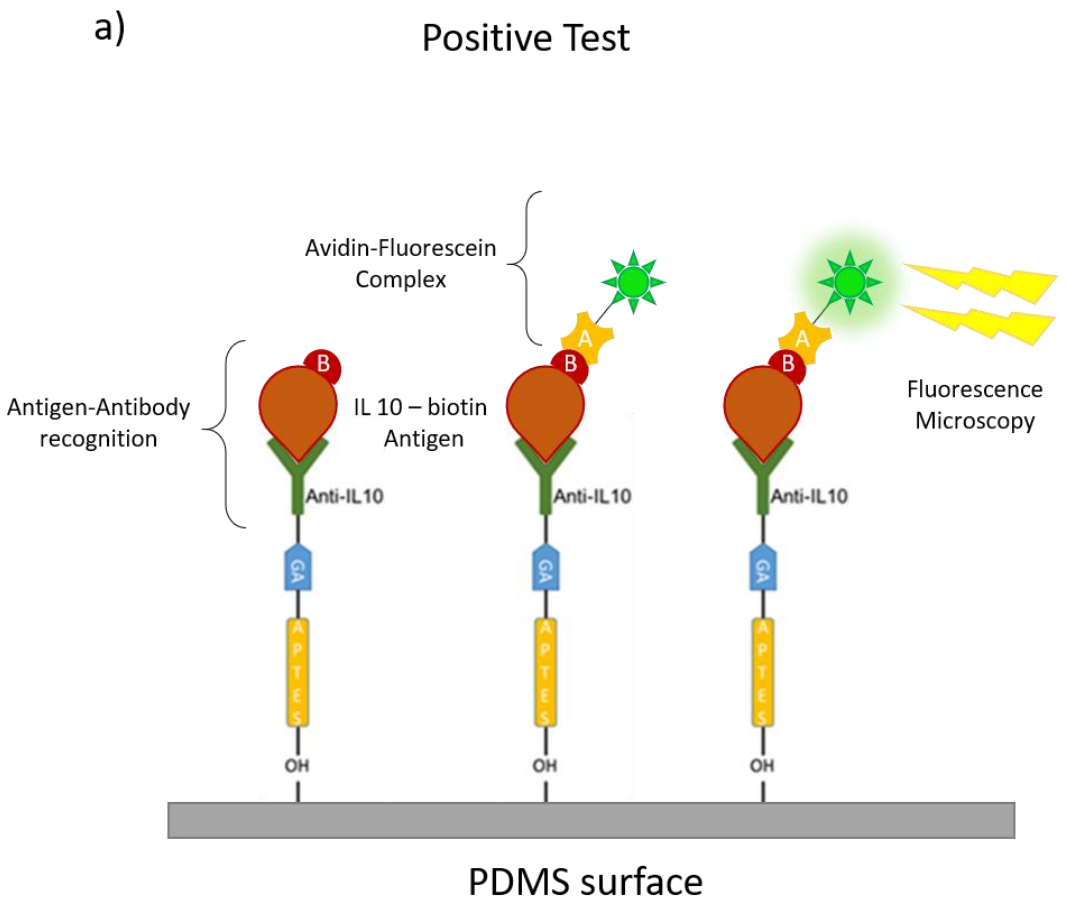

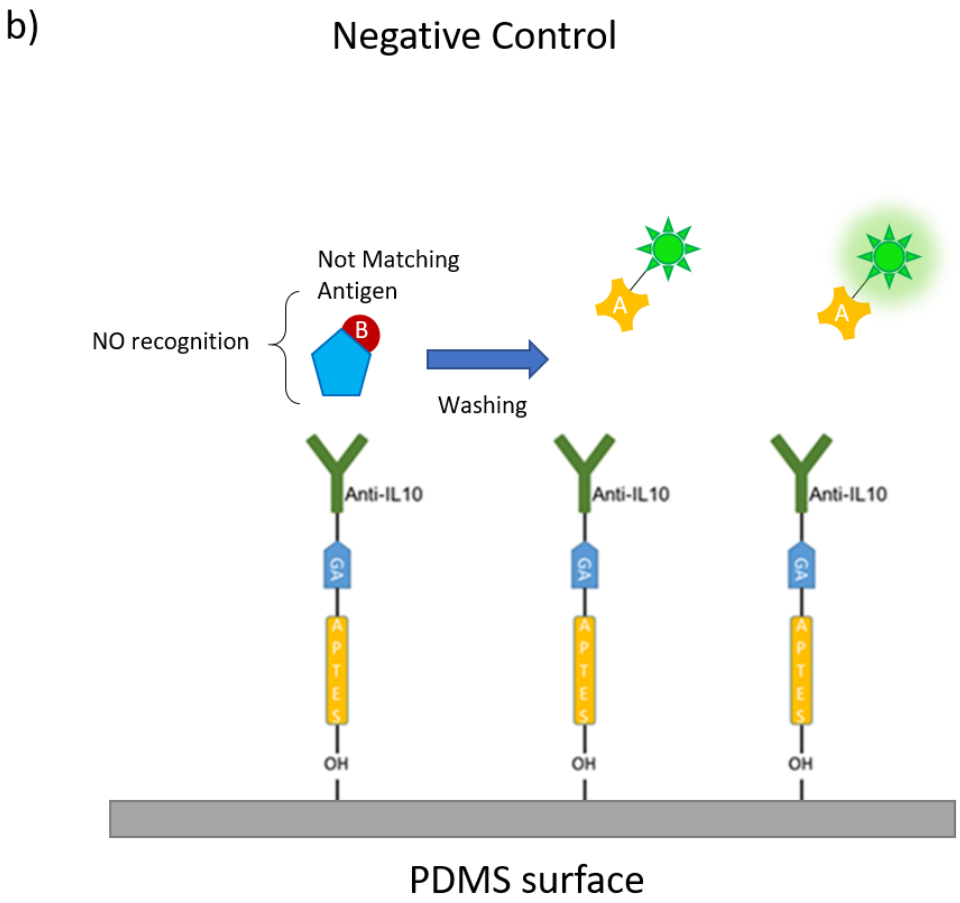

Fig. 5.17 Scheme of the sensing mechanism detected by fluorescence intensity measurements using (a) matching IL-10 antigens and (b) not-matching antigens. When the antigen does not match with then immobilized antibody, no fluorescence is observed.

Avidin-fluorescein binds the biotin on the antigen and allows revealing if successful antigen-antibody recognition occurred through fluorescence microscopy measurements as schematically shown in Fig. 5.17. Before observing the device by fluorescence microscopy, the device was thoroughly washed with PBS and deionized water to remove all excess of fluorescein solution. This procedure was necessary in order to be sure that the recorded fluorescence signal was only due to the avidin-fluorescein linked to the biotinylated antigen that was previously captured by the antibody.

In order to verify the effectiveness of the functionalization process and the correct functioning of the device as a biosensor for detecting small quantities of a specific antigen, a negative test was performed using a device functionalized with the IL10 antibody but inserting a not-matching antigen solution (Fig. 5.17 b).

a)

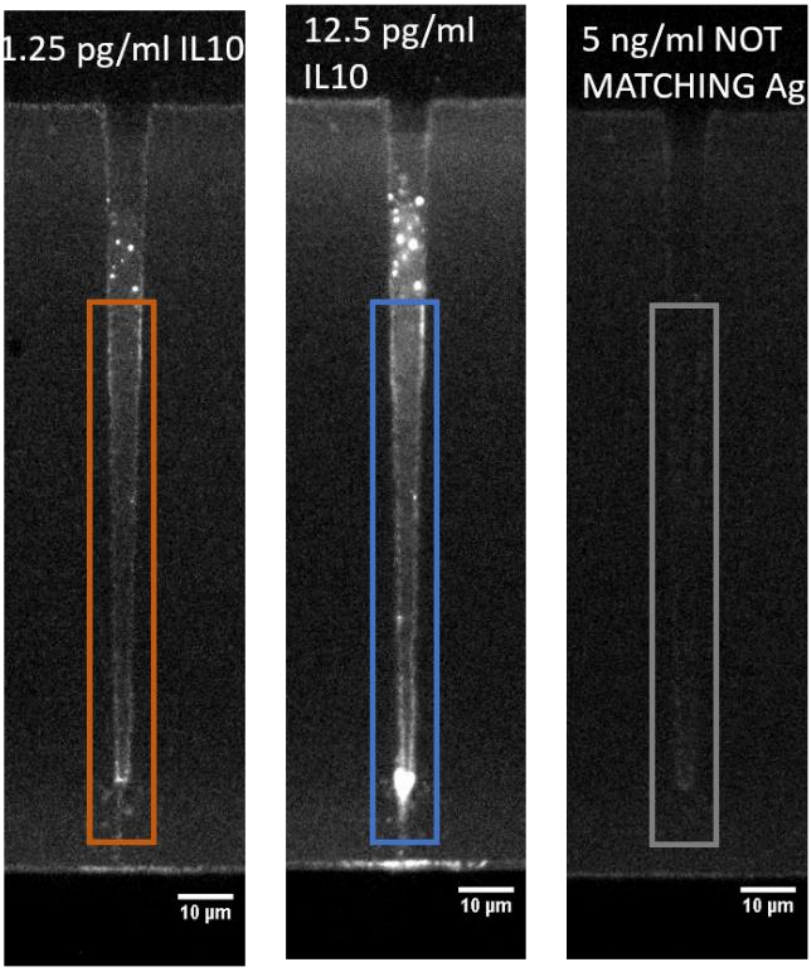

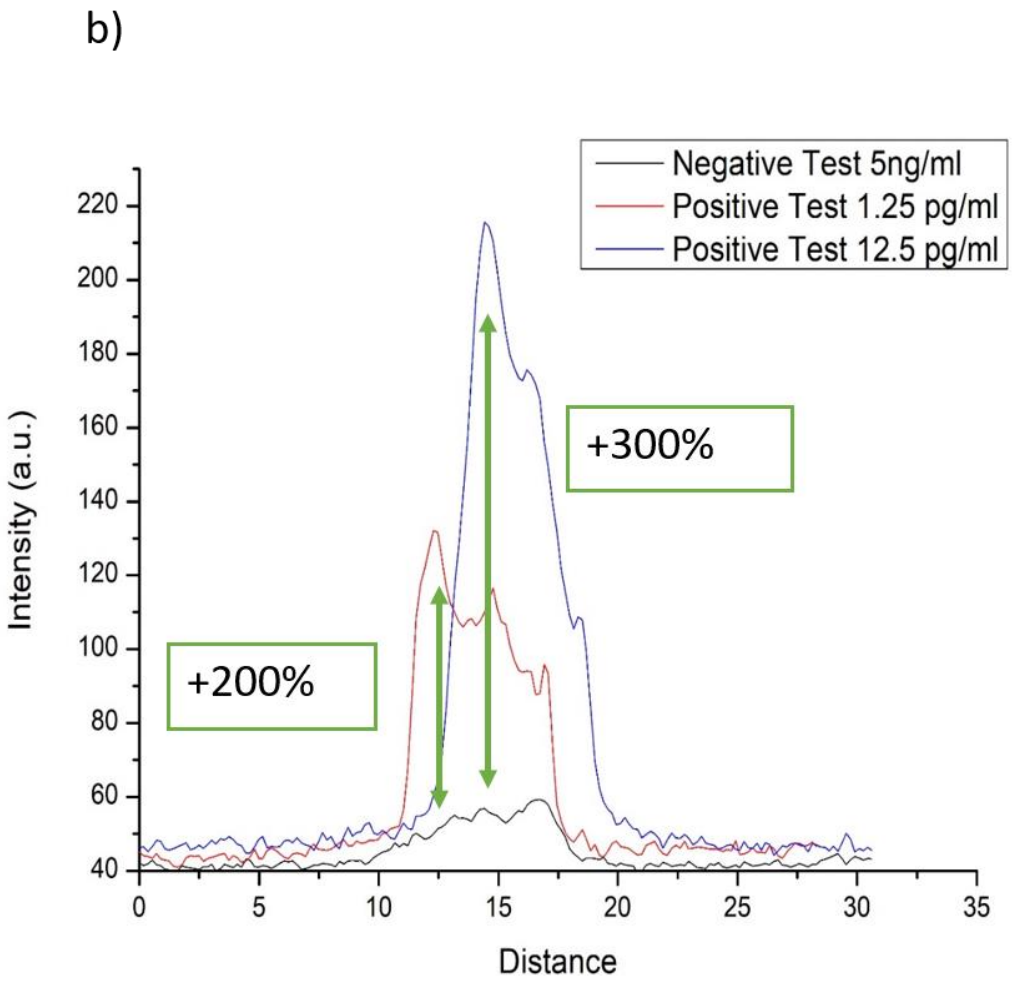

Fig. 5.18 (a) Optical fluorescence images of nanofunnel functionalized with antiIL10 after the injection of 1.25 pg/ml IL10, 12.5 pg/ml of IL10 and 5 ng/ml of not-matching antigens. Voltages applied before imaging: - 10 V. Avidin- fluorescein was inserted in all three devices for optical detection. (b) Fluorescence intensity signals of negative and positive tests acquired in the rectangles shown in (a).

As shown in Fig. 5.18, the experiments were carried on three functionalized devices filled with 12.5 pg /ml of IL 10 (center), 1.25 pg/ml of IL 10 (right) and 5 ng/ml of not-matching antigens (left) .

After the accumulation procedure, by application of a voltage bias, significant fluorescence signal was recorded only for IL-10 antigens while no fluorescence intensity was recorded for non-matching antigens. In particular, I detected fluorescence intensity

values 200 % and 300 % higher than the negative control for 1.25 pg/ml and 12.5 pg/ml of IL-10 solutions, respectively.

The presence of fluorescence signal in Fig. 5.18 a on the walls of the nanochannel indicates the presence of antigen-antibody complexes anchored to nanochannel surface.
This means that a suitable functionalization procedure, combined with the concentration process, allows an easy detection of a specific antigen in an extremely diluted solution only through fluorescence microscopy observation.

5.5 Optimization of the fabrication process – The use of h-PDMS

It has been show how the JGB procedure has made it possible to overcome the "roof collapse" phenomenon of nanostructures, allowing the use of nanofluidic devices for highly sensitive immunological analyzes.
An alternative approach, to solve the collapse problem, goes to an optimization of the fabrication process in order to directly obtain rigid (i.e. mechanically stable) devices, whose nanometric features do not collapse after the bonding procedure.

It is well known that nanofluidic devices have been developed and studied as promising systems for detecting single nano-objects (i.e. nanoplastics and biomolecules such as virus proteins and DNA) in situ and in real-time.
In order to achieve this challenging functionality, the design of these devices must contain a well-defined nanostructured region with dimensions close to the objects to be investigated. This means that re-opening the device through the JGB technique is not a good strategy for using these devices for single-particle label-free sensing. Therefore, it was necessary to optimize the fabrication process to avoid nanostructures collapse during the bonding procedure.

Usually, solid-state nanochannels are produced on silicon or glass substrates by using a high-resolution nanopatterning technique (i.e. FIB, EBL and laser machining)**[84–86]**.

These techniques allow excellent control of the geometry and high reproducibility of the devices but are much expensive and not easily scalable to a production stage.

An effective method, developed in order to overcome these limitations, consisted of pairing the latter techniques with PDMS based soft-lithography **[63,87,88]** . This approach resulted to be crucial for reducing the fabrication costs, preserving the ability to produce sub-micrometric nanofluidic structures (see section 4.1 for fabrication details). The main disadvantages of using PDMS are related to (i) its high viscosity and (ii) the "roof collapse" mechanism. The first tends to limit the ability to reproduce the structures compromising the replica fidelity **[89]** , while the second is a mechanism that occurs during the sealing process making the device unusable (see section 5.1 for more information) **[75,76]**.

The most obvious solution to prevent the risks of "roof collapse" consists of using a polymer with a higher Young's modulus than standard PDMS. For example, hard-PolyDiMethylSiloxane (h-PDMS) offers all the interesting properties of PDMS (i.e optical transparency, biocompatibility and low cost) but with a higher Young's modulus: around 8.2 MPa [65].

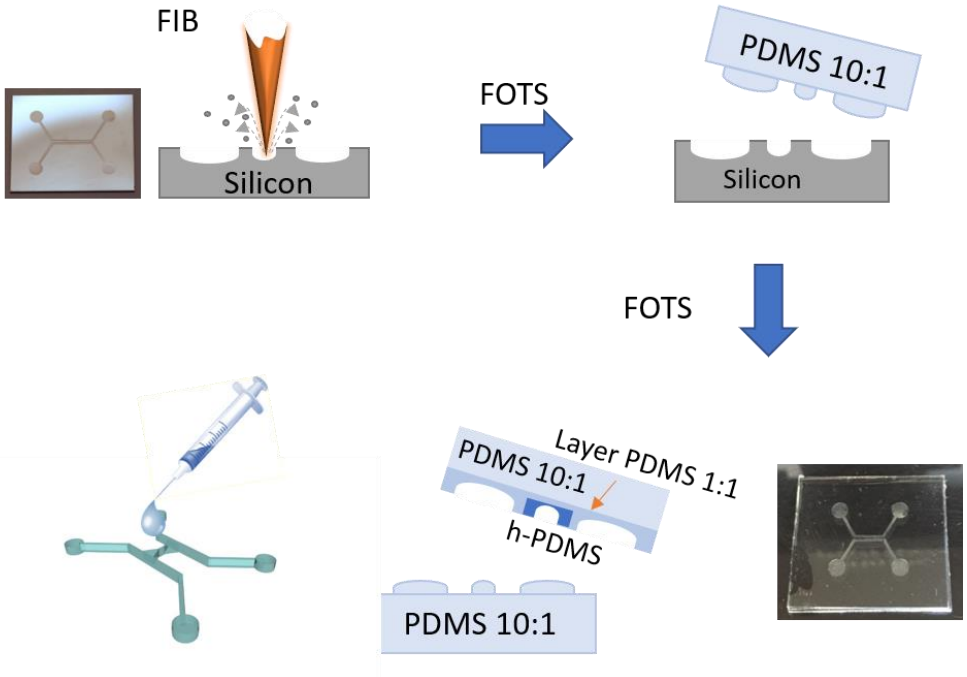

Fig. 5.19 (a) Scheme of the fabrication process of a polymeric nanofluidic device. h-PDMS was poured in a "focused drop-casting" way, i.e. only on the nanostructured region.

Fig. 5.19 shows a schematic representation of the fabrication method developed for exploiting the properties of h-PDMS. In particular, the “roof collapse” problem was solved acting on the second step of the fabrication process, i.e. during the production of the positive replica.

During this phase, h-PDMS was poured on a confined region of the negative replica in order to use the stiffer material only for replicating the nanometric structures of the device. This procedure was called “focused drop-casting”.

5.5.1 Optical detection

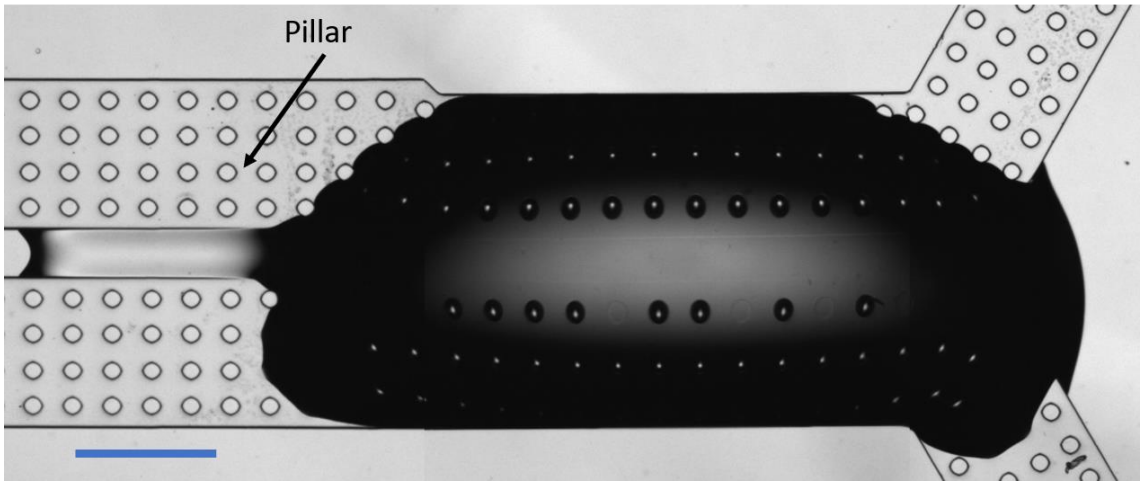

Fig. 5.20 Optical microscope image of the polymeric negative replica with a drop of h-PDMS spread in correspondence of the nanopatterned region. Scale bar 500 µm.

Fig. 5.20 reports the optical microscope image of a h-PDMS drop on the polymeric negative replica. It is possible to observe the polymer spreading horizontally along the gap between the microchannels, covering the entire nanostructure. On the contrary, in the perpendicular direction, it remains confined due to the geometrical configuration of the microchannels that act as a guide, preventing the polymer from widening.

After a short pre-curing of the deposited h-PDMS prepolymer, the leftover negative replica was covered with a thin layer of PDMS 1:1 and then with a thicker layer of PDMS 10:1 to complete the positive replica fabrication. PDMS 1:1 layer was deposited between h-PDMS and PDMS 10:1 in order to decrease the stiffness of the material progressively. Moreover, between the deposition of the two layers, the device was cured for 1h at 68°C.

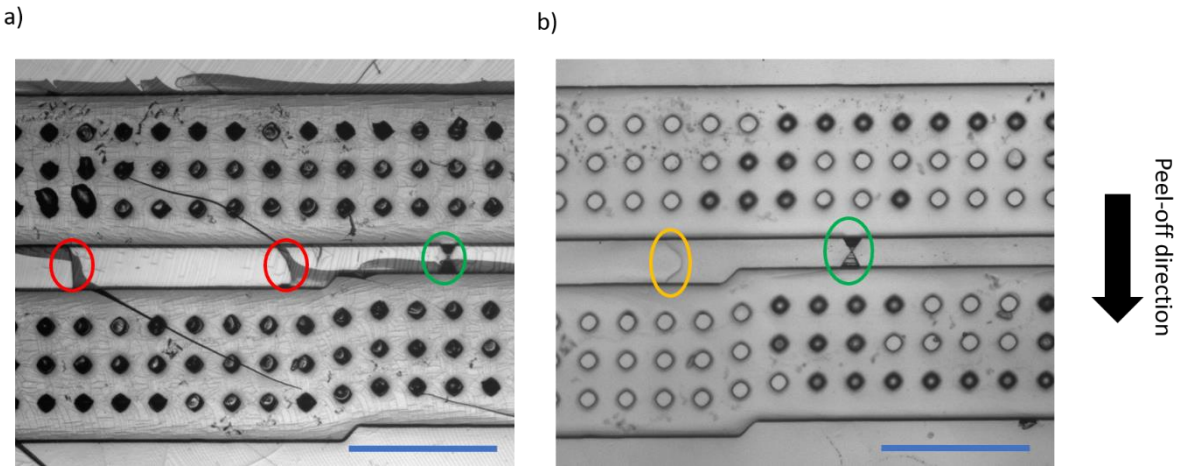

Fig. 5.21 (a) Optical microscope image of a positive replica made with a layer of h-PDMS all over the negative replica surface. This method generates undesired cracks (red circles) while the nanostructure, a short nanochannel linking two trapezoidal access regions, is highlighted by the green circle. (b) Optical microscope images of the positive replica obtained using h-PDMS in a "focused drop-casting" way. No cracks are visible with this procedure. Here, it is possible to observe the interface between the h-PDMS drop and standard PDMS (yellow circle). Scale bar 500 µm.

After the final curing step, the positive replicas were peeled-off and observed by means of optical microscopy. Fig. 5.21 shows optical images of a positive replica made both with the entire layer of h-PDMS and with h-PDMS poured with the "focused drop casting" approach. From the first picture, it is possible to observe several cracks (red circle – Fig. 5.21 a), probably due to the high stiffness of material, that make the device unusable for sensing applications as they represent competitive points of connection, linking the two microchannels. Instead, when h-PDMS is poured with a "focused drop casting" strategy, the positve replica presents planar heterogeneity of the material, in fact from the Fig.21 b - yellow circle is possible to observe the interface h-PDMS/PDMS 1:1. This novel approach allows obtaining a positive replica with stiff nanostructures and

more flexible in the other regions of the device. This means that, with a correct peel off direction (as shown from the black arrow in Fig. 5.21 b) which allows reducing torsion and thanks to the low polymer spreading in that direction, an excellent replica release, without undesired cracks formation can be performed.

After the observation of the positive replica by optical microscopy, the replica was bonded with a glass coverslip and compared with a bonded device made only with PDMS 1:1 and 10:1.

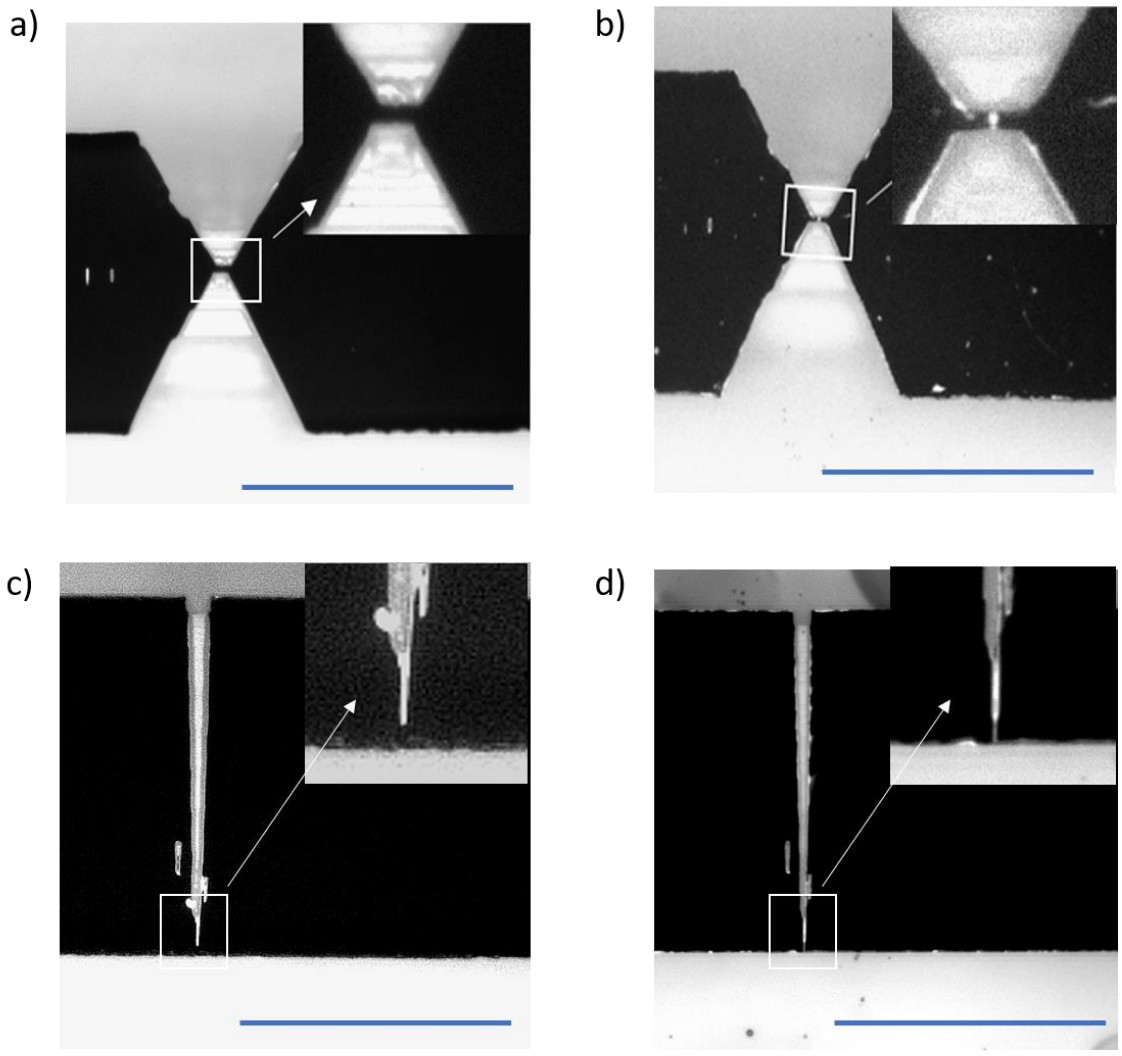

Fig. 5.22 Optical microscope images of (a) hourglass and (c) funnel-shaped nanostructures, after the bonding procedure, made with PDMS 1:1 and PDMS 10:1 (a, c) and made using h-PDMS with the "focused drop-casting" approach (b,d). Insets show a zoom in the nanochannel region that allows appreciating if the collapse occurred or not. Scale bar 100 µm.

Optical microscopy images, acquired in reflection mode, of the bonded nanofluidic devices are shown in Fig. 5.22.

For both nanostructures made with the standard fabrication process, that employs only standard PDMS in 1:1 and 10:1 mixing ratio, the nanochannels tend to completely collapse (see inset of fig 5.22 a-c) causing an interruption between the two microchannels of the nanofluidic devices making them useless for sensing applications. Instead, for devices made with the "focused-drop-casting" strategy, h-PDMS nanochannels did not collapse during the bonding (see inset of fig 5.22 b-d). This means that h-PDMS allows winning the surface interaction between polymeric replica and the glass coverslip, during the bonding procedure, which is the main cause of the roof-collapse phenomenon **[75,76]**.

The obtained single nanochannel in the hourglass devices (see Fig. 5.22 b) has a nominal length of ~ 2 µm, a width of ~ 500 nm and a height of ~ 90 nm, the nanochannel in Fig. 5.22 d has nominal a length of ~ 8 µm, a width of ~ 500 nm and a height of ~ 90 nm.

5.5.2 AFM characterization

In order to analyze the nanochannel dimensions obtained using h-PDMS and Sylgard 184, two NOA casts of the two positive polymeric replicas were fabricated and analyzed by AFM.

The two casts were fabricated bringing into conformal contact the polymeric replica with a glass coverslip and then inserting the resin and curing it under UV-light (see section 4.2.1 for details).

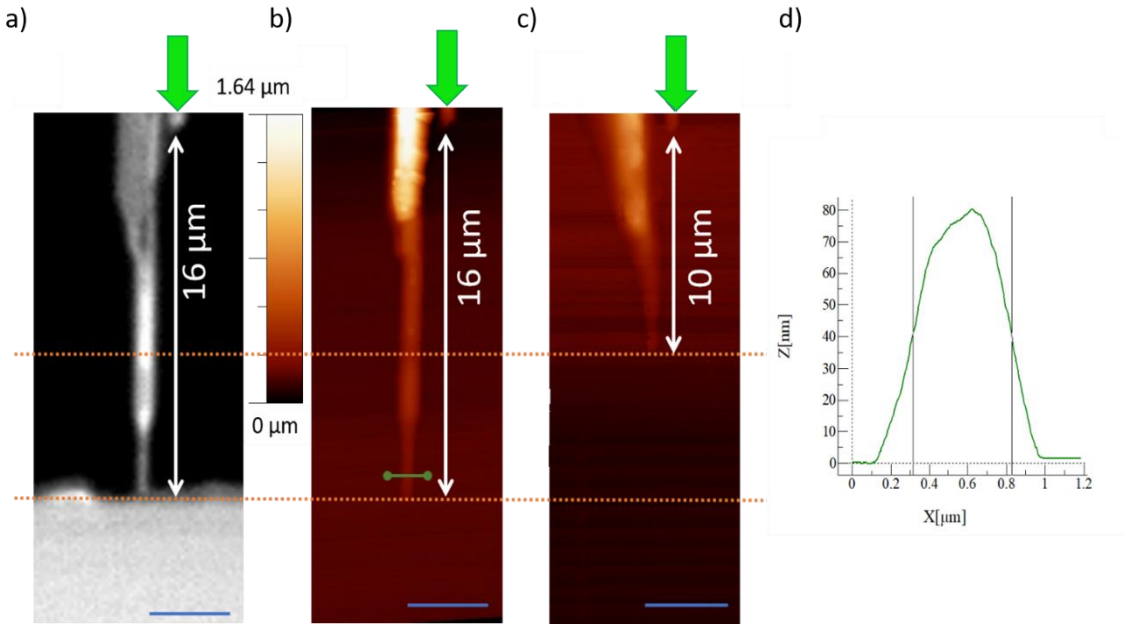

Fig. 5.23 AFM measurements. (a) Optical microscope image of the tip of a nanochannel made with h-PDMS deposited with "focused drop casting" approach. AFM images of the NOA (Norland Optical Adhesive) cast of a funnel-shaped nanochannel made (b) with and (c) without h-PDMS. (d) Height profile acquired in correspondence of the tip in (b). Scale bar 4 µm.

Fig. 5.23 shows two AFM images of the casts of the replicas fabricated with and without the use of h-PDMS, called cast 1 and cast 2 respectively.

The main difference is the distance of the tip from the same reference point (green arrow in Fig. 5.23) that for cast 1 is 16 µm and for cast 2 is 10 µm.

This means that the resin, during the cast fabrication, completely fills nanochannel made with h-PDMS, demonstrating how this material allows replicating with high-fidelity the nanostructures of the master.

On the contrary, when only standard PDMS is used for fabricating replicas, even when I just put into conformal contact, the replica with a glass coverslip, a partial collapse of the nanostructure occurs. This implies that, when the resin is inserted, it does not reach the tip of the channel.

Thus, it is possible to conclude that the cast 2 (made from a standard PDMS replica) collapsed for a length of 6 µm and thus results to be interrupted, while the cast obtained from the h-PDMS replica is open up to the apex, and thus it can properly connect the

two microchannels. The reduction of the nanochannel length is due to the “roof collapse” phenomenon that occurs when the replica is put into contact with the glass. From the topography of the casts near the funnel tip (Fig. 5.23 b – green line), it is possible to trace the profile, reported in Fig. 5.23 d, from which one can estimate the nanochannel’s width and height that result in being 500 nm and 80 nm, respectively.

5.5.3 Electrical characterization

To test the device's functionality, I characterized them through electrical measurements. Two different devices' geometries were studied: funnel and hourglass.

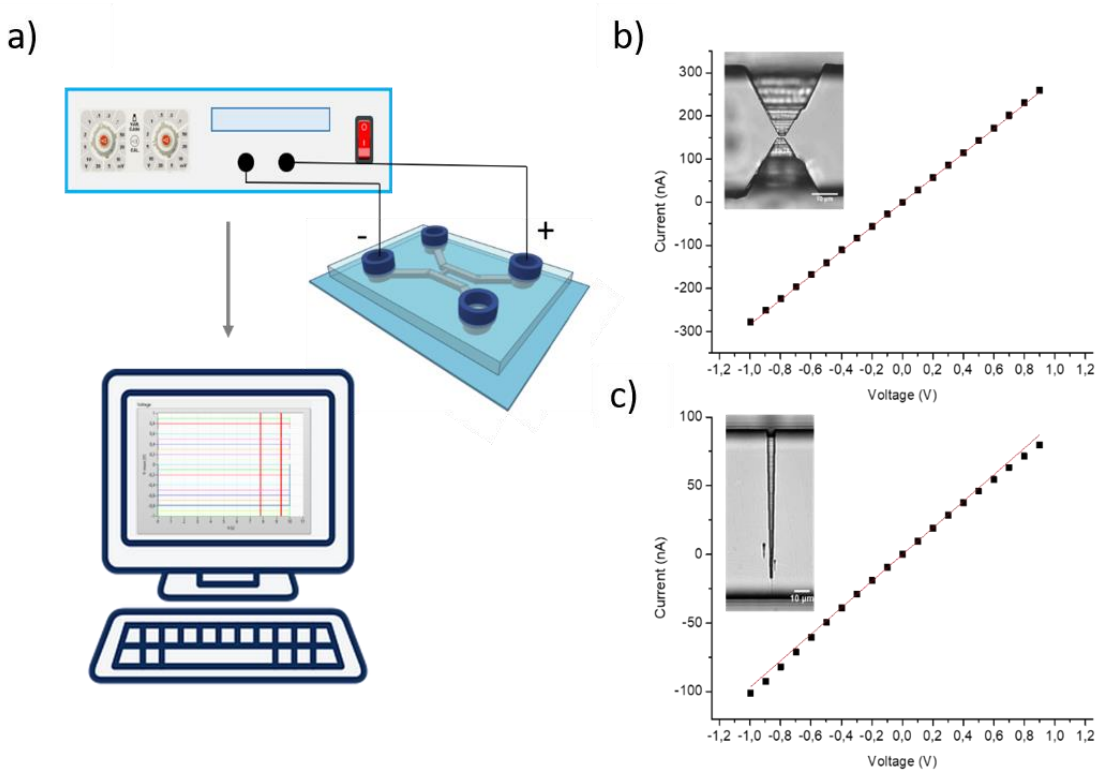

Fig. 5.24 Electrical device characterization. (a) Schematic representation of the electrical measurements set-up. (b) I-V curve of the nanofluidic device provided of an hourglass-shaped nanochannel. The red line represents the linear fitting. (c) I-V curve of the nanofluidic device equipped with a funnel-shaped nanochannel. The red line represents the linear fitting.

Fig 5.24 shows a schematic representation of the experimental set-up used for electrical measurements. The devices were both filled with KCl 1 M and two electrodes were placed across them in order to apply a voltage bias. Applying constant voltages across the device and recording the current, it is possible to determine the nanochannel resistance and from its value understanding if the nanochannel collapsed or not.

The resistance of nanochannels was estimated by a linear fit of the experimental points (red line). For the nanostructure with hourglass geometry the resistance results (3.5 ± 0.1) MΩ and, as expected, the curve had an ohmic behavior while the I–V curve of the funnel geometry shows a slightly rectifying behavior. This response is typically due to the asymmetric geometry of the structure [90] and the estimated resistance is (10.3 ± 0.1) MΩ.

Knowing the resistivity of a KCl 1M solution that is 0.07 Ωm and approximating the nanochannel section with a triangle, a reasonable assumption looking at the profile in Fig 5.23 d it is possible to deduce that the experimental resistance value is consistent with nanochannel's NOA cast dimensions.

Furthermore, the nanochannel dimensions of the positive replica results similar to the nominal dimensions of the device, allowing to confirm the fidelity of the "focused-drop-casting" approach in replicating nanostructures, and to prove the efficiency of this method for the fabrication of devices not affected by leakage or cracks problems, a fundamental advantage when they are employed for electro-kinetic measurements.

The polymeric nanostructures, fabricated with this approach, were exploited for a variety of applications and, in this case, for the development of a new class of nanosensors for single nano-sized objects detection [91].

5.6 Single nanoparticles detection and sizing through RPS

As anticipated in the previous section, in order to use nanofluidic devices as nanosensors capable of detecting single particles, it is necessary that these devices are equipped with nanostructures with well-defined geometry and with dimensions comparable to the objects to be analyzed.

In this section, by combining miniaturized polymeric devices, that have suitable geometry and dimensions, with the RPS (Resistive Pulse Sensing) technique, it is shown how it is possible to perform in-situ, high-sensitivity, label-free and low-cost analysis of single nano-objects.

Based on the size of the nano-objects, two types of devices with different aspect ratios were used, both with symmetric geometry.

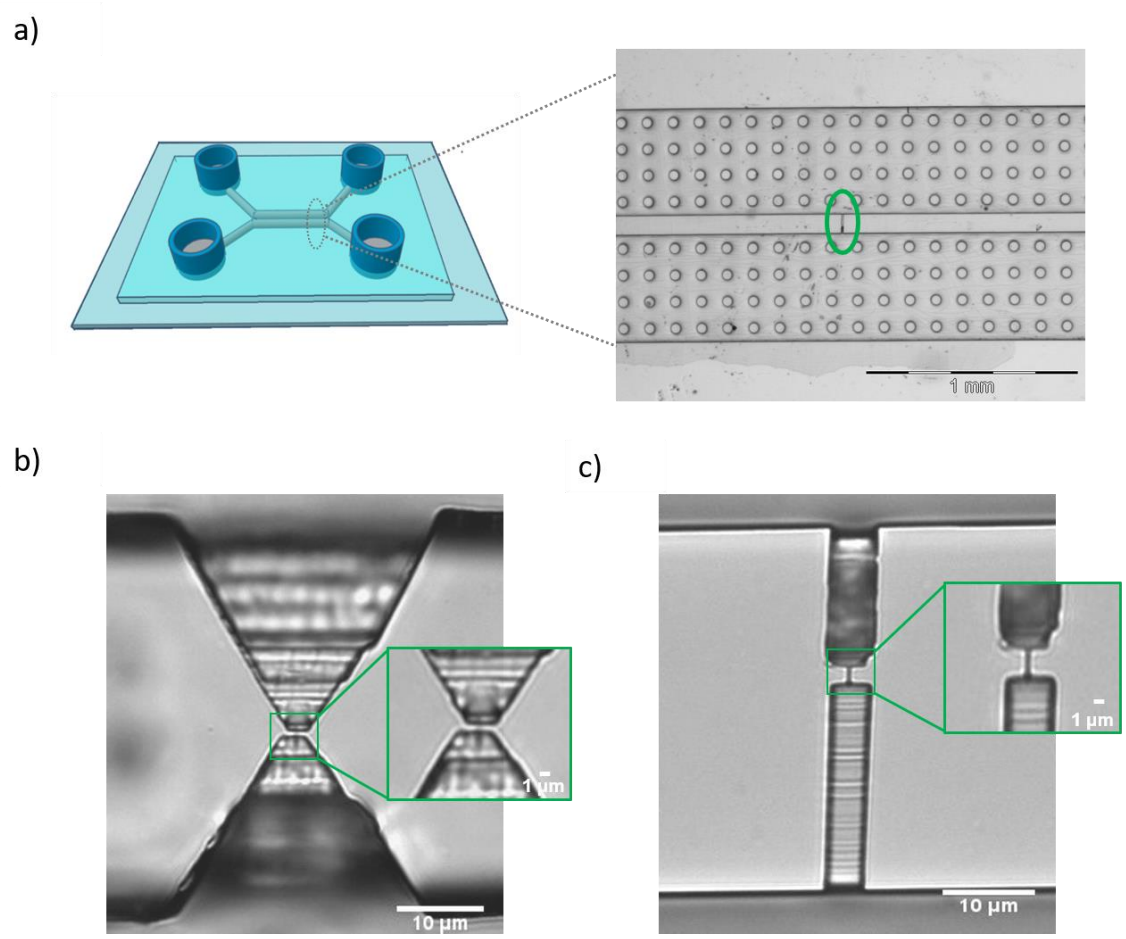

Fig. 5.25 (a) Schematic representation of a nanofluidic sensor and optical microscope image of the central area of the polymeric device. Two pillared microchannels are connected by a nanochannel with trapezoidal access regions Device 1 (b) and rectangular access region device 2 (c).

The first device (Fig 5.25 b) has two trapezoidal access regions and between them a nanochannel with a length of ~ 2 µm, a width of ~ 500 nm, and depth of ~ 90 nm. The second one (Fig 5.25 c) has two rectangular access areas and a longer nanochannel about 4 µm long, 500 nm wide and 800 nm deep. Hereafter, these two devices are called Device 1 and Device 2, respectively.
The insets of Fig 5.25 b and c highlight the functional part of the devices.
Device 1 with an aspect ratio <0.4 was made, using h-PDMS, by means of a "focused drop casting" approach, instead, Device 2, with larger dimensions and an aspect ratio > 0.4, was fabricated without using h-PDMS.

Nano-objects or nanoparticles (NPs) were characterized and studied by the resistive pulse sensing technique. It consists of applying a constant voltage across the device while ionic currents are recorded (see section 4.8 for details); and, when one NP passes through the nanochannel, a typical current blockade, and thus a resistance increase, occurs. The magnitude of the current blockade results proportional to nanoparticle size as foretold by De Blois equation **[92]**:

$$\Delta \boldsymbol{R} = \frac{\boldsymbol{4\pi\rho r^3}}{\boldsymbol{3S^2}}$$

This means that, given the nanochannel dimensions (the cross-section area *S*), working solution resistivity (ρ) and the current variation from which I can determine the nanochannel resistance variation *ΔR*, it is possible to infer a coarse evaluation of the radius *r* of the nanoparticle that is passing through the nanochannel.

5.6.1 40 nm and 100 nm nanoparticles detection

	Device 1		*Device 2*
	40nm Beads	100nm Beads	100nm Beads
Nanochannel Section	$S = (3.5 \pm 0.2) \cdot 10^{-14}\ m^2$	$S = (2.2 \pm 0.1) \cdot 10^{-14}\ m^2$	$S = (1.6 \pm 0.1) \cdot 10^{-13}\ m^2$
Expected Spikes Intensity	$\Delta I = 0.14 \pm 0.02$ nA	$\Delta I = 2.2 \pm 0.2$ nA	$\Delta I = 0.14 \pm 0.02$ nA
Normalized Expected Spikes Intensity	$\Delta I_{norm} = 0.44 \pm 0.05$	$\Delta I_{norm} = 1.9 \pm 0.2$	$\Delta I_{norm} = 0.39 \pm 0.05$

Table 1. Valuation of current spikes intensity expected for 40 nm and 100 nm nanoparticles translocation events. Applied voltage: -300 mV

Table 1 shows the expected current spikes intensities for 40 nm and 100 nm particles translocating through the nanochannel of *Device 1* and of 100 nm particles passing through *Device 2,* respectively. The table highlights that, for a given nanochannel section and for a voltage value of - 300 mV, I should observe spike's in current intensities, due to the nanoparticles' passage in Device 1, of (0.44 ± 0.05) nA and (2.2 ± 0.2) nA for 40 nm and 100 nm, respectively. While, for 100 nm particles detected by *Device 2,* I estimated (0.39± 0.05) nA. All values are normalized.

Experimentally, the voltages were applied with a patch-clamp amplifier and by using Ag/AgCl electrodes in the range of ± 1000 mV. The experiments were performed filling one microchannel with a solution containing nanoparticles, and the other with an electrolytic solution of the same molarity. Constant voltages were applied in order to drive particles through the nanochannel, exploiting electro-kinetic effects.

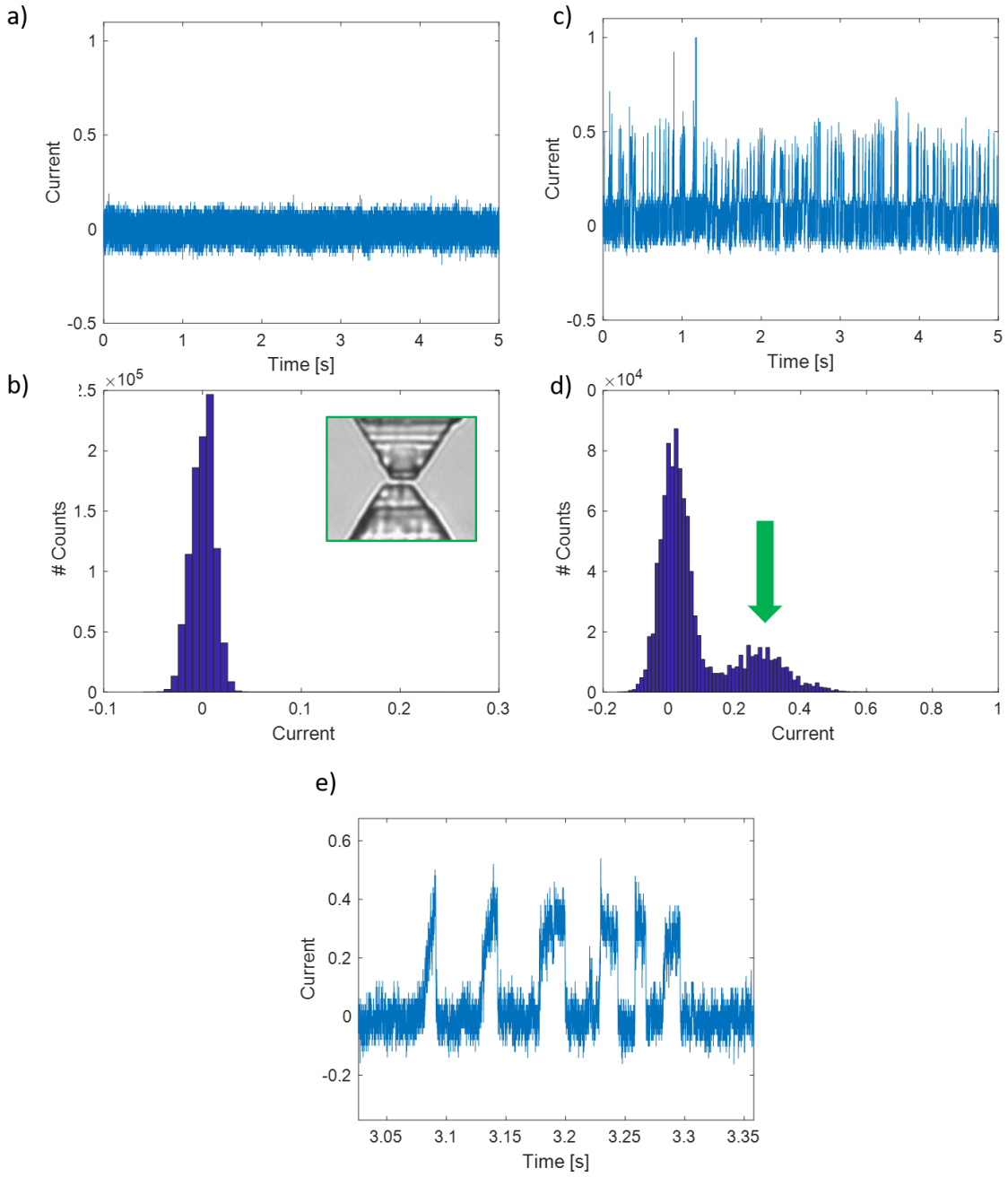

Fig. 5.26 Resistive Pulse Sensing Experiments. (a) Current trace recorded when the device was filled with only KCl 1 M solution, i.e., when the nanochannel is in the open state. (b) Histogram of current distribution levels of the nanochannel in open-state. (c) Current traces recorded when 40 nm beads were inserted in Device 1, (d) and its current levels' distribution. (e) Zoom of the current trace showed in (c). The applied voltage value was -300 mV.

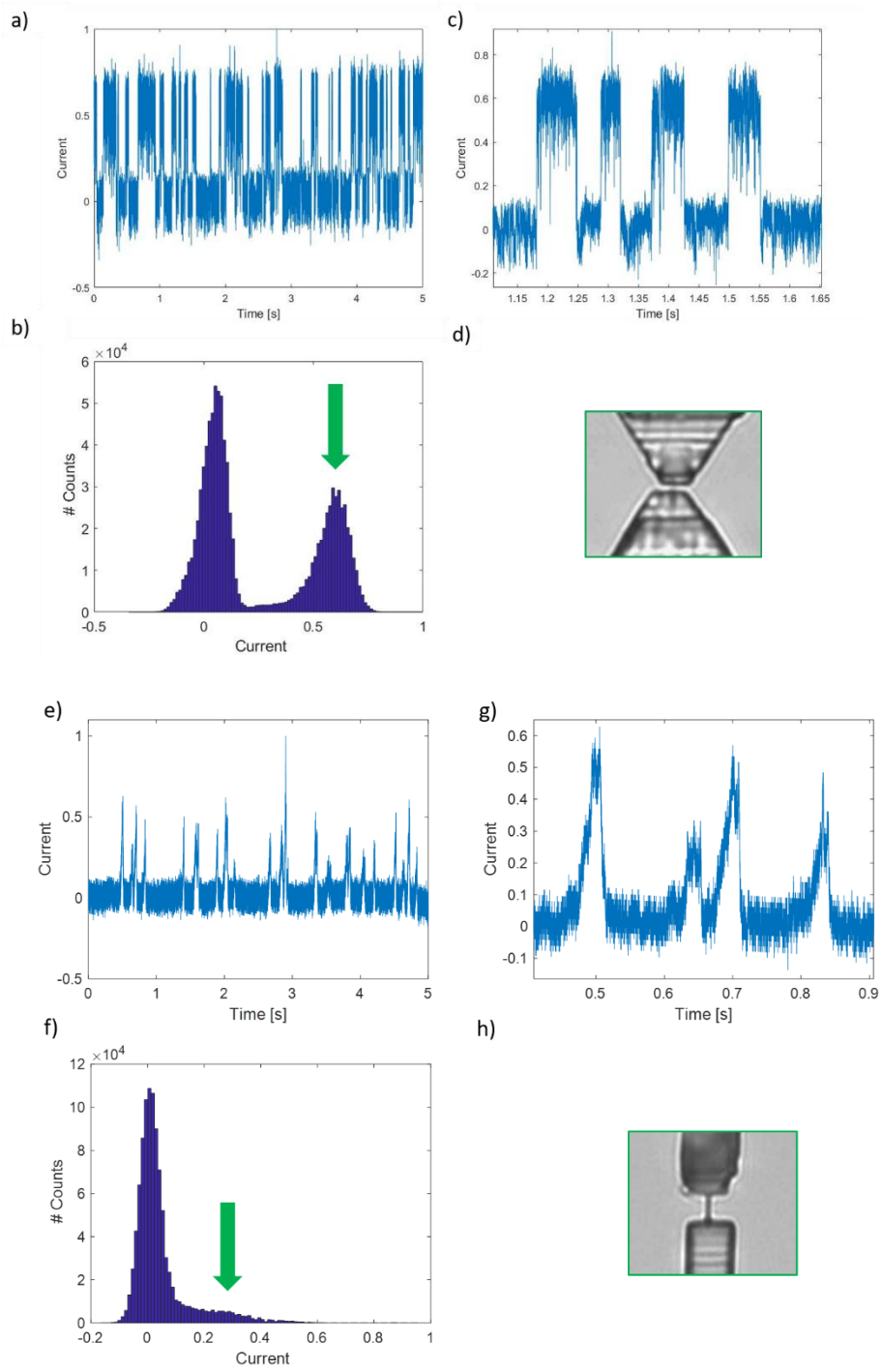

Fig. 5.27 (a) Current traces recorded when a solution with 100 nm beads was inserted in Device 1 and (b) current distribution levels. (c) Zoom of the current trace (a). Image (d) shows the functional nanostructured part of Device 1.
(e) Current traces recorded when a solution with 100 nm beads was inserted in Device 2 and (f) current distribution levels. (g) Zoom of the current trace (e). Image (h) shows the functional nanostructured part of Device 2. Applied voltages were ± 300 mV.

Fig. 5.26 and Fig. 5.27 show RPS signals of 100 nm and 40 nm nanoparticles detected by Device 2 and 1. Good signals were recorded applying ± 300 mV. The resistance values of the nanochannels filled with KCl 1 M, were (1.7 ± 0.1) MΩ and (1.8 ± 0.1) MΩ for Device 2 and 1, respectively.

Fig. 5.26 a shows a current trace recorded after filling the device only with KCl 1 M solutions. The trace resulted in being completely flat with a noise of about 100 pA and 80 pA for Device 1 and 2, respectively. Noise were estimated as the standard deviation of the current signal fluctuations. When NPs are present in solutions (Fig 5.26 c and 5.27 a - e) the acquired current traces show a lot of sudden current drops. Fig 5.26 b-d and Fig 5.27 b-f show histograms of current levels distribution obtained from corresponding current traces analysis.

Only for KCl 1 M, I obtained a symmetric distribution centred on zero because only the open-state nanochannel current was measured. Instead, when the solution with beads was inserted, in all cases, the arise of a new peak were observed in the histograms of the current level distribution. This means that the two current levels registered correspond to two possible device states: open and closed.

The higher peak (centred on zero) corresponds to the channel open state, while the lower peak corresponds to the closed state, i.e., when the nanochannel results partially clogged by the nanoparticle. In other words, the second lower peak arise because of the translocation of nanoparticles through the nanochannel. The lower peaks of histograms are centred on a precise value that represents the mean variation of current intensity related to translocations events. Analysing the recorded current traces, an average spike's magnitude of (0.31 ± 0.07) and (0.62 ± 0.04) for 40 nm and 100 nm beads with Device 1 and (0.36 ± 0.13) for 100nm with Device 2 were determined and all these values are in good agreement with the values estimated with De Blois model (see Table 1). Definitely, RPS technique allows not only to size and count nanoparticle, as disclosed previously, but it also allows studying the nanoparticle's motion inside the nanochannels. In particular, recording current traces when applying different voltages, it has been possible to analyze the spikes behaviour.

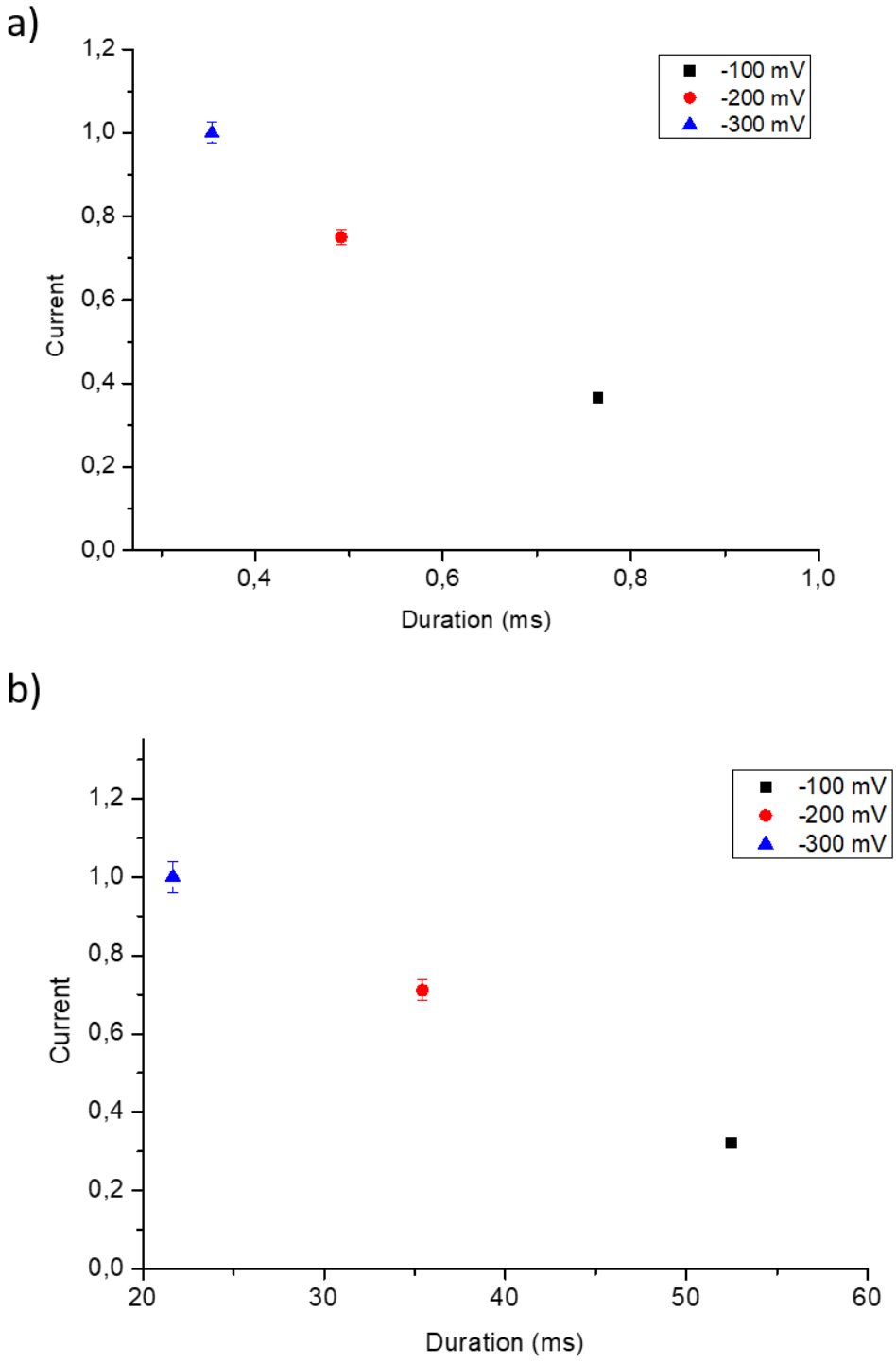

Fig. 5.28 Voltage dependence on current variations during nanoparticles translocations. Average current spike's intensity as a function of event's duration at different applied voltages for 40 nm beads (a) and 100 nm beads (b) detected with Device 1 and Device 2, respectively.

Fig 5.28 shows the average current spikes intensity as a function of the event duration time for 40 nm beads passages in Device 1 and 100 nm beads passages in Device 2. Measurements were performed at -100mV, -200mV and -300mV with KCl 1M as working solution.

The spikes show a similar behaviour for both nanoparticles analysed: at the voltage increase, I recorded a progressive shift of their magnitude towards higher values and a shift of their duration towards shorter values. This means that in both devices nanoparticles tend to translocate faster as the voltage increases.

5.6.2 λ-DNA detection

λ-DNA is a complex molecule of 48502 base pairs, that correspond to ~ 17 μm of contour length. It is known that, when the molecule is in solution, it assumes a "ball-like" conformation, instead, when it is forced to enter a nanoconfined structure, conformational changes take place.

Moreover, DNA represents a good prototype of polymeric complex molecule and it is at the base of many biological processes, so the study of its dynamic behavior under nanoconfinement becomes important. In particular, RPS was exploited to study the conformational changes taking place when λ-DNA is forced to pass through the nanochannel by applying an electric field.

Typically, the dynamic of the passage is divided in two different steps:

(i) The DNA-ball moves close to the nanochannel entrance by diffusion and also for the electrical field applied across the device being a charged molecule.

(ii) The correspondent driving force drags the molecule extremity into the nanochannel forcing it to unroll completely or partially depending both on the force intensity and nanochannel dimensions.

Device 2 was used for detecting and identifying current drops due to λ-DNA translocation through the sensing gate.

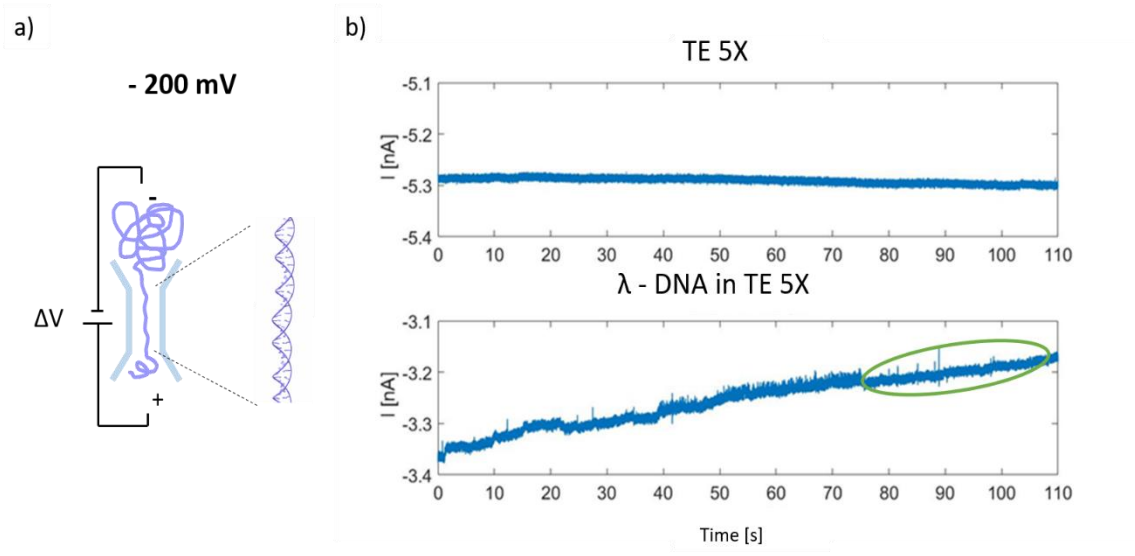

Fig. 5.29 (a) Schematic representation of λ-DNA molecule translocation event through nanochannel. (b) Current trace recorded under -200 mV of voltage application on the device filled with and without λ-DNA.

Fig. 5.29 shows a schematic representation of a λ-DNA molecule translocation event through the nanochannel and the current trace recorded experimentally. The first trace is related to the device filled with TE 5X buffer solution (no λ-DNA), and it is possible to observe a current level of about 5.28 nA and a peak-to-peak noise of 10 pA. Instead, when λ-DNA was diluted in TE 5X, several sudden current variations were visible in the trace. Moreover, from the second trace, besides current spikes, a current drop of 40% and a reduction of the current spike events occurs. This means that λ-DNA tends to stick along the nanochannel walls causing its partial obstruction.

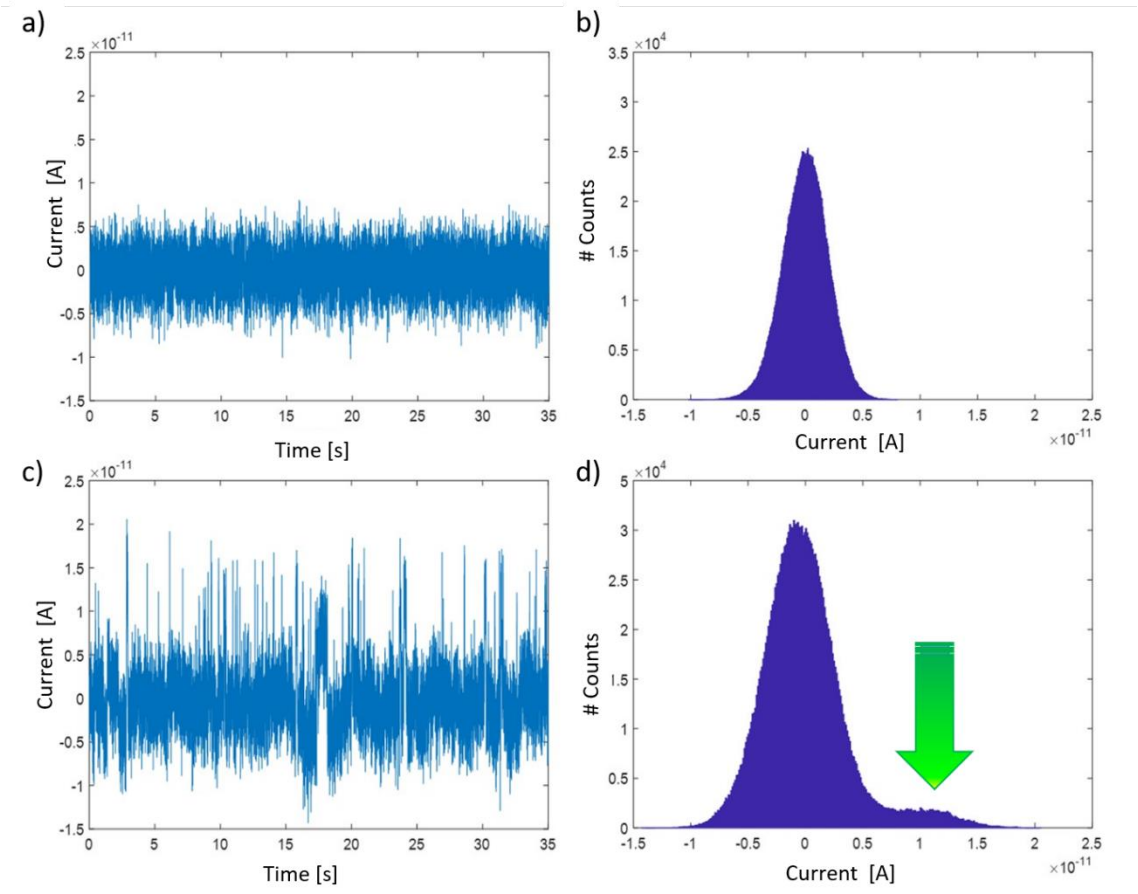

Fig. 5.30 Current trace recorded at -200mV after filling the device (a) with only TE 5X and (c) with λ-DNA diluted in TE 5X solution. (b, d) Histograms of the current level distributions of trace (a) and (d), respectively.

Typically, λ-DNA molecules tend to uncoil even at relatively low voltages (in general from ± 50 mV to ± 300 mV). Fig. 5.30 shows the current measured, at -200 mV, after inserting into *Device 1* a solution of TE 5x with λ-DNA molecules. The current trace recorded and the relative current levels' distribution (Fig. 5.30 d) underline that each biomolecule passage is associated with a current blockade whose average figure is $\Delta I = (13 \pm 2)$ pA. . The average event duration is $t = (8 \pm 1)$ ms .

Also in this case, current traces, recorded for different applied voltages, were analyzed for studying the spikes' behaviour.

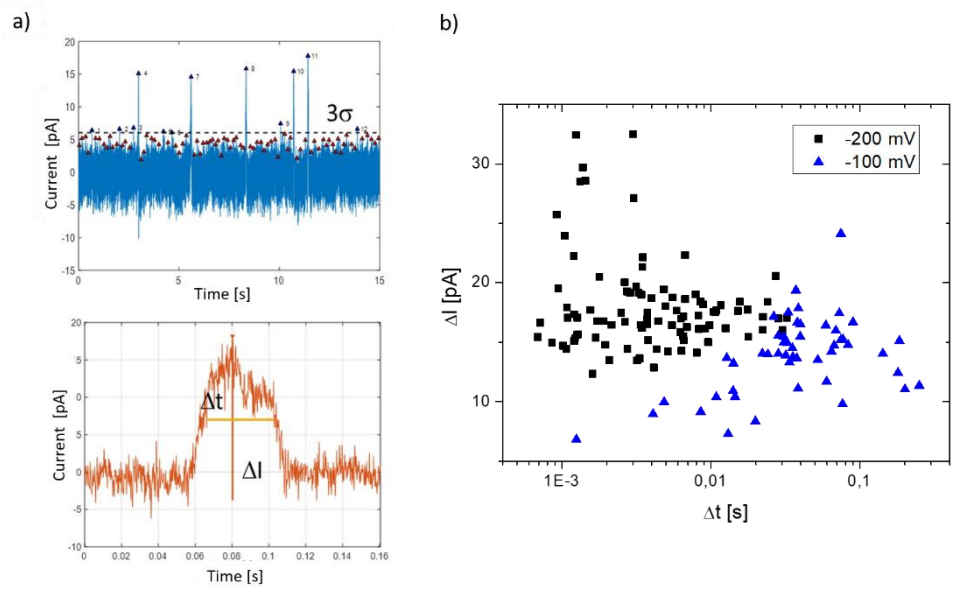

Fig. 5.31 (a) Example of current trace analysis and example of the evaluation of spikes duration and intensity. (b) Distribution of spikes intensities as a function of duration acquired for two different voltages.

Fig. 5.31 is a semi-logarithmic plot of the current spikes as a function of the translocation time estimated from the analysis of the traces acquired at -100 mV and -200 mV. During the analysis, only spikes above a threshold of 3σ were selected and used for calculating the intensity and duration of each spike.

From this analysis, it is evident that the increase of the applied voltage results in an increase of the current spike intensity, a decrease of the event's duration and an increase of events' frequency, in agreement with electrophoretic effects. Furthermore, the decrease of the translocation time is also due to the fact that when raising the voltage, λ-DNA interactions with nanochannel's walls are less frequent, so it tends to enter and transit in the sensing zone much unfolded **[93]**.

In addition, focusing on -200 mV spikes, it is possible to observe (Fig. 5.31 b) several data points with high values of ΔI. Probably, this means that λ-DNA pass through the nanochannel in a partially (one, two, etc…) folded arrangements causing a bigger obstruction and consequently a high current blockage, while in other cases, λ-DNA was supposed to pass unfolded **[92]**. So, it is possible to conclude that the probability to

observe folded λ-DNA passages seem to be greater when electric fields, and thus the driving force, increase.

6. Conclusions

In conclusion, in this Ph.D. thesis I studied, characterized and optimized polymer-based nanofluidic devices. These kinds of devices result very interesting because, currently, they represent good candidates for the exploitation of powerful functionalities offered by nanofluidics in many fields such as in biomedicine and environmental field.

The main advantage of using polymeric materials is represented by their low cost and ease of handling compared to the semiconductor industry-derived materials. In fact, it was seen how soft lithography and poly(dimethylsiloxane) (PDMS) have, since long, been the basic ingredients for producing low-cost, biocompatible and flexible devices, replicating nanostructured masters.

But, because of nanometric dimension of the fluidic device, when the device is sealed with a glass coverslip in order to be watertight, the so-called "roof collapse" phenomenon occurs. This means that the polymeric material limits become evident when the size of the functional part of fluidic devices is shrunk from micro- to nanoscale, compromising the device functionality.

For this reason, I developed two different methods to solve the “roof-collapse” problem in order to fabricate functional nanofluidic devices useful for biosensing applications.

In the first part of the thesis, I demonstrated that, by exploiting a dielectric breakdown-like process, called Junction Gap Breakdown (JGB) technique, it was possible to fabricate, in-situ, a nanoporous region, at the tip of an asymmetric PDMS microfluidic structure, in order to reconnect the two main microchannels of the fluidic device.

Devices fabricated in this manner show marked ionic current rectification features, when filled with high ionic strength solutions. Moreover, this nanoporous region can be used as an accumulation area that was exploited for sensing applications.

Indeed, studing the distribution of fluorescein diluted KCl solutions at different molarity, it was observed, exploiting the Ion Concentration Polarization (ICP) phenomenon, that the probe tends to accumulate inside the funnel and the accumulation results stronger and more evident for low molarity solutions.

This behavior makes these devices good candidates for developing high sensitivity detectors.

Indeed, combining the accumulation phenomenon, governed by electro-hydrokinetic effects, that occurs when applying high voltage across the device, and an appropriate functionalization of the nanochannel walls with antibodies (IL 10 antibodies) linked by using APTES (3-Aminopropyl)triethoxysilane and GA (Glutaraldheyde), I have demonstrate how it was possible to improve the sensing limit for the detection of one or several targeted counterparts (i.e. IL 10 antigens). In particular, only through fluorescence optical microscopy, I was able to evaluate the uptake of a specific antigen, diluted in solution (from 12.5 pg/ml to 1.25 pg/ml), to the nanochannel surface functionalized with antibodies. In this condition, I successfully detected antigen-antibody binding on the surface of the nanostructure. This represents a promising step for fabricating a high-sensitivity nanofluidic immunoassay sensors.

In the second part of the thesis, to overcome the “collapse” problem a new fabrication strategy was developed to make the nanostructured parts stiffer than the others region of the replica.

I have developed a “focused-drop casting” approach for fabricating polymeric nanofluidic devices hosting nanochannels of different geometries. This approach has

allowed to easily obtain sub-100 nm nanostructures with an aspect ratio less than 0.4. In particular, to avoid the collapse phenomenon, we optimized the fabrication process by exploiting the larger stiffness of h-PDMS, yet avoiding the drawbacks brought by its introduction.

In particular, I exploited a “focused drop-casting” approach, that consist in the pouring of h-PDMS only on the nanostructured region. This approach allows to making only the nanochannels stiffer avoiding their collapse during the bonding procedure. At the same time it left the other regions of the device flexible enough to prevent the formation of undesired cracks. The method described provides a powerful and simple solution for making polymeric nanofluidic systems, reducing the fabrication costs and improving their reliability.

These platforms, thus fabricated, represent a powerful tool for detecting and characterizing nanoparticles, DNA and nano-objects in general by means of the Resistive Pulse Sensing method. In particular, they were used for detecting and sizing nanoparticles as small as 40 nm showing a high sensitivity and reliability. Sensing experiments for detecting λ-DNA molecules were also validated.

Definitely, these platforms based on nanofluidic principles may result very useful both in the biomedical field allowing to study several biomolecules that usually are related to specific pathologies and in the environmental field allowing to detect nanoplastics and nano-powders that nowadays represent one of the most dangerous sources of pollution.

7. Publications

1. “Increased flexibility in lab-on-chip design with a polymer patchwork approach”

   D. Pezzuoli, E. Angeli, D. Repetto, P. Guida, G. Firpo and L. Repetto

   Nanotmaterials (2019) DOI: 10.3390/nano9121678

2. “Junction gap breakdown-based fabrication of PDMS ionic rectifiers”

   D. Pezzuoli & E. Angeli, D. Repetto, P. Guida, G. Firpo, R. Lo Savio, L. Repetto and U. Valbusa

   Journal of Micromechanics and Microengineering (2019) DOI: 10.1088/1361-6439/ab5fa9

3. “Nanofluidic concentration for high-sensitivity immunoassay”

   D. Pezzuoli & E. Angeli, D. Repetto, P. Guida, G. Firpo, R. Lo Savio, L. Repetto and U. Valbusa (Submitted-2020)
   Sensors- 734896

4. “The role of surfaces in gas transport through polymer membranes”

   G. Firpo, E. Angeli, P. Guida, D. Pezzuoli, D. Repetto, L. Repetto and U. Valbusa, *Polymers* (2019) DOI: 10.3390/polym11050910

5. “Enhancing miRNAs Capture on Polydimethylsiloxane Surface Nanostructuration”

   P. Guida, R. Lo Savio, C. Potrich, V. Vaghi, E. Angeli, L. Vanzetti, D. Pezzuoli, L. Pasquadrini, G. Firpo, L. Repetto, D. Repetto, C. Pederzolli and U. Valbusa
   Journal of J Nanomedicine & Nanotechnology (2017) DOI: 10.4172/2157-7439.1000437

8. Attended Conferences

1. Workshop participation at “Luce per la Biofisica” (Parma, 7 June 2019)
2. “Development of nanofluidic devices for DNA detection and nanoparticles sizing” D. Pezzuoli, E. Angeli, P.Guida, G. Firpo, R. Lo Savio, L. Repetto and U. Valbusa, Biophysics at Rome (Rome, 15-16 May 2019) **ORAL PRESENTATION**.
3. “Nanofluidic chip for DNA and nanoparticles detection and manipulation” D. Pezzuoli, E. Angeli, D. Repetto, G. Firpo, P. Guida, R. Lo Savio, L. Repetto and U. Valbusa 63nd Biophysical Society Annual Meeting (Baltimore, 2-6 March 2019, MD, USA) **POSTER.**
4. “Nanofluidic devices for nano-plastics label-free detection” D. Pezzuoli, E. Angeli, D. Repetto, G. Firpo, P. Guida, R. Lo Savio, L. Repetto and U. Valbusa. ICOBSI-Nanomax (Firenze, 17-20 December 2018) **ORAL PRESENTATION**.
5. “High sensitivity miniaturized immunoassay sensor based on biomolecules concentration phenomena at nanoscale” D. Pezzuoli, E. Angeli, D. Repetto, F. Ferrera, G. Firpo, P. Guida, R. Lo Savio, L. Repetto, U. Valbusa. SIBPA XXIV National Conference (Ancona, 10-13 September 2018) **POSTER.**
6. “Fabrication and characterization of elastomeric nanofluidic device for nanoparticles’ sizing and counting” D. Pezzuoli, E. Angeli, A. Voiello, G. Firpo, P. Guida, R. Lo Savio, D. Repetto, L. Repetto, U. Valbusa Nanofluidics in Physics and Biology (Lyon, France, 9-12 July 2018) **POSTER.**
7. “Nanofluidic Sensor for Antigen-Antibody Binding Detection” D. Pezzuoli, A. Cazzulo, E. Angeli, F. Ferrera, G. Firpo, P.Guida, R. Lo Savio, D.Repetto, L.Repetto, U. Valbusa. 62nd Biophysical Society Annual Meeting (San Francisco, 17-21 February 2018, CA, USA) **ORAL PRESENTATION.**

References

[1] Richard P. Feynman 1960 There's Plenty of Room at the Bottom *There's Plenty of Room at the Bottom*

[2] N. Taniguchi 1974 On the Basic Concept of "Nano-Technology" *Proc. Intl. Conf. Prod. Eng. Tokyo, Part II,*

[3] V.M. Arole, S.V. Munde A V M and Munde S. V. 2014 Fabrication of nanomaterials by top-down and bottom-up approaches - An overview **1** 89–93

[4] Wei R, Gatterdam V, Wieneke R, Tampé R and Rant U 2012 Stochastic sensing of proteins with receptor-modified solid-state nanopores *Nature Nanotech* **7** 257–63

[5] Han A, Creus M, Schürmann G, Linder V, Ward T R, de Rooij N F and Staufer U 2008 Label-Free Detection of Single Protein Molecules and Protein−Protein Interactions Using Synthetic Nanopores *Anal. Chem.* **80** 4651–8

[6] Fan R, Karnik R, Yue M, Li D, Majumdar A and Yang P 2005 DNA Translocation in Inorganic Nanotubes *Nano Lett.* **5** 1633–7

[7] Menard L D and Ramsey J M 2013 Electrokinetically-Driven Transport of DNA through Focused Ion Beam Milled Nanofluidic Channels *Anal. Chem.* **85** 1146–53

[8] Harms Z D, Mogensen K B, Nunes P S, Zhou K, Hildenbrand B W, Mitra I, Tan Z, Zlotnick A, Kutter J P and Jacobson S C 2011 Nanofluidic Devices with Two Pores in Series for Resistive-Pulse Sensing of Single Virus Capsids *Anal. Chem.* **83** 9573–8

[9] Mitra A, Deutsch B, Ignatovich F, Dykes C and Novotny L 2010 Nano-optofluidic Detection of Single Viruses and Nanoparticles *ACS Nano* **4** 1305–12

[10] Yang L and Yamamoto T 2016 Quantification of Virus Particles Using Nanopore-Based Resistive-Pulse Sensing Techniques *Front. Microbiol.* **7**

[11] Abgrall P and Nguyen N-T 2009 *Nanofluidics* (Boston: Artech House)

[12] Bruus H 2008 *Theoretical microfluidics* (Oxford ; New York: Oxford University Press)

[13] Nguyen N-T and Wereley S T 2006 *Fundamentals and applications of microfluidics* (Boston: Artech House)

[14] Schoch R B, Han J and Renaud P 2008 Transport phenomena in nanofluidics *Reviews of Modern Physics* **80** 839–83

[15] Kirby B J 2010 *Micro- and nanoscale fluid mechanics: transport in microfluidic devices* (New York: Cambridge University Press)

[16] Dukhin A S 2017 *Characterization of liquids, dispersions, emulsions, and porous materials using ultrasound* (Amsterdam, Netherland ; Cambridge, MA: Elsevier)

[17] Hałka-Grysińska A, Gwarda R Ł and Dzido T H 2016 Planar chromatography using electroosmotic flow *Forced-Flow Layer Chromatography* (Elsevier) pp 223–83

[18] Kim M, Beskok A and Kihm K 2002 Electro-osmosis-driven micro-channel flows: A comparative study of microscopic particle image velocimetry measurements and numerical simulations *Exp Fluids* **33** 170–80

[19] Wu D, Qin J and Lin B 2008 Electrophoretic separations on microfluidic chips *Journal of Chromatography A* **1184** 542–59

[20] Smoluchowski 1903 Contribution à la théorie de l'endosmose électrique et de quelques phénomènes corrélatifs (ut supra) **8** 182–199

[21] Hückel, E 1924 Die kataphorese der kugel **25** 204

[22] Li D 2014 Single-Phase Electrokinetic Flow in Microchannels *Heat Transfer and Fluid Flow in Minichannels and Microchannels* (Elsevier) pp 175–219

[23] Yager P, Edwards T, Fu E, Helton K, Nelson K, Tam M R and Weigl B H 2006 Microfluidic diagnostic technologies for global public health *Nature* **442** 412–8

[24] Duan C, Wang W and Xie Q 2013 Review article: Fabrication of nanofluidic devices *Biomicrofluidics* **7** 026501

[25] Pimpin A and Srituravanich W 2012 Review on Micro- and Nanolithography Techniques and their Applications *EJ* **16** 37–56

[26] Wang Z M 2013 *FIB Nanostructures* (Cham: Springer)

[27] Li H-W, Kang D-J, Blamire M G and Huck W T S 2003 Focused ion beam fabrication of silicon print masters *Nanotechnology* **14** 220–3

[28] Frey L, Lehrer C and Ryssel H 2003 Nanoscale effects in focused ion beam processing *Applied Physics A: Materials Science & Processing* **76** 1017–23

[29] Sahin O, Ashokkumar M and Ajayan P M 2018 Micro- and nanopatterning of biomaterial surfaces *Fundamental Biomaterials: Metals* (Elsevier) pp 67–78

[30] De Paoli F. 2015 *Measuring Polydimethylsiloxane (PDMS) Mechanical Properties Using Flat Punch Nanoindentation Focusing on Obtaining Full Contact* (University of South Florida)

[31] Xia Y, McClelland J J, Gupta R, Qin D, Zhao X-M, Sohn L L, Celotta R J and Whitesides G M 1997 Replica molding using polymeric materials: A practical step toward nanomanufacturing *Adv. Mater.* **9** 147–9

[32] Rechnitz G A, Kobos R K, Riechel S J and Gebauer C R 1977 A bio-selective membrane electrode prepared with living bacterial cells *Analytica Chimica Acta* **94** 357–65

[33] Napoli M, Eijkel J C T and Pennathur S 2010 Nanofluidic technology for biomolecule applications: a critical review *Lab Chip* **10** 957

[34] Bakajin O, Duke T A J, Tegenfeldt J, Chou C-F, Chan S S, Austin R H and Cox E C 2001 Separation of 100-Kilobase DNA Molecules in 10 Seconds *Anal. Chem.* **73** 6053–6

[35] Yeh J-W, Sriram K K, Taloni A, Chen Y-L and Chou C-F 2015 Quantitative analysis of reptation of partially extended DNA in sub-30 nm nanoslits *arXiv:1502.05115 [cond-mat, physics:physics]*

[36] Yamamoto T 2012 Single molecular level analysis and processing in nanochannels *Front Biosci* **S4** 1461–74

[37] Han J and Craighead H G 1999 Entropic trapping and sieving of long DNA molecules in a nanofluidic channel *Journal of Vacuum Science & Technology A: Vacuum, Surfaces, and Films* **17** 2142–7

[38] Turner S W P, Cabodi M and Craighead H G 2002 Confinement-Induced Entropic Recoil of Single DNA Molecules in a Nanofluidic Structure *Phys. Rev. Lett.* **88** 128103

[39] Pennathur S, Baldessari F, Santiago J G, Kattah M G, Steinman J B and Utz P J 2007 Free-Solution Oligonucleotide Separation in Nanoscale Channels *Anal. Chem.* **79** 8316–22

[40] Karnik R, Castelino K and Majumdar A 2006 Field-effect control of protein transport in a nanofluidic transistor circuit *Appl. Phys. Lett.* **88** 123114

[41] Fu J, Schoch R B, Stevens A L, Tannenbaum S R and Han J 2007 A patterned anisotropic nanofluidic sieving structure for continuous-flow separation of DNA and proteins *Nature Nanotech* **2** 121–8

[42] Foote R S, Khandurina J, Jacobson S C and Ramsey J M 2005 Preconcentration of Proteins on Microfluidic Devices Using Porous Silica Membranes *Anal. Chem.* **77** 57–63

[43] Eggenberger O M, Ying C and Mayer M 2019 Surface coatings for solid-state nanopores *Nanoscale* **11** 19636–57

[44] Sparreboom W, van den Berg A and Eijkel J C T 2010 Transport in nanofluidic systems: a review of theory and applications *New J. Phys.* **12** 015004

[45] Dai J, Ito T, Sun L and Crooks R M 2003 Electrokinetic Trapping and Concentration Enrichment of DNA in a Microfluidic Channel *J. Am. Chem. Soc.* **125** 13026–7

[46] Kim S J, Song Y-A and Han J 2010 Nanofluidic concentration devices for biomolecules utilizing ion concentration polarization: theory, fabrication, and applications *Chem. Soc. Rev.* **39** 912

[47] Zhang Y and Timperman A T 2003 Integration of nanocapillary arrays into microfluidic devices for use as analyte concentrators *Analyst* **128** 537

[48] Wang Y-C, Stevens A L and Han J 2005 Million-fold Preconcentration of Proteins and Peptides by Nanofluidic Filter *Anal. Chem.* **77** 4293–9

[49] Findlay J W A, Smith W C, Lee J W, Nordblom G D, Das I, DeSilva B S, Khan M N and Bowsher R R 2000 Validation of immunoassays for bioanalysis: a pharmaceutical industry perspective *Journal of Pharmaceutical and Biomedical Analysis* **21** 1249–73

[50] Li D 2014 Nanofluidic Systems for Single-Molecule Detection *Encyclopedia of Microfluidics and Nanofluidics* ed D Li (Boston, MA: Springer US) pp 1–8

[51] Kasianowicz J J, Brandin E, Branton D and Deamer D W 1996 Characterization of individual polynucleotide molecules using a membrane channel *Proceedings of the National Academy of Sciences* **93** 13770–3

[52] Lyon W A and Nie S 1997 Confinement and Detection of Single Molecules in Submicrometer Channels *Anal. Chem.* **69** 3400–5

[53] Foquet M, Korlach J, Zipfel W R, Webb W W and Craighead H G 2004 Focal Volume Confinement by Submicrometer-Sized Fluidic Channels *Anal. Chem.* **76** 1618–26

[54] Komal Saxena K S, Sapna Jain, D. K. Sharma, Rajiv Dua and Mohit Kamthania 2014 Applications of Integrated Microfluidic Devices in Environmental Monitoring: A Review 521–30

[55] Kalogerakis N, Karkanorachaki K, Kalogerakis G C, Triantafyllidi E I, Gotsis A D, Partsinevelos P and Fava F 2017 Microplastics Generation: Onset of Fragmentation of Polyethylene Films in Marine Environment Mesocosms *Front. Mar. Sci.* **4**

[56] Koelmans A A, Besseling E and Shim W J 2015 Nanoplastics in the Aquatic Environment. Critical Review *Marine Anthropogenic Litter* ed M Bergmann, L Gutow and M Klages (Cham: Springer International Publishing) pp 325–40

[57] Ng E-L, Huerta Lwanga E, Eldridge S M, Johnston P, Hu H-W, Geissen V and Chen D 2018 An overview of microplastic and nanoplastic pollution in agroecosystems *Science of The Total Environment* **627** 1377–88

[58] Bhargava S, Chen Lee S S, Min Ying L S, Neo M L, Lay-Ming Teo S and Valiyaveettil S 2018 Fate of Nanoplastics in Marine Larvae: A Case Study Using Barnacles, *Amphibalanus amphitrite ACS Sustainable Chem. Eng.* **6** 6932–40

[59] Jeong C-B, Kang H-M, Lee Y H, Kim M-S, Lee J-S, Seo J S, Wang M and Lee J-S 2018 Nanoplastic Ingestion Enhances Toxicity of Persistent Organic Pollutants (POPs) in the Monogonont Rotifer *Brachionus koreanus* via Multixenobiotic Resistance (MXR) Disruption *Environ. Sci. Technol.* **52** 11411–8

[60] Qu M, Nida A, Kong Y, Du H, Xiao G and Wang D 2019 Nanopolystyrene at predicted environmental concentration enhances microcystin-LR toxicity by inducing intestinal damage in Caenorhabditis elegans *Ecotoxicology and Environmental Safety* **183** 109568

[61] Lehner R, Weder C, Petri-Fink A and Rothen-Rutishauser B 2019 Emergence of Nanoplastic in the Environment and Possible Impact on Human Health *Environ. Sci. Technol.* **53** 1748–65

[62] Fanzio P, Manneschi C, Angeli E, Mussi V, Firpo G, Ceseracciu L, Repetto L and Valbusa U 2012 Modulating DNA Translocation by a Controlled Deformation of a PDMS Nanochannel Device *Scientific Reports* **2**

[63] Manneschi C, Fanzio P, Ala-Nissila T, Angeli E, Repetto L, Firpo G and Valbusa U 2014 Stretching of DNA confined in nanochannels with charged walls *Biomicrofluidics* **8** 064121

[64] Delamarche E, Schmid H, Michel B and Biebuyck H 1997 Stability of molded polydimethylsiloxane microstructures *Adv. Mater.* **9** 741–6

[65] Choi K M and Rogers J A 2003 A Photocurable Poly(dimethylsiloxane) Chemistry Designed for Soft Lithographic Molding and Printing in the Nanometer Regime *J. Am. Chem. Soc.* **125** 4060–1

[66] Bhattacharya S, Datta A, Berg J M and Gangopadhyay S 2005 Studies on surface wettability of poly(dimethyl) siloxane (PDMS) and glass under oxygen-plasma treatment and correlation with bond strength *J. Microelectromech. Syst.* **14** 590–7

[67] Seghir R and Arscott S 2015 Extended PDMS stiffness range for flexible systems *Sensors and Actuators A: Physical* **230** 33–9

[68] Kuddannaya S, Chuah Y J, Lee M H A, Menon N V, Kang Y and Zhang Y 2013 Surface Chemical Modification of Poly(dimethylsiloxane) for the Enhanced Adhesion and Proliferation of Mesenchymal Stem Cells *ACS Applied Materials & Interfaces* **5** 9777–84

[69] Kim D and Herr A E 2013 Protein immobilization techniques for microfluidic assays *Biomicrofluidics* **7** 041501

[70] Abrosimova K V, Shulenina O V and Paston S V 2016 FTIR study of secondary structure of bovine serum albumin and ovalbumin *Journal of Physics: Conference Series* **769** 012016

[71] Carneiro L B, Ferreira J, Santos M J L, Monteiro J P and Girotto E M 2011 A new approach to immobilize poly(vinyl alcohol) on poly(dimethylsiloxane) resulting in low protein adsorption *Applied Surface Science* **257** 10514–9

[72] Harrer S, Kim S C, Schieber C, Kannam S, Gunn N, Moore S, Scott D, Bathgate R, Skafidas S and Wagner J M 2015 Label-free screening of single biomolecules through resistive pulse sensing technology for precision medicine applications *Nanotechnology* **26** 182502

[73] Song Y, Zhang J and Li D 2017 Microfluidic and Nanofluidic Resistive Pulse Sensing: A Review *Micromachines* **8** 204

[74] Vaclavek T, Prikryl J and Foret F 2019 Resistive pulse sensing as particle counting and sizing method in microfluidic systems: Designs and applications review *J. Sep. Sci.* **42** 445–57

[75] Zhou W, Huang Y, Menard E, Aluru N R, Rogers J A and Alleyne A G 2005 Mechanism for stamp collapse in soft lithography *Appl. Phys. Lett.* **87** 251925

[76] Huang Y Y, Zhou W, Hsia K J, Menard E, Park J-U, Rogers J A and Alleyne A G 2005 Stamp Collapse in Soft Lithography *Langmuir* **21** 8058–68

[77] Hsia K J, Huang Y, Menard E, Park J-U, Zhou W, Rogers J and Fulton J M 2005 Collapse of stamps for soft lithography due to interfacial adhesion *Appl. Phys. Lett.* **86** 154106

[78] Momotenko D and Girault H H 2011 Scan-Rate-Dependent Ion Current Rectification and Rectification Inversion in Charged Conical Nanopores *J. Am. Chem. Soc.* **133** 14496–9

[79] White H S and Bund A 2008 Ion Current Rectification at Nanopores in Glass Membranes *Langmuir* **24** 2212–8

[80] Sa N and Baker L A 2013 Experiment and Simulation of Ion Transport through Nanopipettes of Well-Defined Conical Geometry *J. Electrochem. Soc.* **160** H376–81

[81] Fu L-M, Hou H-H, Chiu P-H and Yang R-J 2018 Sample preconcentration from dilute solutions on micro/nanofluidic platforms: A review *ELECTROPHORESIS* **39** 289–310

[82] Zangle T A, Mani A and Santiago J G 2010 Theory and experiments of concentration polarization and ion focusing at microchannel and nanochannel interfaces *Chem. Soc. Rev.* **39** 1014

[83] Harshil D. Dhruv 2009 *CONTROLLING NONSPECIFIC ADSORPTION OF PROTEINS AT BIOINTERFACES FOR BIOSENSOR AND BIOMEDICAL APPLICATIONS* (Logan, Utah: Utah State University)

[84] Gates B D, Xu Q, Stewart M, Ryan D, Willson C G and Whitesides G M 2005 New Approaches to Nanofabrication: Molding, Printing, and Other Techniques *Chem. Rev.* **105** 1171–96

[85] Tseng A A 2004 Recent developments in micromilling using focused ion beam technology *J. Micromech. Microeng.* **14** R15–34

[86] Altissimo M 2010 E-beam lithography for micro-/nanofabrication *Biomicrofluidics* **4** 026503

[87] Chantiwas R, Hupert M L, Pullagurla S R, Balamurugan S, Tamarit-López J, Park S, Datta P, Goettert J, Cho Y-K and Soper S A 2010 Simple replication methods for producing nanoslits in thermoplastics and the transport dynamics of double-stranded DNA through these slits *Lab Chip* **10** 3255

[88] McDonald J C, Duffy D C, Anderson J R, Chiu D T, Wu H, Schueller O J and Whitesides G M 2000 Fabrication of microfluidic systems in poly(dimethylsiloxane) *Electrophoresis* **21** 27–40

[89] Odom T W, Love J C, Wolfe D B, Paul K E and Whitesides G M 2002 Improved Pattern Transfer in Soft Lithography Using Composite Stamps *Langmuir* **18** 5314–20

[90] Cao L, Guo W, Wang Y and Jiang L 2012 Concentration-Gradient-Dependent Ion Current Rectification in Charged Conical Nanopores *Langmuir* **28** 2194–9

[91] Angeli E, Volpe A, Fanzio P, Repetto L, Firpo G, Guida P, Lo Savio R, Wanunu M and Valbusa U 2015 Simultaneous Electro-Optical Tracking for Nanoparticle Recognition and Counting *Nano Letters* **15** 5696–701

[92] DeBlois R W and Bean C P 1970 Counting and Sizing of Submicron Particles by the Resistive Pulse Technique *Review of Scientific Instruments* **41** 909–16

[93] Wanunu M, Sutin J, McNally B, Chow A and Meller A 2008 DNA Translocation Governed by Interactions with Solid-State Nanopores *Biophysical Journal* **95** 4716–25

[94] Peng R and Li D 2017 Detection and sizing of nanoparticles and DNA on PDMS nanofluidic chips based on differential resistive pulse sensing *Nanoscale* **9** 5964–74